JIMMA UNIVERSITY

JIMMA INSTITUTE OF TECHNOLOGY

FACULTY OF ELECTRICAL AND COMPUTER ENGINEERING

Modeling and Control of Series Resonant Converter for High Voltage Application Using Adaptive Sliding Mode Controller

A Thesis Submitted to Jimma Institute of Technology, School of Graduate Studies, Jimma University

In Partial Fulfillment of the Requirement for the Degree of Master of Science in Electrical and Computer Engineering (Control and Instrumentation Engineering)

By: Negasa Cherena

Wednesday, February 27, 2019

JIMMA ETHIOPIA

JIMMA UNIVESITY

JIMMA INSTITUTE OF TECHNOLOGY

FACULTY OF ELECTRICAL AND COMPUTER ENGINEERING

Modeling and Control of Series Resonant Converter for High Voltage Application Using Adaptive Sliding Mode Controller

A Thesis Submitted to Jimma Institute of Technology, School of Graduate Studies, Jimma University

In Partial Fulfillment of the Requirement for the Degree of Master of Science in Electrical and Computer Engineering (Control and Instrumentation Engineering)

By: Negasa Cherena

Approved by Board Examiners

Chairman, School of Graduate Committee	Signature	Date
Dr-Ing .Gebremichael Teame Advisor	Signature	Date
External examiner	Signature	Date
Internal examiner	Signature	Date

Declaration

I declare that this thesis entitled as Modeling and Control of Series Resonant Converter for High Voltage Application Using Adaptive Sliding Mode Controller is my own original work. This thesis has not been presented for a master's degree in this or any other universities, and all sources of materials used have been fully acknowledged.

Negasa Cherena

Name	Signature	Date

This thesis has been submitted for examination with my approval as a university advisor.

Dr-Ing .Gebremichael Teame

Name of Main Advisor	Signature	Date

Mr. Mengistu Fentaw (MSc.)

Name of Co-advisor	Signature	Date

Acknowledgment

I have immense pleasure in expressing deep sense of gratitude to my almighty God for everything I have got through my life giving me the strength all the time.

I am very delightful to give gratitude to my advisor, Dr-Ing. Gebremechael Teame, for his guidance throughout this thesis. He delivered his whole knowledge which is indispensable for the completion of this thesis. I am very happy with all his comments, guidance and support. He always guide me sacrificing his expensive time.

I have great thanks for my co-advisor, Mr. Mengistu Fentaw, for his firm guidance during simulation and all report writing. He supported me without any hesitation at any time I need his help. I would also like to thank the academic staffs of Electrical and Computer Engineering, and colleagues for their vital comments, advice and idea contribution on the thesis.

Abstract

Inductor inductor capacitor (LLC) series resonant converter is used for high frequency and high voltage applications. The converter operates in zero voltage swithching (ZVS) region to reduce swithching loss happened in swithches used to turn ON and OFF the system. This operation makes the output voltage to be regulated for wide input voltage and load resistance variation with small variation of switching frequency. This is the main advantage of LLC resonant converter compared to other resonant converters. But, LLC series resonant DC-DC converter have a problem of the voltage regulation due to nonlinearity, the uncertainity and disturbance which is caused by the deviation of input voltage (300-400)V, load resistance (3-8)kΩ and resonant components from the nominal value. Extended describing function and Jacobian Linearization methods is used to develop small signal modeling of the converter. But, the linearized system has seven states wich are not measurable and needs obsrever for controller design. Hence, seven state small signal modeling of the converter is reduced to two measurable states using the relationship between the state variables. Model reference adaptive sliding mode controller is designed for simplified second order system of LLC converter to control the output voltage and rectifier current. The lyapunov adaptive method is used to estimate the sliding mode controller parameters to solve the disturbance caused by parameter variation in the converter. The stabilty of controller is checked using Lyapunov stability criteria. The converter is designed for 4kV output voltage, 0.5A output current and 2kW output power. The simulation is done using MATLAB/SIMULINK® software. The simulation result indicates that the adaptive sliding mode controller has better performance compared to supper twiting sliding mode controller. The setling (t_s) is reduced to 2.5msec and rise time (t_r) is increased to 334.24μsec respectively, while the steady state error (e_{ss}) is reduced to 0.2%.

Keywords: Controller design, Extended describing function, DC-DC converter, LLC resonant converter, Parameter variation

Table of Contents

List of Tables

List of Figures

List of Acronyms

BJT-Bipolar Junction Transistor

DC-Direct Current

DCM-Discomtinuos Conduction Mode

DSP-Digital Signal Processing

EDF-Extended Describing Function

EMI-Electromagnetic Interference

FHA-First Harmonic Approximation

HVDC-High Voltage Direct Current

KCL-Kirchofs Current Law

KVL-Kirchofs Voltage Law

MIMO-Multi Input Multi Output

MOSFET-Metal Oxide Semiconductor Field Effect Transistor

MRAC-Model Reference Adaptive Control

PID-Proportional Integral Control

PI-Proportional Integral

PRC-Parallel Resonant Converter

PV-Photo Voltage

PWM-Pulse Width Modulation

SMC-Sliding Mode Control

SOSMC-Second Order Sliding Mode Control

SOTC-Simplified Optimal Trajectory Control

SPRC-Series Parallel Resonant Converter

SRC-Series Resonant Converter

STA-Supper Twisting Algorithm

STC-Self Tuning Control

VSC-Variable Structure Control

ZCS-Zero Current Swithching

ZVS-Zero Voltage Crossing

List of Symbols

i_{mc} - Cosine component magnetizing inductor current

V_{Crc} - Cosine component of resonant capacitor voltage

i_{ms} - Sine component magnetizing inductor current

$\delta_{u(t)}$ -Control variation signal

V_{dc} -DC input voltage

t_{dead} -Dead time

u_{ds} -Discontinous control

C_{eq} -Equivalent capacitor

u_{eq} -Equivalent control

C_0 -Filter capacitor

L_m -Magnetizing inductor

f_m -Mathched disturbace

V_0 -Output voltage of the converter

i_{rec} -Rectifier current

f_{r2} -Resonant frequancy due to Lm,Cr and Lr

f_{r1} -Resonant frequency due to Lr and Cr

L_r -Resonant inducctor

C_r -Resonat capacitor

V_{rms1} -Root mean square of primary voltage

V_{rms2} -Root mean square of secondary voltage

R_s -Series internal resistance of resonant components and transformer

V_{Crs} -Sine component of resonant capacitor voltage

s(t) -Sliding surface

$\delta_{x(t)}$ -State variation signal

f_s -Swiching frequncy

f_u -Unmatched disturbance

V-Lyapunov function

LLC-inductor inductor capacitor resonant converter

R_{ac} -AC equivalent resistance

f_n -The ratio of switching frequency to resonant frequency

Q -Quality factor of resonant converter

k -The ratio of magnetizing inductor to resonant inductor

CHAPTER ONE

1. INTRODUCTION

Nowadays, DC-DC converters are being employed for diferent applications i.e. industry and transmision systems to convert one DC voltage level to another voltage level. Photo voltaic (PV) system is one of renewable energy supply in wich DC-DC converter is applied to boost the output voltage to desired level [1]. DC micro grid uses DC-DC converters to solve the problem of inflexibilty due to voltage transformation complexties and incompatabilty of induction motors [2]. Swithed mode DC-DC converter has the potential for HVDC transmission systems [3]. High efficiency and high power density are the main objectives for a DC-DC converter for any area of application.

Pulse width modulation and resonant modulation are two types of the modudation techniques used in DC-DC converters. PWM has large switching loss compared to resonant technique. Due to the capability of achieving zero voltage switching (ZVS) or zero current switching (ZCS), the resonant converters can work at a very high switching frequency, reducing the transformer, filter's dimension and weight to achieve a high efficiency [4].

Resonant converters is classified as series, parallel and the series-parallel resonant converters depending on the region of operation. The series resonant converter can operate in ZCS and ZVS region. But, light load operation requires a very wide range of switching frequencies in order to retain output voltage regulation. In addition, for high input voltage conditions, the series resonant converter suffers from high conduction losses and the switching network transistors experience high turn off current. Compared to the series resonant converter, the parallel resonant converter topology does not require a wide range of switching frequencies to maintain output voltage regulation. However, at high input voltage conditions, the parallel resonant converter shows worse conduction losses and higher turn off currents. Series parallel resonant, which is also known as LCC converter, combines the advantage of both series and parallel resonant converter. But, series parallel resonat converter has a limitation since the conduction loss and switching loss will increase at high input voltage [5].

LLC is series type converter designed by interchanging capacitor and inductor in LCC converter. The benefit of LLC resonant converter is narrow switching frequency range with light load and ZVS capability. This converter operates under no load condition with better performance compared to LCC converter [5].

The application of the sliding mode control (SMC) theory to the model following control system was initiated by Yong [6]. Model reference adaptive sliding mode control is insensitive to the variation of the plant parameters and external disturbance. The the transient response of the plant uncertainty, during sliding mode, can be prescribed in advance by using SMC as a control method.

Integral sliding mode control (ISMC) is a method in which an integral controller was added to a variable structure controller. In this control method not only the parametric variations and/or disturbances can be rejected, but also resulted in zero steady state error. Moreover, it has also been found that ISMC is more robust than conventional linear controllers or conventional sliding mode controller in the applications of electro hydraulic servo control systems [7].

In the conventional sliding mode design, the upper bound of disturbance are bounded and their upper bound is estimated using simulation. However, it is often observed that in most dynamic systems, the statistical characteristics of the uncertainties and nonlinearities of the controlled plant in general are not available or too expensive to asses. Hence, obtaining the boundary values of the disturbance become a practical problem of the application of VSC [8].

1.1 Statement of Problem

LLC series resonant DC-DC converter shows nonlinearity because of the characteristics of switches used to turn ON or OFF the converter. The semiconductor switches creates nonlinearity during switching period which results in nonlinear function of output voltage and current. Moreover, input voltage, load resistance and resonant component is not constant with time as a result of environmental condition, temperature and manufacturing problem. These create the disturbance in the converter which affects the output voltage and rectifier current to deviate from the reference value. The disturbance caused by parameter variation is bounded but the boundary may not known. Therefore, the robust control system should be designed to regulate the output voltage and rectifier current solving the nonlinearity and disturbance effect on the converter.

1.2 Objectives

1.2.1 General Objective

The general objective of the thesis is to model and control LLC series resonant converter for high voltage application using adaptive sliding mode control.

1.2.2 Specific Objectives

- To select specification of LLC converter and design the converter parameters
- To develop small signal model using extended describing function
- To reduce seven unmeasurable states to two measurable states
- To design model reference adaptive sliding mode controller
- To simulate overall system using MATLAB/Simulink® software
- To validate the stability of the system

1.3 Methodology

Different literatures have been reviewed for converter design, modeling and controller design in this thesis. Recent journal articles, conference proceedings, Doctorial dissertation report and different books are reviewed on the areas of adaptive sliding mode controller and mathematical modeling of LLC resonant converter.

Secondary data collection method is used to select design parameters of the converter. The design parameters and specification of the converter is taken from prevously done paper on high voltage application.

DC characteristics of LLC converter is analyzed using graphical method for different values of quality factor and inductor ratio. The simulation result from the converter is analyzed using table and graphical method.

Nonlinear differential eqaution of the converter is developed by applying KVL and KCL method to first harmonic approximation (FHA) model of the full bridge converter. Higher harmonics approximation of the converter is difficult to analyze and to get dominant poles from transfer function. Harmonic balance method is used to get sine and cosine components of resonant inductor current, resonant capacitor voltage and magnetizing inductor current. Extended describing function is used with Jacobian matrix method to get small signal model of the converter at steady

state operating point. Higher order model is reduced to second order system using taylor series approximation.

Resonant parameter, input DC voltage and load resistance are study parameters considered in this thesis. The effects each parametres at different time and at the same time is studied using simulation software. The swithing frequeny is a control signal while output voltage and rectifier current are control parameters to be controlled.

Model reference adaptive sliding mode controller is applied to the system to control output voltage and rectifier current of the converter for different parameter variation and disturbance signal. The performance of this controller is compared with supper twisting second order Sliding Mode controller stated in [21]. Lyapunov stability criteria is used to check the stability of the controller.

Matlab/Simulink® software is used for simulation and signal analysis, while Microsoft Visio 2016 and latex software is used to draw the schematic diagram for converter analysis and design. Matlab/Simulink®2018 release has some important features and good quality signal analysis compared to previous release.

1.5 Scope of Thesis

In this thesis the following parameters are studied:

- Effect of load resistance variation on output voltage and rectifier current
- Effect of resonant tank parameters variation on output voltage and rectifier current
- Effect of input voltage variation on output voltage and rectifier current

To design the converter and controller the following assumption are taken:

- The transformer eddy current and hysteresis loss is neglible
- Only 10% of resonant inductor is varied due to manufacturing problem
- The filter capacitor has no internal resistance

The model reference adaptive sliding mode controller is designed by considering each parameters variation effect individually and at the same time. Integral sliding mode control is used to avoid parameter variation sensitivities of sliding mode control during reaching phase. Continuous function as approximation of discontinuous signal is used rather than higher order sliding mode controller to avoid chattering problem in SMC.

1.6 Outline of the Thesis

Chapter two discusses about topologies of resonant converter, principle of operation and introduction about model reference and sliding mode control. Different control methods of LLC resonant converter are reviewed in this chapter.

Chapter three presents about methods of modeling and linearizing of LLC converter. Large signal and small signal modeling of the converter is done to design controller. The converter design and DC charactetristics is also included in this chapter.

Chapter four is all about controller design. Supper twisting and model reference adaptive controller is designed for the same model derived in chapter three.

Chapter five discusses the simulation result of designed controllers with and without disturbance signal.

In the final chapter, chapter six, the conclusion are drawn depending on simulation result. Recomendation and future work are also discussed in this chapter.

CHAPTER TWO

2. THEORETICAL BACKGROUND and LITERATURE REVIEW

2.1 Switching Schemes of DC-DC Converters

There are two types of switching used in DC-DC converters i.e. hard switching and soft switching.

2.1.1 Hard Switching Scheme

Hard switching occurs when there is an overlap between voltage and current when switching the transistor is ON and OFF. This overlap causes energy loss. This energy loss can be minimized by increasing the change in current and voltage. However, fast changing of voltage causes electromagnetic interference (EMI) to be generated. The buck converter uses power MOSFET switches that shown in Figure 2.1.

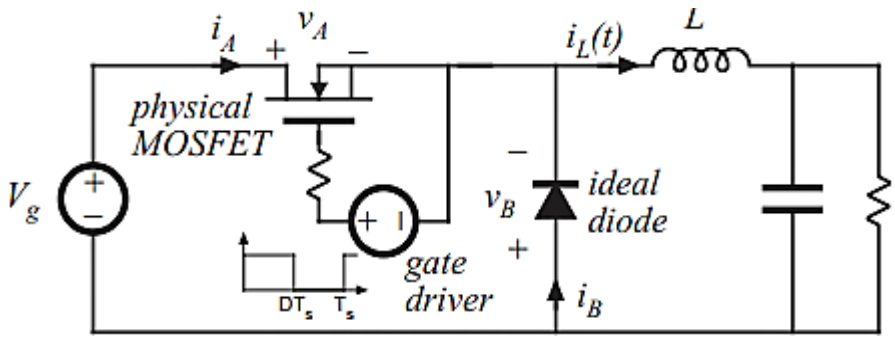

Figure 2.1 Buck converter [9]

The gate of the MOSFET is driven by the duty cycle (D) of the pulse width modulator. In the actual switching period, there is a finite period during which the switch conducts as the voltage (V_A) drops to zero and as the current (i_A) begins to flow. There exists a voltage across the switch and current flows during the switch turn OFF (or ON) cycle. Hence, there is a power loss which is known as the switching loss [9]. The power loss is indicated by the shaded area in Figure 2.2. i_L is inductor current while V_g is DC input voltage.

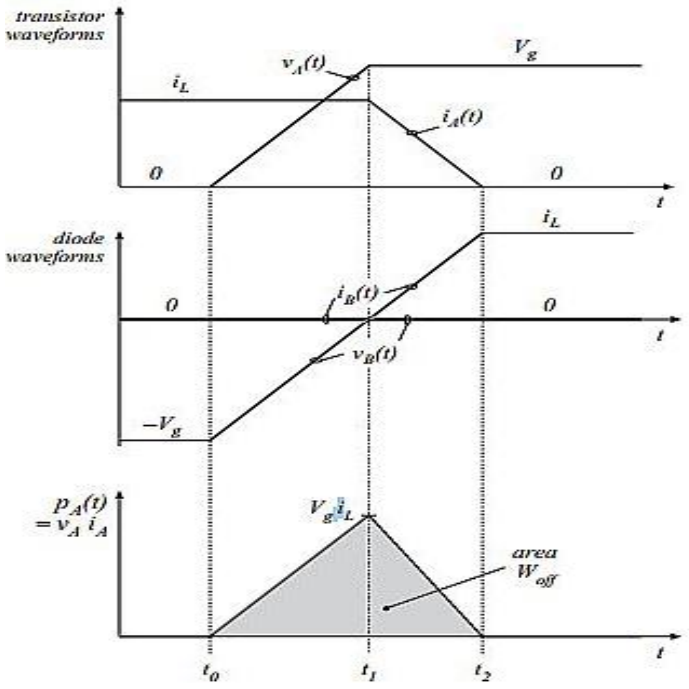

Figure 2.2 Hard switching characteristics of PWM [9]

The energy lost during transistor turn OFF and turn ON transition is the same. The energy lost is calculated as follows which is derived in [9].

$$W_{off/on} = \frac{1}{2} V_A i_A \left(t_2 - t_0\right) \tag{2.1}$$

Then the average power loss is given by

$$p_{loss} = \frac{1}{T_s} \int P_{A(t)} dt = \frac{1}{2} \left(W_{on} + W_{off}\right) \tag{2.2}$$

2.1.2 Soft Switching Scheme

Soft switching brings one electrical parameter to zero (current or voltage) before the switch is turned ON or OFF. This reduces the energy lost during swithching period. The common soft switching schemes described in [10] are:

- Load resonant power converters
- Converters with resonant switches (Quasi- resonant, or multi-resonant)
- Resonant transition power converters –zero voltage transitions (ZVT) and zero current transitions (ZCT)

- Zero voltage switching
- Zero current switching

Among the above listed schemes, ZVS and ZCS are common switching techniques used for resonant converters. Soft switching can mitigate some part of switching loss and reduce the generation of EMI.

i) Zero Voltage Switching (ZVS)

ZVS is defined as the transition phase of the waveforms across the main switch of DC-DC converter from one status to another status. The voltage across the power switch is zero at which the current through the switch is the same with source current during turn ON time. Hence, there is no overlap of current and voltage implies that no power losses take place as shown in Figure 2.3. When the PWM signal is zero, the drain to source voltage (V_{ds}) starts increasing while the current (i_d) still flows through the main power MOSFET. At main switch turn OFF, it is also found that there will be an important quantity of current and voltage at the transition phase which takes into switching power losses. Zero Voltage switching is chosen in favor of high voltage and high power applications [10].

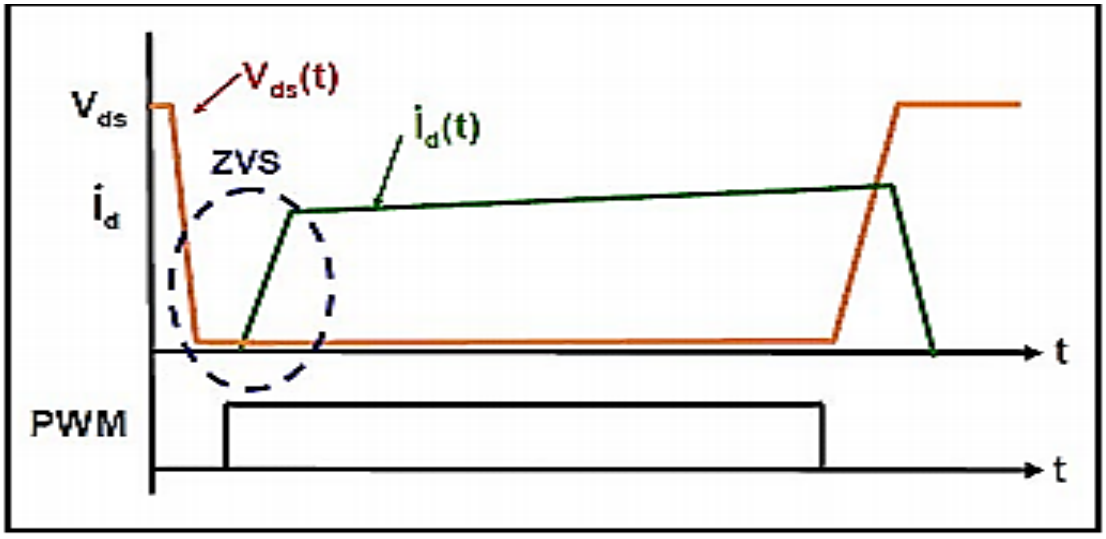

Figure 2.3 Zero voltage switching of PWM [10]

ii) Zero Current Switching (ZCS)

ZCS is a swithching scheme created at main switch turn OFF time. The current is zero at the transition period from one phase to another phase of the power MOSFET; hence, no power losses occurs during the turn OFF period as shown in Figure 2.4. During switch turn OFF, the power MOSFET switching power loss is reduced to zero as the current (i_r) is zero and the drain to source voltage (V_{ds}) is also zero. On switch ON conditions, there will be quantity of current and voltage at the transitions which leads to switching power loss. ZCS enables to cut the noise in the systems, therefore improving EMI performance [10].

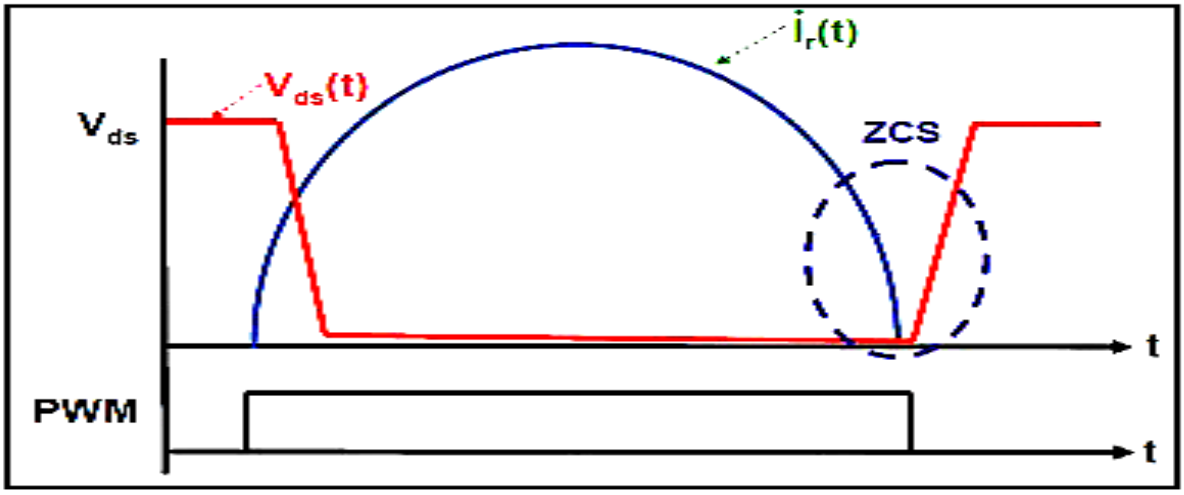

Figure 2.4 Zero current switching PWM [10]

2.2 Resonant Converter Topologies

There are different types of resonant converters used for different applications. Series resonant converter, parallel resonant converter and series parallel resonant converter are the three most popular topologies of resonant converters.

2.2.1 Series Resonant Converter (SRC)

The circuit diagram of a half bridge series resonant converter is shown in Figure 2.5. V_{in} is DC input voltage, Q_1 and Q_2 are half bridge inverter switches, D_1 and D_2 half bridge rectifier diodes, n_p and n_s are transformer turns ratio while C_f is filter capacitor. This converter is named as series since the resonant inductor (L_r) and resonant capacitor (C_r) are series in resonant tank circuit. The

resonant tank circuit is also in series with the load resistance. From this configuration, the resonant tank and the load act as a voltage divider. By changing the frequency of input voltage (V_a), the impedance of resonant tank will change. Since it is a voltage divider, the DC gain of SRC is always lower than 1 as indicated on DC characteristic of SRC shown in Figure 2.6. At resonant frequency, the impedance of series resonant tank will be very small that is all the input voltage will drop on the load. So, for this converter, the maximum DC gain happens at resonant frequency.

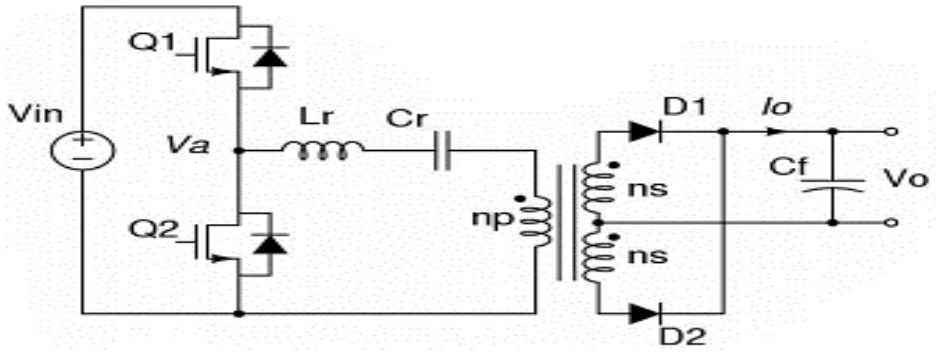

Figure 2.5 Series resonant converter circuit diagram [5]

When the DC gain slope is positive, the converter will work under ZCS condition while it works under ZVS when slope is negative. The major problems of SRC are light load regulation, high circulating energy and turn OFF current at high input voltage condition [5].

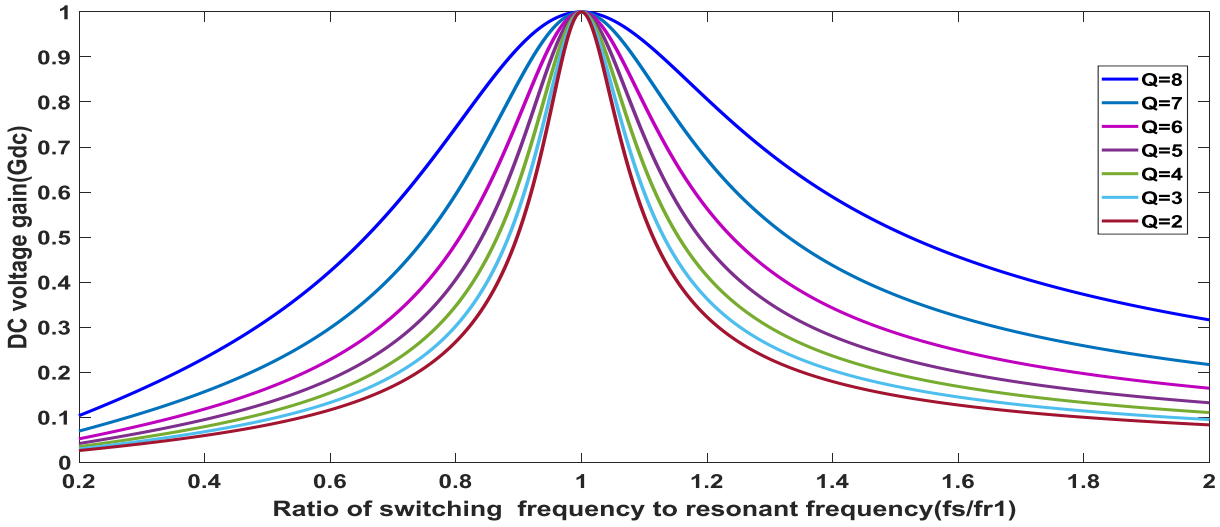

Figure 2.6 DC characteristics of SRC

The DC characteristics curve of all resonant converters is drawn for different Quality factors (Q). Lower quality factor implies heavy load while higher quality factor indicates light load at the output. Quality factor is the ratio of energy storage elements (resonant tank) to energy dissipation element (load resistance).

2.2.2 Parallel Resonant Converter (PRC)

The circuit diagram of parallel resonant converter is shown in Figure 2.7. For parallel resonant converter, the load resistance is in parallel with the resonant capacitor while the resonant tank components are in series. An inductor (L_f) is added on the secondary side to match the impedance of capacitor on transformer primary side.

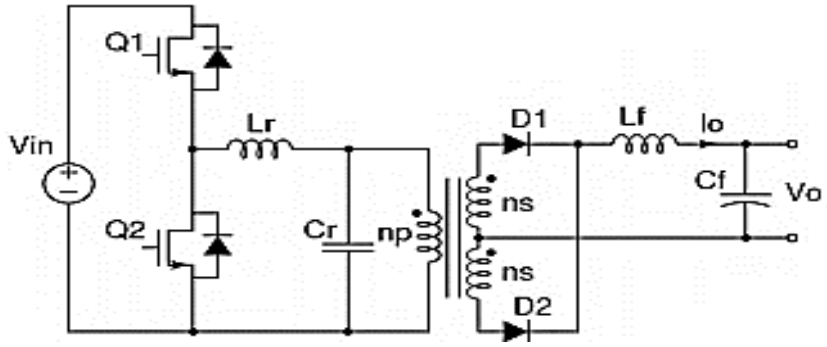

Figure 2.7 Parallel resonant converter circuit diagram [5]

Similar to series resonant converter, the operating region of this converter is also designed on the right hand side of resonant frequency to achieve ZVS. Compared with SRC, the operating region of PRC is much smaller as indicated in Figure 2.8. The switching frequency of the converter doesn't need to change too much to keep output voltage regulated so that light load regulation problem exhibited in SRC is solved in PRC.

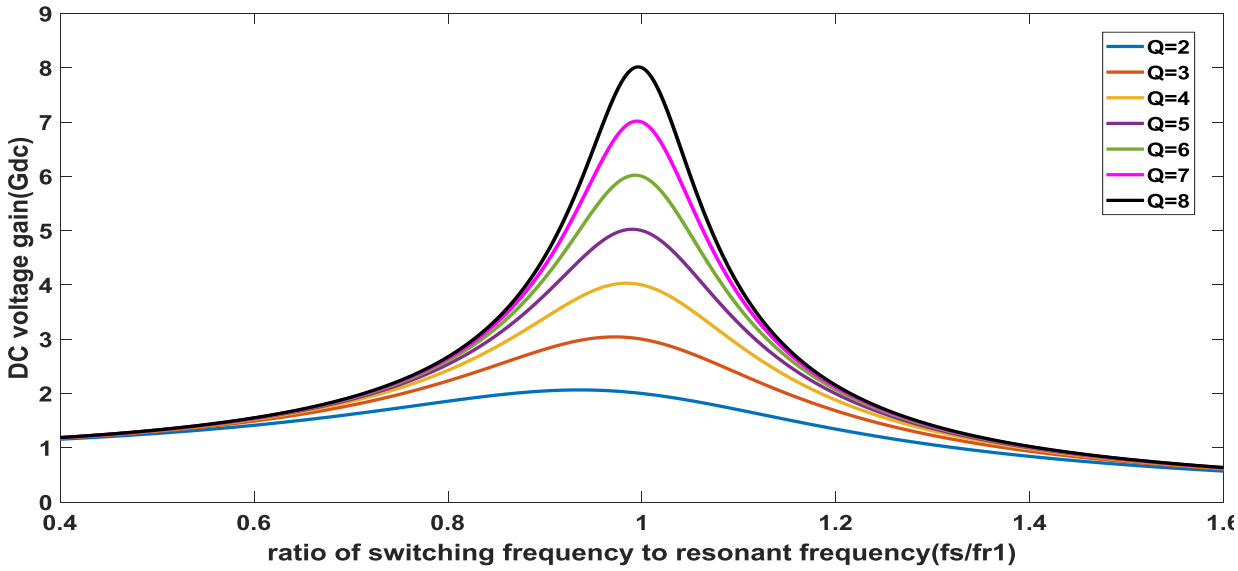

Figure 2.8 DC characteristics of PRC

For PRC, there is small impedance of the resonant tank circuit, even at no load condition, since the load is in parallel with the resonant capacitor. This induces high circulating energy in the converter. The major problems of PRC are high circulating energy and high turn OFF current at high input voltage condition [5].

2.2.3 Series Parallel Resonant Converter (SPRC)

The circuit diagram of series parallel resonant converter is shown in Figure 2.9. Its resonant tank circuit consists of three resonant components i.e L_r, C_{sr} and C_{pr}. It is also known as LCC converter. Similar as PRC, an output filter inductor (L_f) is added on secondary side to match the impedance on primary side. The resonant tank circuit of SPRC is the combination of SRC and PRC which enables it to combine the good characteristic of both converters. When the load resistance is in series with resonant tank components, the circulating energy is smaller compared with PRC. Parallel capacitor (C_{pr}) enables SPRC to regulate the output voltage at no load condition.

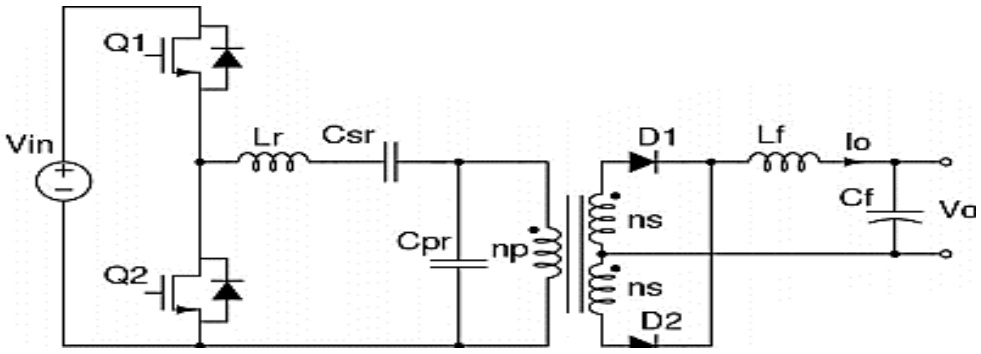

Figure 2.9 Series parallel resonant converter circuit diagram [5]

Similar to SRC and PRC, the operating region is also designed on the right hand side of resonant frequency to achieve ZVS. From the operating region graph shown in Figure 2.10, it can be seen that SPRC has narrow switching frequency range compared with SRC. However, SPRC have a problem with wide input range design. With wide input range, the conduction loss and switching loss will increase at high input voltage. Hence, the switching loss is similar to that of PWM converter at high input voltage [5].

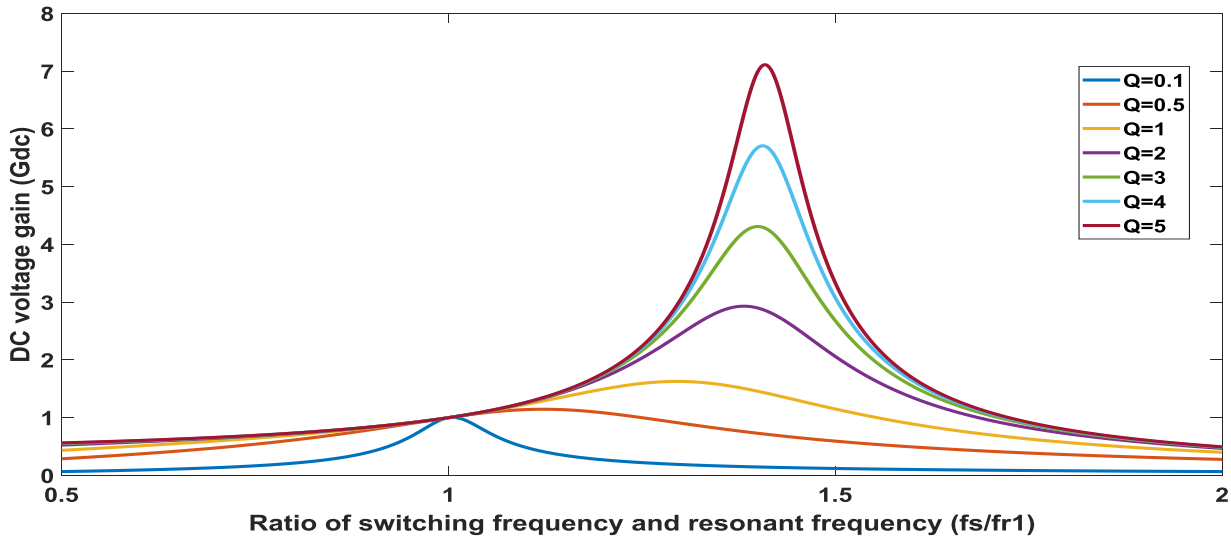

Figure 2.10 DC characteristics of SPRC [5]

The above three converters cannot be optimized at high input voltage. High conduction loss and switching loss will be resulted from wide input range. Moreover, they cannot operate in ZVS region below resonant frequency. Therefore, they are not suitable for front end DC/DC application.

2.2.4 LLC Resonant Converter

By changing the LCC resonant tank to its dual resonant network, a LLC resonant converter could be built [5]. This is done by changing L to C and C to L as shown in Figure 2.11.

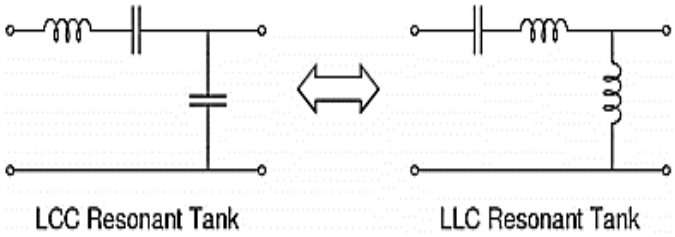

Figure 2.11 LLC and LCC configurations [5]

Full bridge LLC resonant converter circuit is shown in Figure 2.12. S_1, S_2, S_3 and S_4 are full bridge inverter MOSFET switches; D_1, D_2, D_3 and D_4 are reverse recovery diode of MOSFET; D_5, D_6, D_7 and D_8 are full bridge rectifier diode; C_0 is filter capacitor; R_s is resonant tank parameter internal resistance and R_L is load resistance.

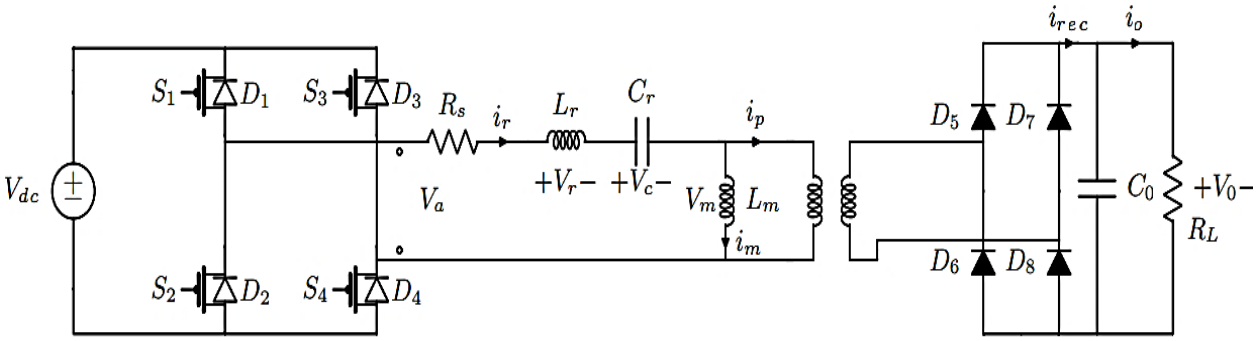

Figure 2.12 Full bridge LLC resonant converter

The benefit of LLC resonant converter is narrow switching frequency range with light load and ZVS capability over other resonant converters.

i) DC Characteristics of the LLC Converter

The DC characteristic of LLC resonant converter could be divided into ZVS region and ZCS region as shown in Figure 2.13. For this converter, there are two resonant frequencies. One is determined by the resonant components (L_r, C_r). The other one is determined by L_m, C_r and load resistance condition. The higher resonant frequency (f_{r1}) is in the ZVS region, which means that the converter could be designed to operate around this frequency. As load getting heavier, the resonant frequency will shift to higher frequency. The two resonant frequencies are:

$$f_{r1} = \frac{1}{2\pi\sqrt{L_r C_r}}$$
$$f_{r2} = \frac{1}{2\pi\sqrt{(L_r + L_m)C_r}} \quad (2.3)$$

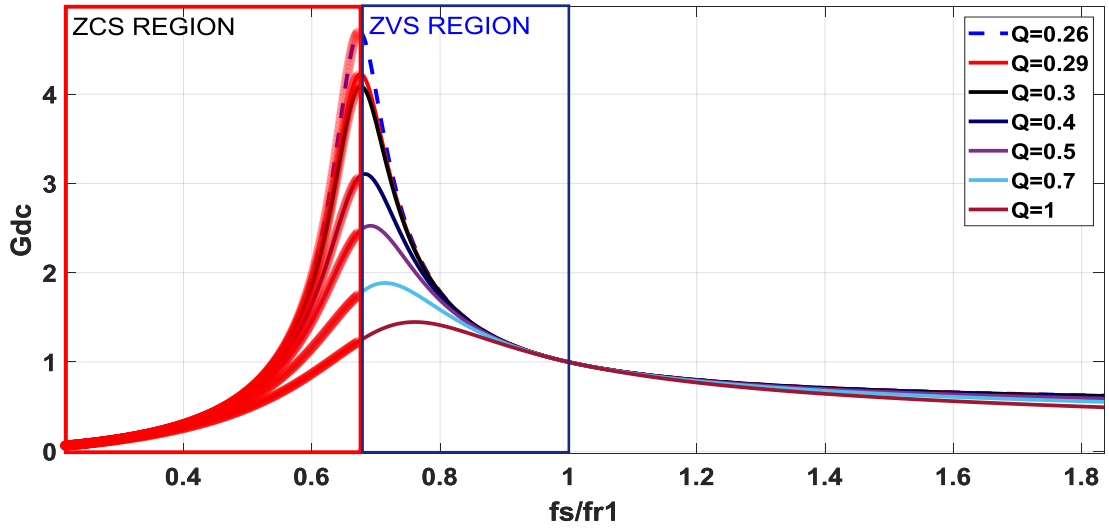

Figure 2.13 DC characteristic of LLC resonant converter

On the right side of frequency ratio (f_n), the converter has same characteristic as SRC. On the left side of f_n, the characteristic of PRC and SRC are fighting to be the dominant. At heavy load, SRC is dominant while the characteristic PRC moves to the top as the load becomes light. With these interesting characteristics, it is possible to design the converter working at the resonant and at lower than resonant frequency of SRC to achieve high efficiency without losing ZVS property.

ii) Operational Principle of LLC Converter

The LLC resonant converter shown in Figure 2.12 operates in ZVS operating region, for which the principal operation waveforms are shown in Figure 2.14. The gating signals and diode current of S_1, S_2, S_3, S_4 are represented as V_{Ds1}, V_{Ds2}, V_{Ds3}, V_{Ds4} and I_{Ds1}, I_{Ds2}, I_{Ds3}, I_{Ds4} respectively. There are three operation modes of in LLC resonant converter in ZVS region described in [31].

Mode 1 (t_0 to t_1):

This mode begins when S_2 and S_3 are turned OFF at t_0. At this moment, resonant inductor current is negative i.e. it will flow through body diode of S_1 and S_4, which creates a ZVS condition. The

gate signal of S_1 and S_4 should be applied during this mode. During this period i_{Lr} begins to rise, which forces rectifier diode D_5 and D_8 conduct and I_0 begins to increase. At this moment, transformer sees output voltage on the secondary side.

Mode 2 (t_1 to t_2)

This mode begins when i_{Lr} becomes positive. Since S_1 and S_4 are turned ON during mode 1, current will flow through them, where output rectifier diode D_5 and D_8 start conducting. The transformer voltage is clamped at V_0 and L_m is linearly charged with output voltage. So, L_m doesn't participate in the resonance during this period. In this mode, the circuit works like a SRC with resonant inductor L_r and resonant capacitor C_r. This mode ends when i_{Lr} is the same as i_{Lm} at which output current reach zero.

Mode 3 (t_2 to t_3)

At t_2, the two inductor's currents are equal which results in i_0 equal to zero. All output rectifier diodes are reverse biased. Transformer secondary voltage is lower than output voltage i.e. output is separated from transformer. During this period, since output is separated from primary, L_m is free to participate in resonance. It will form a resonant tank of L_m in series with L_r and C_r. This mode ends when S_1 and S_4 are turned OFF.

From the waveform shown in Figure 2.14, the MOSFETs are turned ON with ZVS. The ZVS is achieved with magnetizing current, which is not related to load current. So, ZVS could be realized even with zero load condition. With all these, the switching loss of this converter is very small.

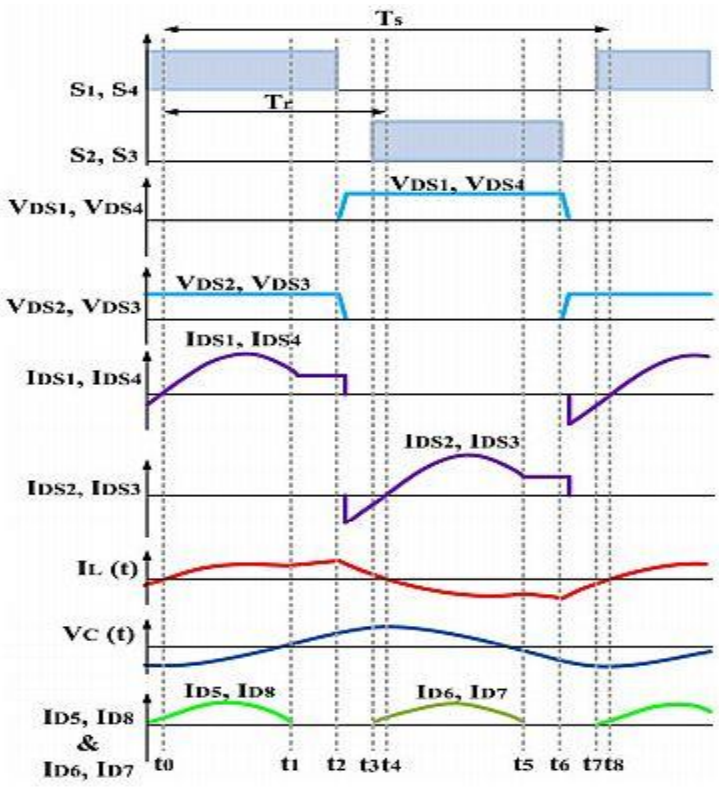

Figure 2.14 Operation mode of LLC converter in ZVS region [31]

2.3 Sliding Mode Control

SMC has been applied to different systems including nonlinear system, MIMO systems, discrete time models, large scale, infinite dimension systems, and stochastic systems. SMC is completely insensitive to parametric uncertainty and external disturbances during sliding mode [11]. SMC is known as variable structure control since control system's structure varies from one to another during the process. VSC utilizes a high speed switching control law to drive the nonlinear plant's state trajectory onto user defined surface in the state space which is called the sliding or switching surface [12] because the controller is swithching between two values for different surface and defined as

$$u(t) = \begin{cases} M, & s(t) \geq 0 \\ -M, & s(t) < 0 \end{cases} \tag{2.4}$$

where M is control signal upper bound, $s(t)$ is sliding surface and u(t) is a control signal.

There are two steps in the SMC design. The first step is designing a sliding surface so that the plant restricted to the sliding surface has a desired system response. The second step is to design the control law to keep the system response around sliding surface.

2.3.1 Integral Sliding Surface

In conventional method, the sliding surface are constructed by the intersection of some hyper surfaces in the state space and this intersection domain is normally called switching plane. Once the system state reaches the switching plane, the structure of the feedback loop is adaptively altered to slide the system state along the switching plane. The system response depends thereafter on the gradient of the switching plane and remains insensitive to variations of system parameters and external disturbances. This motion is called Sliding Mode. The order of equation in the sliding motion is equal to n-m with n being the dimension of the state space and m the dimension of the control input. However, during the reaching phase, the system possesses no such insensitivity property. Therefore, insensitivity cannot be ensured throughout an entire response. The robustness during the reaching phase is normally improved by high gain feedback control. Stability problems that arise certainly limit the application of such high gain feedback control schemes [13].

Integral sliding mode surface is designed using the conventional surface added with its integral part for the robustness of the motion in the whole state space. The order of equation in integral sliding mode surface is equal to the dimension of the state space of the system. Therefore, the robustness of the system can be guaranteed throughout an entire response of the system [14].

Consider the two sytems

$$\dot{x} = f(x) + Bu_0 \tag{2.5}$$

$$\dot{x} = f(x) + Bu + f(t) \tag{2.6}$$

where the state vector f(x) is available for measurement, f(t) represents the whole disturbance and it fulfills the matching condition i.e. $f(x,t) = B(x)u$, with $u \in R$. It is assumed here that function f(t) bounded with known upper bound.

For (2.6), first design a control like

$$u = u_0 + u_{ds} \tag{2.7}$$

where u_0, is the ideal feedback control law which is continuous, such that (2.5) can be stabilized in a desired way and u_{ds}, is designed to be discontinuous for rejecting the disturbance term.

The sliding surface is defined in [14] as

$$s(t) = s_0(t) + z, \text{ with } s_0(t), z \in R^n \tag{2.8}$$

This surface consists of two parts; the first part $s_0(t)$ may be designed as the linear combination of the system states and, the second part z induces the integral term in the surface to get decrease sensitivity of the controller to parameter variation.

To derive the Sliding Mode equation, $\dot{s}(t)$ should be made equal to zero on the system trajectories. Solving algebraic equation $\dot{s}(t) = 0$, an equivalent control is obtained as follows upon the required performances.

$$u_{eq} = -u \tag{2.9}$$

From this equivalent control it is possible to determine the formulation of variable z. The eqaution (2.9) is satisfied if

$$\dot{z} = -(\frac{\partial}{\partial x} s_0(t))\dot{x} \tag{2.10}$$

Integrating (2.10) gives

$$z = s_0(0) - \int (\frac{\partial s_0(t)}{\partial x})(f(x) + Bu_0) \tag{2.11}$$

Substituting (2.11) into (2.8) the sliding surface becomes

$$s(t) = s_0(t) - \int (\frac{\partial s_0(t)}{\partial x})(f(x) + Bu_0) + s_0(0) \tag{2.12}$$

where $s(0)$ is initial condition, $s_0(t)$ is the tracking error and u_0 is initial continuous control law.

2.3.2 Sliding Mode Control Law

For the system described in (2.6), the control objective is to stabilize x(t) when only the bounds of uncertainty are known. To stabilize the uncertain system in (2.6), if initial value of x(t) is positive then $\dot{x}(t)$ should be negative. Therefore, depending on the sign of x(t), control law should be altered to ensure stabilization of x(t).

The first step is to design equivalent control law as stated in [15]. In this approach, the discontinuous control is replaced by a linear (continuous) control. The linear control is called equivalent control and is obtained by setting $\dot{s}(t) = 0$ for the nominal system.

Let $e(t) = x_r - x$, where x_r is a reference signal and x is measured states. Then the integral sliding surface is defined as

$$s(t) = \lambda e(t) - \lambda \int e(t)dt \tag{2.13}$$

The derivative of the surface is

$$\dot{s}(t) = \lambda \dot{e(t)} - \lambda e(t) = \lambda(\dot{x}_r - \dot{x}) - \lambda(x_r - x) \tag{2.14}$$

Substituting (2.5) into (2.14),

$$\dot{s}(t) = \lambda(\dot{x}_r - (f(x) + Bu + f(t)) - \lambda(x_r - x) \tag{2.15}$$

Setting $\dot{s}(t) = 0$, the equivalent control law is derived as

$$\lambda(\dot{x}_r - (f(x) + Bu_{eq} + f(t))) - \lambda(x_r - x) = 0 \tag{2.16}$$

$$u_{eq} = -B^{-1}((x_r - x) + f(x) + f(t)) \tag{2.17}$$

The second step is to design discontinuous control law. To ensure finite time reaching for general n^{th} order single input system the following conditions should be satisfied is stated in [15].

$$\begin{aligned} \lim_{x \to 0^+} \dot{s}(t) < 0 \\ \lim_{x \to 0^-} s(t) > 0 \end{aligned} \tag{2.18}$$

The above conditions precisely ensure that s(t) and $\dot{s}(t)$ should have opposite sign and due to this

$$s\dot{s} < 0 \tag{2.19}$$

The above condition is also known as the reachability condition. The condition in (2.19) ensures only asymptotic reaching on sliding surface. A stronger condition for finite time reaching is given as follows

$$s\dot{s} < -\eta |s| \tag{2.20}$$

where $\eta > 0$

The control law which satisfies condition (2.20) is designed as follows

$$u = u_{eq} + u_{dis} = -B^{(-1)}((x_r - x) + f(x) + f(t)) + Q\text{sign}(s) \tag{2.21}$$

The above control law ensures a minimum rate of decrease (or increase) of $x(t)$. Therefore $x(t)$ reaches sliding surface in finite time. At the origin, the discontinuous part of the control law is undefined. However, at the moment the trajectory crosses the origin from either direction, again it is forced back on $x(t) = 0$. This situation is explained in Figure 2.15 which shows the state trajectories in the vicinity of $s = 0$. Because the control law is discontinuous about x(t), it demands switching at very high frequency. If this switching occurs at a very high frequency then $x(t) = 0$ can be consistently maintained with this discontinuous control law. The initial phase when the trajectory is forced towards $x(t) = 0$ is called the reaching phase which also known as the sliding phase or sliding mode. During the sliding phase, with this discontinuous control law, $x(t) = 0$ is maintained even in presence of consistent disturbances. Therefore system motion is insensitive to disturbances [15].

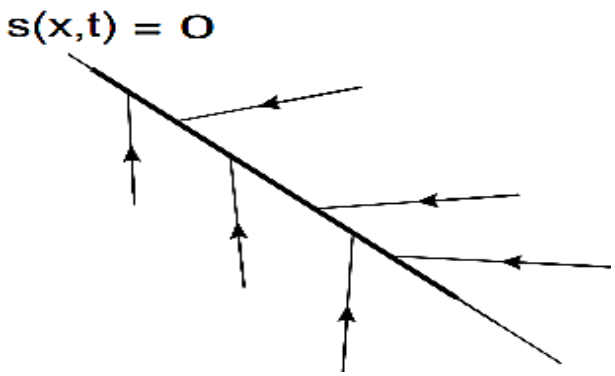

Figure 2.15 Sliding surface trajectory [15]

Alternatively, the discontinuous control law can be obtained by the so called reaching law approach stated in [13] which the upper bound of perturbation is known previously.

• The constant rate reaching law:

$$\dot{s} = -Q\,\mathrm{sign}(s) \tag{2.22}$$

• The constant plus proportional rate reaching law:

$$\dot{s} = -ks^{-1}Q\,\mathrm{sign}(s) \tag{2.23}$$

• The power rate reaching law:

$$\dot{s} = -Q^{-}\,|\,s_i\,|^{\alpha_i}\,\mathrm{sign}(s) \tag{2.24}$$

where Q and K are diagonal matrices with positive elements, Q^{-} is a positive scalar, and $\alpha_i \in (0,1)$

In the above discontinuous control law, the controller pushes the state trajectory from either side on to x(t)=0. This process continues and the control law switches between two values. This phenomena is known as chattering which needs to be addressed appropriately. Among the well known approaches based on smooth approximations of the discontinuities and asymptotic state observers, the use of the high order sliding mode control approach can attenuate the chattering phenomenon significantly [16].

2.4 Model Reference Adaptive Control (MRAC)

Model Reference Adaptive Control (MRAC) is one of adaptive control methods used to adapt the system states to uncertainty due to parameter variation. It consists of a reference model which produces the desired output. The difference between the plant output and the reference output is then used to adjust the control parameters and the control input directly. MRAC is often continuous time domain, and used for both deterministic and stochastic plants. Furthermore, MRAC adapts to the changes in the controller parameters, and is referred to as direct adaptive control which do not need a separate identification procedure for estimation of the system parameters.

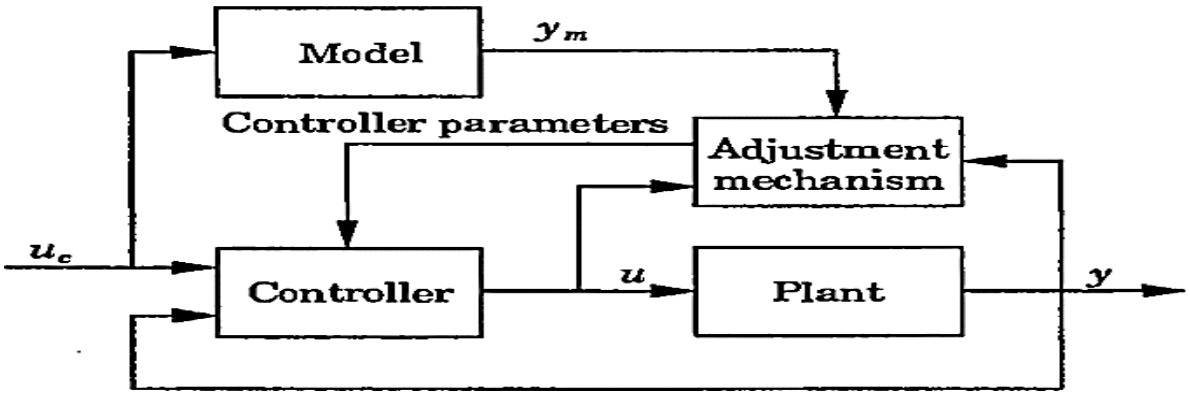

Figure 2.16 MRAC structure [18]

Self-Tuning Control (STC) estimates system parameters and then computes the control input from the estimated parameters so that it is referred to as indirect adaptive control. STC is often in discrete time and for stochastic plants [17].

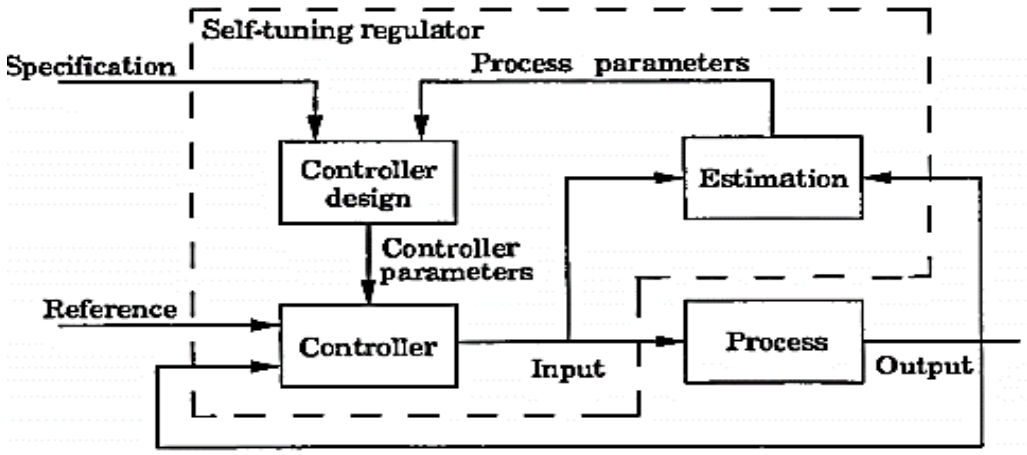

Figure 2.17 STC control structure [18]

Consider a first order system given as,

$$\dot{y} + ay = bu \tag{2.25}$$

where y and u are the system output and input respectively, and a and b are unknown constant parameters. The output of the reference model which y is to follow is defined as

$$\dot{y}_m + a_m y_m = b_m u_c \tag{2.26}$$

The reference model is stable, if $a_m>0$. The signal u_c is the reference input. The design objective is to make the tracking error $e = y - y_m$ converge to zero. The derivative of the error is

$$\begin{aligned} \dot{e} &= -a_m (y - y_m) + b\left(u + \frac{(a_m - a)}{b} - \frac{b_m}{b} u_c \right) \\ \dot{e} + a_m e &= b(u - \theta_1 y - \theta_2 u_c) \end{aligned} \tag{2.27}$$

For the resultant error to be zero ($\dot{e} + a_m e = 0$), the right hand side equation should be zero($u - \theta_1 y - \theta_2 u_c = 0$).

The control law is defined as

$$u = \theta_1 y + \theta_2 u_c \tag{2.28}$$

where $\theta_1 = \frac{(a - a_m)}{b}$ and $\theta_2 = \frac{b_m}{b}$ are nominal values that controller reaches at steady state.

The certainty equivalence principle suggests that the parameters in the control design are replaced by their pararemeter update law [17]. Hence, when the controller parameters are unknown, let $\hat{\theta}_1$ and $\hat{\theta}_2$ denote parameter update law of θ_1 and θ_2. Then the control law, based on the certainty equivalence principle, is given by

$$u = \hat{\theta}_1 y + \hat{\theta}_2 u_c \tag{2.29}$$

The certainty equivalence principle only suggests a way to design the adaptive control input, not how to update the parameter estimates. Stability issues must be considered when deciding the adaptive laws, i.e., the way how controller parameters are updated. MIT update rule is simple and works for the system which reference input varies with time. But, there is no guarantee that an adaptive controller based on the MIT rule will give stable closed loop system. Lyapunov function is good method for designing adaptive controllers that can guarantee the stability of the system and design estimated parameters [18]. With the proposed adaptive control law, the closed loop system dynamics are described by

$$\dot{e} + a_m e = b(u - \tilde{\theta}_1 Y - \tilde{\theta}_2 u_c) \tag{2.30}$$

where $\tilde{\theta}_1 = \theta_1 - \hat{\theta}_1$ and $\tilde{\theta}_2 = \theta_2 - \hat{\theta}_2$

Consider the Lyapunov function candidate

$$V = \frac{1}{2}e^2 + \frac{|b|}{2\gamma_1}(\tilde{\theta}_1)^2 + \frac{|b|}{2\gamma_2}(\tilde{\theta}_2)^2 \tag{2.31}$$

The derivative of lyapunov function is

$$\dot{V} = -a_m e + \tilde{\theta}_1(\frac{|b|}{\gamma_1}\dot{\tilde{\theta}}_1 - eby) + \tilde{\theta}_2(\frac{|b|}{\gamma_2}\dot{\tilde{\theta}}_2 - ebu_c) \tag{2.32}$$

For the derivative of lyapunov function to be semi_negative definite, $\dot{V} \leq 0$.

Therefore, if $\frac{|b|}{\gamma_1}\dot{\tilde{\theta}}_1 - eby = 0$ and $\frac{|b|}{\gamma_2}\dot{\tilde{\theta}}_2 - ebu_c = 0$,

$$\dot{V} = -a_m e \tag{2.33}$$

The adaptive laws are

$$\begin{aligned} \dot{\hat{\theta}}_2 &= \text{sign}(b)\gamma_2 e u_c \\ \dot{\hat{\theta}}_1 &= \text{sign}(b)\gamma_1 e y \end{aligned} \tag{2.34}$$

2.5 Model Reference Adaptive Sliding Mode Controller

Sliding mode control is a robust control technique which has many attractive features such as robustness to parameter variations and insensitivity to disturbances. It has some limitations such as chattering or high frequency oscillation in practical applications. Adaptive control is an effective approach to handle parameter variations. Adaptive methods are used to automatically adjust the response of the controller to compensate for changes in the response of the plant. Therefore adaptive sliding mode control has the advantages of combining the robustness of variable structure methods with the tracking capability of adaptive control [19].

2.6 Literature Review

Various control methods [20-30] have been applied to LLC resonant converter to control output voltage and track resonant frequency.

Lai, Yen and Min [20] proposed a control system to deal with resonant frequency variation caused by the resonant components tolerance and variation. The voltage reference of power factor correction output voltage is tuned to achieve both switching frequency tracking and output voltage regulation of resonant converter[20]. The proposed method is simple and needs no knowledge of resonant frequency in prior. But voltage regulation due to load resistance and input voltage variation is not solved.

Geng, Zhao and Sun [21] designed sliding mode control technique which performs well against wide input voltage and load variations at constant operating frequency. The proposed controller has better performance compared to PID controller and rejects the disturbance caused by input voltage and load resistance variation. However, the output voltage control with resonant tank parameter variation is considered together with input voltage and load resistance variation.

Chen, Tianpei and etal [22] applied fuzzy self-adaptive PI controller to improve the LLC resonant converter with nonlinear, time-varying feature control performance. The control system has voltage outer loop and the current inner loop in which traditional PI controller is used. The outer control parameters are adjusted using fuzzy rules to make the output voltage to keep track the reference voltage in the adjustment process. The inner PI control loop prevent current spikes and ripples caused by external changes [22]. But, fuzzy logic needs a knowledge base controller which needs different rule base for different operating point and varying parameters i.e. it needs huge lookup table for rulebase.

Degioanni, Ignacio, and Martin [23] designed a simple and dual loop control scheme i.e.an inner current loop and outer voltage loop in which Proportional Integral (PI) controllers are employed as compensators for each control loop. This dual-loop scheme enables numerous advantages as tight current regulation and over current protection. The implementation of an inner current loop minimizes the variations of the small signal characteristics of the converter at different operating points achieving similar transient responses over a wide range of frequencies [23]. However, this

dual-loop control works only for an accurate large signal average and a simplified linearized model of the converter operating at resonant frequency. A simplified linearized model cannot work for high resonant frequency range.

Amghar, Darcherif, Jean, and Djamel [24] applied a petrinet and PI hybrid control strategy in series resonant converter for high voltage applications for minimizing the no load conduction losses. Petri nets are among the powerful tools for modeling and control of such systems which have discontinuities in their mathematical models [24]. In this method the amplitude is considered fixed leaving the frequency as the only control variable. Resonant frequency variation caused by the resonant tank components and load resistance effect on output voltage regulation due to uncertainties is not solved by this method.

Maguiri, Ouadia and etal [25] designed adaptive control strategy to regulate series resonant converter output voltage, despite load uncertainty. An adaptive controller is designed using the tuning functions backstepping technique. The proposed controller achieved the perfect output reference tracking and exact converter load estimation [25]. But, the disturbance due to input voltage and resonant tank components variation is left uncontrolled. Moreover, backstepping algorithm needs complex analysis.

Shahzad, Imran, Iqbal and Taib [26] applied PID controller to LLC converter for battery charging application. The controller performance is analyzed for adjustment of output voltage for both line and load variations. The controller has adjusted the effects of step variations in line, load and also tracked the reference signal for both step and linear variations in the reference value [26]. But, PID is linear controller which cannot handle nonlinear characteristics in LLC converter due to parameter variation.

Zhijian, Junhua, Shanxu, Kaipei and Tao [27] proposed a nonlinear control strategy using load feedback linearization for an LLC resonant converter. Compared with the conventional PI controllers, the proposed strategy can achieve better performance with elimination of the nonlinear characteristics. The LLC resonant converter's dynamic model is built based on fundamental harmonic approximation using extended describing function. The LLC resonant converter's model

is simplified from seventh order state equations to second order to design double loop PI controller which regulates output voltage. The switching frequency can be calculated as a function of the load, input voltage and modulation voltage [27]. However, such a simplified two-order model can't replace the small signal model which provides detailed dynamics of an LLC resonant converter and the effect of input voltage, load resistance and resonant paramater variation cannot be regulated by this method since the controller is linear controller.

Feng, Weiyi, Fred, and Paolo [28] applied simplified optimal trajectory control (SOTC) for the LLC resonant converter. The method used a linear controllers during the steady state and SOTC method during load transients, immediately changing the pulse widths of the gate driving signals. Using the state plane analysis, the pulse widths are estimated, letting the state variables track the optimal trajectory locus in the minimum period of time. The proposed solution is implemented in a digital controller, and experimental results show that while the digital logic requirement is very small, the performance improvement is significant [28]. But, The variable equal load resistor values need be calculated at every instantaneous time online which is nonlinear and complicated. Thus, it is very difficult to implement this method. Moreover, PWM cannot be used for high frequency application to control the output voltage of the converter.

Hwa-Pyeong and Jee-Hoon [29] designed and implemented a high frequency LLC resonant converter to verify the power density enhancement achieved by decreasing the size of the passive components. The effect of the smaller output capacitance is analyzed for stability using a proper small signal model of the LLC resonant converter. Finally, the proper design methods of a feedback compensator are proposed to obtain sufficient phase margin in the bode plot of the converter's loop gain for stable operation at high switching frequency [29].

Buccella,Concettina ,and etal [30] designed a nonlinear observer based controller and implemented with a digital signal processor (DSP). A nonlinear model for the LLC resonant converter was developed using the extended describing function (EDF) method; then, based on the derived model, transient responses obtained under input voltage and output load variations show that the proposed controller is capable to stabilize the output effectively. In this system the output voltage is the unique measured state variable, while the other state variables are estimated using the

Luenberger-like observer [30]. But, this method cannot be applied to control rectifier current since it is unable to measure rectifier current directly. Moreover, the effect of resonant component variation is not considered.

2.6.1 Sliding Mode Control (SMC) of LLC Resonant DC-DC Converters

Robust control using second order sliding mode technique is proposed for the LLC resonant DC-DC converter in [21]. Firstly, a nonlinear model of LLC converter is obtained via the extended describing function method. Then, based on the derived model, a second order sliding mode (SOSM) controller is designed. SMC is known for its finite time convergence, high accuracy and robustness against parametric uncertainties and external disturbances. The super twisting algorithm (STA) is a continuous sliding mode algorithm among the SOSM algorithms. Therefore, it does not suffer from the chattering problem compared with classical sliding mode method. The conventional sliding variable is used to design the controller. Moreover, the upper bound of disturbance is assumed known in priori. The controller performance is better than conventional PID controller. But, SMC has low performance if upper bound of the disturbance is not known and there is parameter variation in resonant tank.

In this thesis, model reference adaptive sliding mode controller is applied to LLC resonant converter for high voltage application. The proposed system is a nonlinear controller in which nonlinearity existing in the converter is solved. The adaptive control method adjusts the controller parameters to control output voltage and rectifier current. Even though there is disturbance caused by input voltage, load resistance and resonant component variation, the controller rejects the disturbance and reduces the tracking error. A switching surface consisting of an ordinary linear term plus an integral term is proposed. In this thesis, to avoid overestimation of upper bounds of the disturbance in sliding mode control, an adaptation scheme that can adapt the unknown upper bound of disturbance is proposed, so that the objective of globally asymptotical stability can be achieved.

CHAPTER THREE

3. LLC CONVERTER DESIGN and MATHEMATICAL MODELING

3.1 Design of LLC Resonant Converter for High Voltage Application

The parameters and specifications of the converter for the high voltage and low current output application are taken from [31]. The specifications have been established for the simulation of a proposed LLC converter is given Table 1 in appendix B.

The converter shown in the Figure 2.12 is composed of inverter, resonant tank, and transformer and rectifier circuit. Each circuit is designed as follows.

3.1.1 Inverter Design

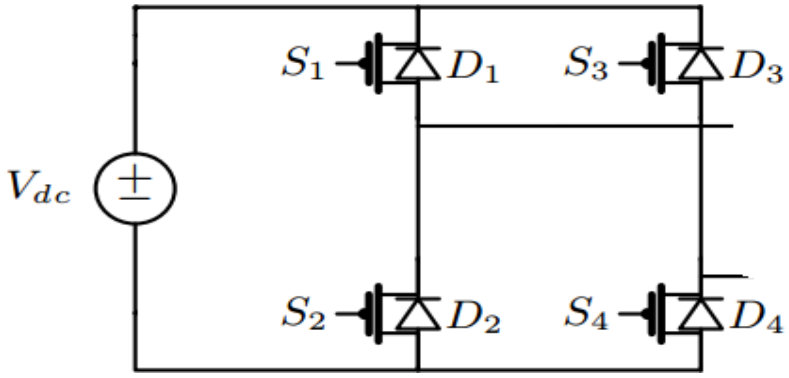

Figure 3.1 Switch network (Inverter)

Inverter is used convert DC to AC signal. Single phase inverter can be designed by using half or full bridge (H- bridge) circuit depending on desired output signal. The bridges are constructed by using power switches such as IGBT, MOSFET and BJT. Pulse modulation or frequency modulation technique is used to derive the gates of power switches depending on switching frequency of the converter. In these techniques, the gate signal is controlled by varying the duty cycle. Pulse width modulation is common for low frequency application. However, in resonant converters for which the frequency is very high, voltage controlled oscillator is used to derive gate signal of switches. MOSFETs are preferred to other power switches since they have high input impedance and operate at high switching frequency. H-Bridge inverter generates quasi square

wave with frequency is equal to switching frequency of MOSFET [32]. This quasi square wave is expressed as follows using Fourier series is derived as

$$V_{square} = \sum_{1}^{n} \frac{4V_{DC}}{n\pi} \sin\left(n2\pi f_s t\right) \tag{3.1}$$

The rms voltage of quasi square wave of equation (3.1) is given by

$$V_{rms} = \frac{V_{s1}}{\sqrt{2}} \tag{3.2}$$

where V_{s1} is of fundamental component of (3.1) given as

$$V_{s1} = \frac{4V_{DC}}{\pi} \tag{3.3}$$

i) Dead time

Dead time is a minimum time inserted between the switching periods of MOSFETs to discharge completely the effective capacitance appeared in parallel with drain to sources of the power MOSFETs. This is to realize the ZVS operation at the worst case conditions applied to converter. The dead time selection should ensure ZVS of four primary side MOSFET at maximum switching frequency, where the magnetizing current to charge and discharge MOSFET's C_{eq} is the maximum [33]. The dead time is derived as follows

$$t_{dead} = \frac{2C_{eq}V_{in}}{I_m\ max} \tag{3.4}$$

where $I_m$max is the maximum magnetizing current to charge and discharge C_{eq}, defined as

$$I_m\ max = \frac{nV_0}{4L_m f_s} \tag{3.5}$$

,C_{eq} is equivalent capacitor of the MOSFET.

The excessive dead time results in reduced efficiency; thus, it is recommended to reduce dead time.

ii) Selection of MOSFET

Two key factors most important to consider for selecting the MOSFET for LLC topology are ZVS of MOSFET and body diode reverse recovery. A rule for selecting suitable MOSFETs based on ZVS point of view is to select a MOSFET with lower C_{eq} in the same internal resistance between drain and source of MOSFET (Rds) device which determines the charging/discharging time during the dead time in LLC topology. The lower the C_{eq} value, the shorter the discharging time of the MOSFET's.

The body diode reverse recovery issue in LLC topology comes from the charging speed of the resonant capacitance during startup. The higher resonant capacitance is selected in LLC topology to increase the voltage gain of the converter. It is difficult to make the body diode reverse recovery completely when resonant capacitance and initial startup switching frequency are high. The recommended solution to resolve the body diode hard commutation issue is to select the CoolMOSTM CFD series with the extremely low reverse recovery charge [33].

It is stated in [33] , if the voltage break down is 400V which is the same as DC input, the MOSFET is selected with the following specification

Table 3.1 MOSFET specification for LLC converter

Specification	Tdead	Ceq	R_{ds}	$I_r$max
APT6024BFLL	1.5ms	90 nF	0.24Ω	12A

3.1.2 Resonant Tank Parameter Design

Resonant tank circuit consists of resonant inductor and resonant capacitor which are designed as follows.

i) Resonant inductor (L_r)

By using the relationship between resonant inductor and magnetizing inductor, the resonant inductor is designed as

$$L_r = \frac{L_m}{k} = \frac{56\mu H}{1.24} = 45\mu H \tag{3.6}$$

where k is inductor ratio defined as $k = \frac{L_m}{L_r}$

ii) Resonant capacitor (C_r)

The resonant capacitor is calculated as

$$C_r = \frac{\left(\frac{1}{2\pi f_{r1}}\right)^2}{L_r} = \frac{\left(\frac{1}{2\pi(61250)}\right)^2}{45\mu H} = 150nF \quad (3.7)$$

3.1.3 Transformer Parameter Design

The conventional 50/60 Hz design of the transformer is robust and simple. But, this design has low quality input currents, low power factor, sluggish operating characteristics, low power supply efficiency and large size and weight. High frequency switched mode operation has advantage of more precise control over the operating parameters such as output voltage level, current level, voltage rise times and response to variations in load demand, significant reduction in the size and weight of the high voltage transformer. This reduction in size and weight leads to a compact design, which minimizes the installation and maintenance costs. Moreover reactance of the transformer core to be much lower and hence the efficiency of the power supply can be improved [34]. High voltage, high frequency transformer is designed with some specifications stated in [35]. The specification are selected depending on converter switching frequency and square voltage. The specification of the transformer is in given Table 2 in appendix C. The transformer parameters are designed as follows.

i) Magnetizing inductor (L_m)

The magnetizing inductor should meet the following condition so that the primary switches turn ON under ZVS.

$$L_m \leq \frac{nV_0 t_{dead}}{8C_{eq} V_{in} f_s} \quad (3.8)$$

Sustituting the values, $L_m \max = 56\mu H$

ii) Total estimated losses (p_Σ)

$$p_\Sigma = \frac{p_{out}}{\eta} - p_{out} = \frac{2000}{0.98} - 2000 = 40.8w \tag{3.9}$$

For maximum efficiency, copper loss (p_{cu}) is equal to eddy loss (p_{eddy}). Thus both can be calculated as

$$\begin{aligned} p_\Sigma &= p_{cu} + p_{eddy} = 2p_{cu} \\ p_{cu} &= p_{eddy} = \frac{p_\Sigma}{2} = \frac{40.8}{2} = 20.4w \end{aligned} \tag{3.10}$$

iii) Transformer ratio (n)

Transformer ratio is calculated by using number of primary and secondary turns.

$$n = \frac{N_p}{N_s} = \frac{5}{50} = 0.1 \tag{3.11}$$

where

$$N_p = \frac{V_{ab} x 10^4}{4 B_m f_s} = 4.19 \approx 5$$

$$Ns = \frac{N_p V_0}{V_{ab}} = \frac{5x4000}{510} = 39.2$$

To allow use of nominal duty cycle of 80% on the primary side the secondary number of turn is

$$N_s = \frac{N_s}{0.8} = \frac{39.2}{0.8} = 49.01 \approx 50$$

iv) Primary resistance (R_p)

It is calculated as

$$R_p = M_{ltp} N_p R_{\frac{p}{t}} \xi = 19.5x5x8.85x10^{-6} x1.24 = 1.06m\Omega \tag{3.12}$$

v) **Secondary resistance**

$$R_s = M_{lts} N_s R_{\frac{s}{t}} \xi = 2\pi x15.5x50x418.9x10^{-6} x1.24 = 2.5\Omega \tag{3.13}$$

Eddy current loss resistance (R_c)

$$p_{cu} = \frac{(nV_0)^2}{R_c}$$
$$R_c = \frac{(nV_0)^2}{p_{cu}} = \frac{(0.1x4000)^2}{20.4} = 7843\Omega \quad (3.14)$$

3.1.4 Rectifier Bridge Parameter Design

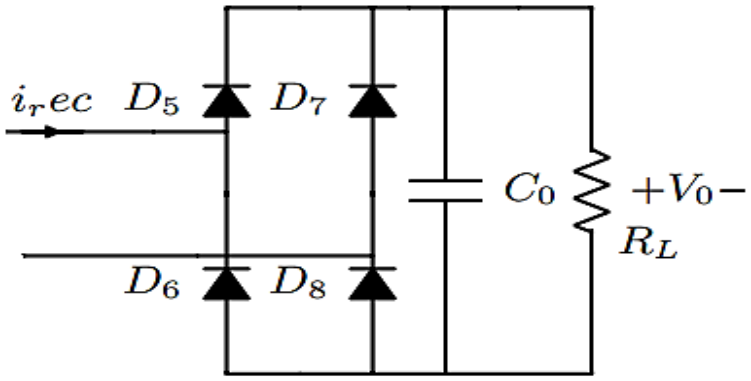

Figure 3.2 First harmonic approximation model of rectifier circuit

The full bridge rectifier, the last part of LLC converter, shown in Figure 3.2 is used to convert AC to DC wave form. The Bridge is used with output capacitor to filter the ripple output voltage at a load. The full bridge used with capacitor is modeled as AC equivalent resistance (R_{ac}). AC equivalent load resistance seen from primary side of transformer is derived as

$$R_{ac} = \frac{8}{\pi^2} n^2 \frac{V_0}{i_0} = \frac{8}{\pi^2} n^2 R_L = \frac{8}{\pi^2} x0.1^2 x \frac{4000}{0.5} = 64.845\,\Omega \quad (3.15)$$

Output filter capacitor design

To design output capacitor it is assumed that the ripple factor is 0.1%. Thus, output capacitor is calculated as:

$$rf\% = \frac{1}{2f_s R_L C_0};$$
$$C_0 = \frac{1}{2f_s R_L rf\%} = \frac{1}{2x50000x8000x0.001} = 1.25x10^{-6}\,F \quad (3.16)$$

3.1.5 DC Characteristics of LLC Converter for Different Values of k and Q

The DC characteristics equation of LLC converter is derived by applying first harmonic approximation to full bridge converter shown in Figure 2.12.

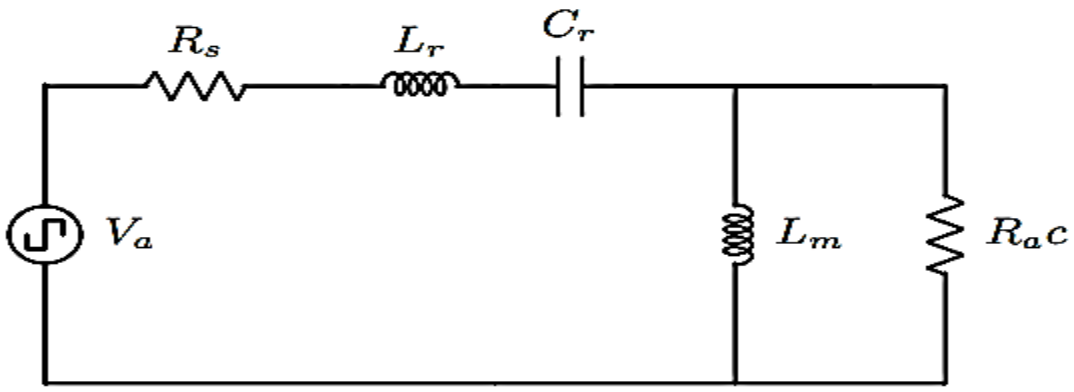

Figure 3.3 AC equivalent circuit of full bridge LLC converter

Based on Figure 3.3, the LLC equivalent impedance and voltage gain can be calculated by:

$$Z_{in}(j\omega) = \frac{1}{j\omega C_r} + j\omega L_r + (j\omega L_m \,||\, R_{ac}) = \frac{R_{ac}(\omega L_m)^2}{R_{ac} + (\omega L_m)^2} + j(R_{ac}\omega L_m)^2 + \omega L_r - \frac{1}{\omega C_r} \tag{3.17}$$

$$G_{dc}(j\omega) = \frac{(j\omega L_m \,||\, R_{ac})}{\frac{R_{ac}(\omega L_m)^2}{R_{ac} + (\omega L_m)^2} + j\frac{R_{ac}{}^2\omega L_m}{R_{ac} + (\omega L_m)^2} + \omega L_r - \frac{1}{\omega C_r}} \tag{3.18}$$

$$G_{dc}(j\omega) = \frac{\frac{R_{ac}(\omega L_m)^2}{R_{ac} + (\omega L_m)^2} + j\left(\frac{(Rac)^2\omega L_m}{R_{ac} + (\omega L_m)^2}\right)}{\frac{R_{ac}(\omega L_m)^2}{R_{ac} + (\omega L_m)^2} + j\left(\frac{Rac^2\omega L_m}{R_{ac} + (\omega L_m)^2}\right) + \omega L_r - \frac{1}{\omega L_r}} \tag{3.19}$$

$$|G_{dc}| = \frac{\sqrt{\left(\frac{R_{ac}(\omega L_m)^2}{R_{ac} + (\omega L_m)^2}\right)^2 + \left(\frac{R_{ac}{}^2\omega L_m}{R_{ac} + (\omega L_m)^2}\right)^2}}{\sqrt{\left(\frac{R_{ac}(\omega L_m)^2}{R_{ac} + (\omega L_m)^2}\right)^2 + \left(\frac{R_{ac}{}^2\omega L_m}{R_{ac} + (\omega L_m)^2} + \omega L_r - \frac{1}{\omega L_r}\right)^2}} \tag{3.20}$$

Rearranging the variables

$$|G_{dc}|=\frac{1}{\sqrt{\left(1+\frac{1}{k}(1-\frac{1}{f_n^{\,2}})^2\right)^2+Q^2\left(f_n-\frac{1}{f_n}\right)^2}} \tag{3.21}$$

where $k=\frac{L_m}{L_r}$, $f_n=\frac{f_s}{f_{r1}}$ and $Q=\frac{\sqrt{\frac{L_r}{C_r}}}{R_{ac}}$; Q-Quality factor of the converter and f_n-ratio of switching frequency to resonant frequency.

The minimum Quality factor at heavy load and maximum Quality factor at light load is calculated as

$$\begin{aligned} Q_{min}&=\frac{\sqrt{\frac{L_r}{C_r}}}{R_{ac}\,max}=0.27\\ Q_{max}&=\frac{\sqrt{\frac{L_r}{C_r}}}{R_{ac}\,min}=3.36 \end{aligned} \tag{3.22}$$

The inductor ratio should be small (k=1.24) for high voltage applications. But, this will reduce the efficiency of the converter. The optimal quality factor and inductor ratio value selected depending on the equation stated as

$$\sqrt{Qk}<1 \tag{3.23}$$

The minimum Quality factor Q_{min}=027 and the small value of inductor ratio k=1.24 are selected as a nominal DC characteristics design parameters by assuming LLC resonant the converter operates at heavy load for high voltage output.

For k=1.24 and different values of quality factor

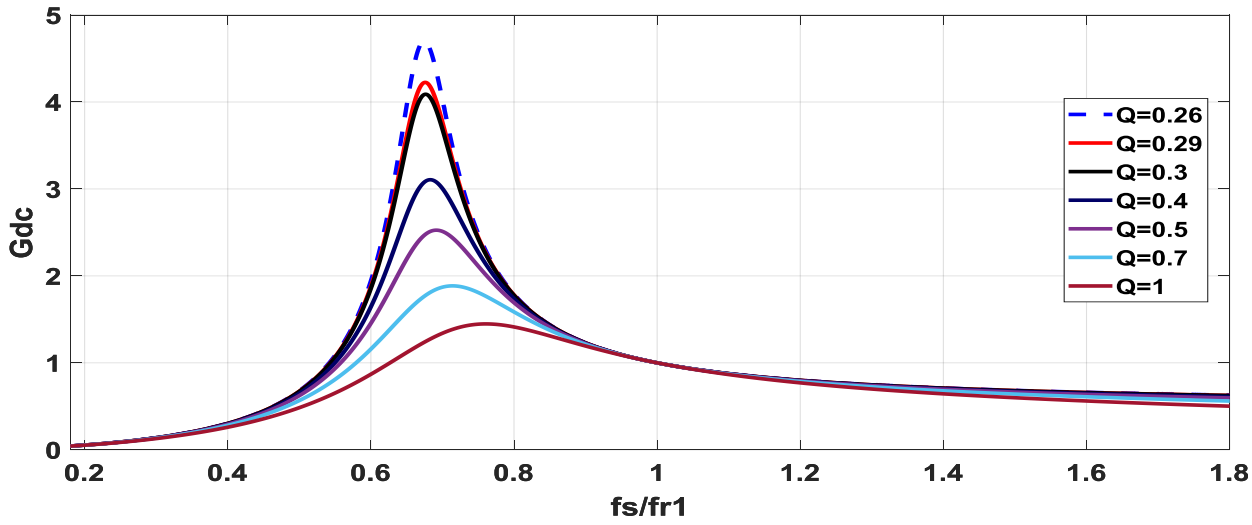

Figure 3.4 DC characteristics for different values of Q

For Q=0.27 and different values of ratio of inductor

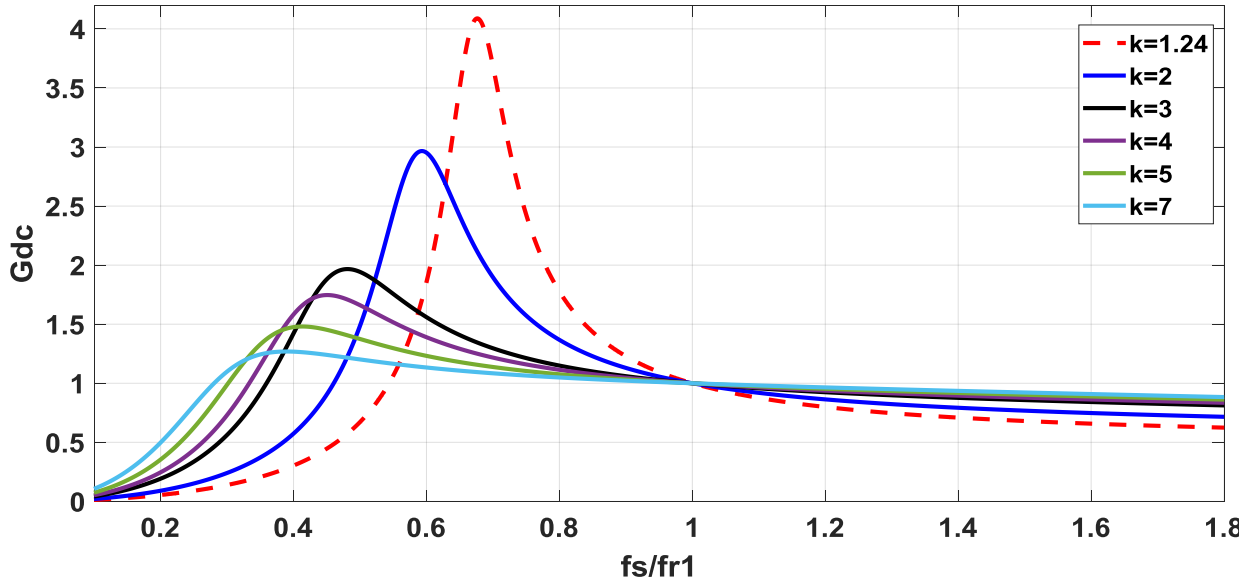

Figure 3.5 DC characteristics for different values of k

Taking the nominal value of Q and k as 0.27 and 1.24 respectively; the graph is:

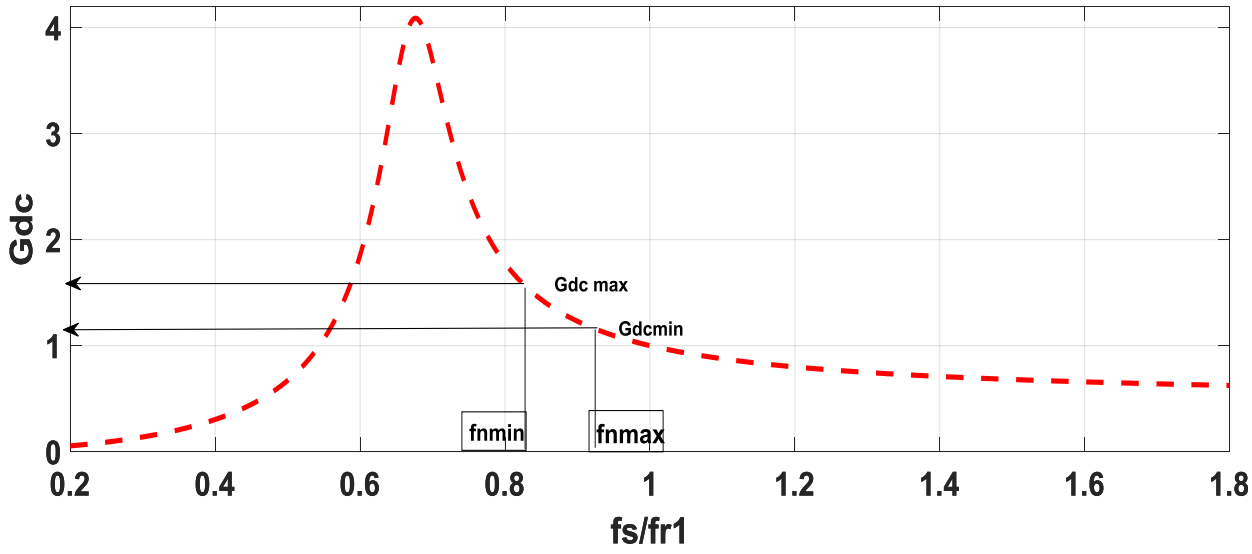

Figure 3.6 DC characteristics for optimal value of Q and k

The maximum and minimum DC gain is calculated as follows

$$G_{DC}\,\max = \frac{nV_o\,\max}{V_{in}\,\min} = \frac{0.1x4700}{300} = 1.566$$
$$G_{DC}\,\min = \frac{nV_o\,\max}{V_{in}\,\max} = \frac{0.1x4700}{400} = 1.175 \qquad (3.24)$$

The minimum and maximum frequency range is determined from the graph shown in Figure 3.6 using maximum and minimum DC gain. The minimum frequency ratio at maximum gain is 0.828 and the maximum frequency ratio at minimum gain is 0.918. Therefore, the minimum and maximum switching frequency are 50,715Hz and 56,227.5 Hz respectively.

3.2 Mathematical Modeling of LLC Resonant Converter

3.2.1 Small Signal Modeling of LLC Resonant Converter

For PWM modulated converter, state space average method has been widely used. State space average method provides simple and accurate solution for up to half switching frequency. With the small signal model derived from state space average method, small signal characteristic of PWM modulated converter can be analyzed and control system can be designed accordingly. The natural frequency of the linear network (output filter) is much lower than the switching frequency

which makes the modulation of the converter through the low frequency content in the control signal. With this character, the average method can provide approximate linear solution of the nonlinear state equations. The derived model has a continuous form and is accurate up to half of switching frequency [5].

However, for resonant converter, the switching frequency is close to the natural frequency of the linear network (resonant tank). The states contain mainly switching frequency harmonics instead of low frequency content in PWM converter. The modulation of the resonant converter is achieved by the interaction between switching frequency and resonant frequency. Since average method will eliminate the information of switching frequency, it cannot predict the dynamic performance of resonant converter [5].

Resonant DC-DC converters are nonlinear systems which is caused by MOSFET's nonlinear characteristics. Time variant nonlinear state equations are obtained by writing the circuit equations using Kirchhoff's Laws for each state variable. LLC resonant tank parameters i.e. resonant current, magnetizing current, and voltage across resonant capacitor are approximated to their first harmonic signal while current and voltage of the output filter are approximated to their DC components. The small signal model of the LLC converter is derived by applying extended describing function method and Jacobean linearization at steady state operating point.

i) Derivation of Nonlinear State Equations

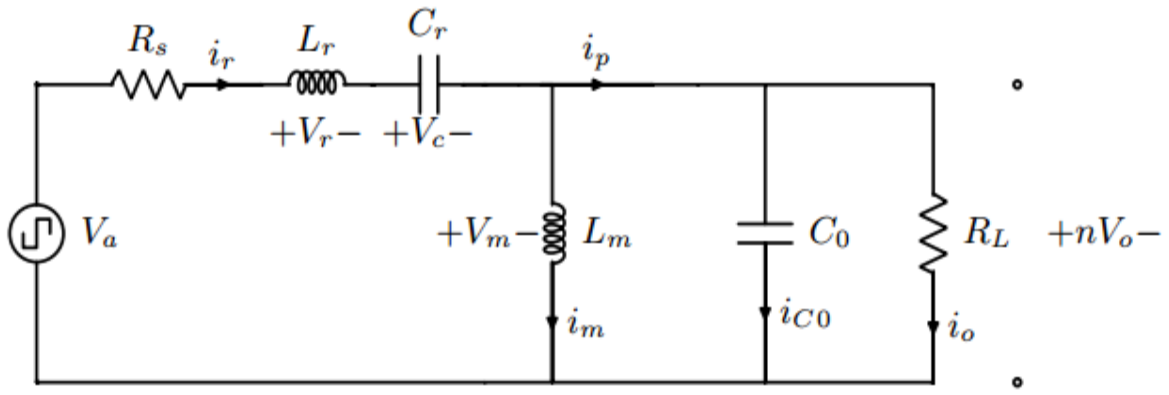

Figure 3.7 FHA model of full bridge LLC converter

A quasi-square wave voltage generated from the active full bridge network, is applied to the resonant tank of the LLC resonant converter. The state equations are obtained as shown in (3.25-3.28)

Resonant inductor voltage

$$L_r \frac{d(i_r)}{dt} = V_{ab} + i_r R_s - v_{Cr} - \text{sign}\left(i_r - i_m\right) n V_0 \tag{3.25}$$

where $\text{sign}\left(i_r - i_m\right) = \begin{cases} -1, V_0 < 0 \\ +1, V_0 > 0 \end{cases}$

Resonant inductor current

$$i_r = \frac{d(V_{Cr})}{dt} \tag{3.26}$$

Magnetizing inductor voltage

$$L_m \frac{d(i_m)}{dt} = \text{sign}\left(i_r - i_m\right) n V_0 \tag{3.27}$$

Output voltage of the load

$$C_0 \frac{d}{dx} V_0 + \frac{1}{R_L} V_0 = \left|i_r - i_m\right| \tag{3.28}$$

ii) Harmonic balance approximation

This method is used to approximate the given AC signal to its fundamental component by ignoring higher order harmonic signal. The general Fourier expansion of any function is expressed as:

$$f\left(x\right) = a_0 + \sum_1^n \left(a_n \cos\frac{n\pi x}{L} + b_n \sin\frac{n\pi x}{L} \right) \tag{3.29}$$

Expressing f(x) by considering only the fundamental components and ignoring the DC component, and other harmonic terms

$$f(x) = a_1 \cos(x) + b_1 \sin(x) \tag{3.30}$$

Resonant current, magnetizing current and voltage across resonant capacitor are approximated using FHA as follows.

$$\begin{aligned}
&i_r(t) = i_{rs}\sin(\omega t) + i_{rm}\cos(\omega t)\\
&i_m(t) = i_{ms}\sin(\omega t) + i_{mc}\cos(\omega t)\\
&v_{Cr}(t) = v_{Crs}\sin(\omega t) + v_{Crc}\cos(\omega t)\\
&v_{in}(t) = f_{1dc}\sin(\omega t)\\
&\text{sign}(i_r - i_m) = f_2(i_s, i_m)\sin(\omega t) + f_3(i_c, i_p)\cos(\omega t)\\
&|i_r - i_m| = f_4(i_p)
\end{aligned} \tag{3.31}$$

Differentiating (3.31) gives

$$\begin{aligned}
&\frac{d}{dt}i_r(t) = \sin(\omega t)\frac{d}{dt}i_{rs} + \omega i_{rs}\cos(\omega t) + \cos(\omega t)\frac{d}{dt}i_{rc} - \omega i_{rc}\sin(\omega t)\\
&\frac{d}{dt}i_m(t) = \sin(\omega t)\frac{d}{dt}i_{ms} + \omega i_{ms}\cos(\omega t) + \cos(\omega t)\frac{d}{dt}i_{mc} - \omega i_{mc}\sin(\omega t)\\
&\frac{d}{dt}V_{cr}(t) = \sin(\omega t)\frac{d}{dt}V_{crs} + \omega V_{crs}\cos(\omega t) + \cos(\omega t)\frac{d}{dt}V_{crc} - \omega V_{crc}\sin(\omega t)\\
&v_{in}(t) = f_{1dc}\sin(\omega t)\\
&\text{sign}(i_r - i_m) = f_2(i_s, i_p)\sin(\omega t) + f_3(i_c, i_p)\cos(\omega t)\\
&|i_r - i_m| = f_4(i_p)
\end{aligned} \tag{3.32}$$

where f_{1dc}, $f_2(i_s, i_m)$, $f_3(i_c, i_p)$ and $f_4(i_p)$ are coefficients of nonlinear states ,and **s** indicates sine component while **c** indicates cosine component of current and voltage.

iii) Extended describing function (EDF)

The describing function method is used to represent a nonlinear function in a linear manner by considering only the fundamental component of the response of the nonlinear system. Higher order harmonics are ignored as they are considered to be negligible. This principle of describing functions is extended to model resonant converters, in which the discontinuous terms in the nonlinear state equations are approximated to their fundamental or DC components [36]. For a nonlinear component described by a function given below, its output is periodical function to a sinusoidal input. Assuming that the function f(x) is piecewise continuous,

$$w(t) = f\left(A\sin(\omega t)\right) \tag{3.33}$$

$w(t)$ is a piecewise continuous periodic function with the same period as the input signal. A piecewise periodical function can be expanded in Fourier series as follows.

$$w(t) = \frac{a_0}{2} + \sum_{1}^{n} a_n\cos(\omega t) + b_n\sin(\omega t) \tag{3.34}$$

where $a_n = \frac{1}{\pi}\int_{-\pi}^{\pi}\cos(\omega t)d(\omega t)$ and $b_n = \frac{1}{\pi}\int_{-\pi}^{\pi}\sin(\omega t)d(\omega t)$

Taking the approximation to the first order, it becomes,

$$w_1(t) = a_1\cos(\omega t) + b_1\sin(\omega t) \tag{3.35}$$

Hence, the frequency response of this nonlinear component can be analyzed as follows.

$$w_1(t) = M\sin(\omega t - \phi) \tag{3.36}$$

where $M(A,\omega) = \sqrt{a_1^{\,2} + b_1^{\,2}}$ and $\phi = \arctan\frac{b_1}{a_1}$

The equation (3.36) can be expressed in the form of complex expression as:

$$w_1(t) = Me^{i(\omega t+\phi)} = (a_1 + b_1 j)e^{i\omega t} \tag{3.37}$$

The describing function is defined, similar to frequency response, as the complex ratio of the fundamental component of the nonlinear element against the input.

$$N(A,\omega) = \frac{Me^{i(\omega t+\phi)}}{Ae^{i\omega t}} = \frac{a_1 + b_1 j}{A} \tag{3.38}$$

In nonlinear state, $V_{in}(t) = f_{1dc}(\sin(\omega t))$, the coefficient term f_{1dc} is calculated by approximation of switch network to its DC component.

The switch network is the full bridge inverter. Applying the fourier transform to the inverter, the output voltage is described as

$$V_{ab} = \sum_{0}^{n} 2V_{dc}\sin(n\omega t) \tag{3.39}$$

However by only considering fundamental components of harmoniic equation the average output voltage is given by

$$V_{avg}(f_{1dc}) = \frac{2}{Ts}\int_{0}^{\frac{Ts}{2}} V_{ab}dt = \frac{2}{Ts}\int_{0}^{\frac{Ts}{2}} V_{dc}\sin(\omega t)dt = \frac{4}{\pi}V_{dc} \tag{3.40}$$

The nonlinear state $\text{sign}(i_r - i_m) = f_2(i_s, i_m)\sin(\omega t) + f_3(i_c, i_p)\cos(\omega t)$ and $|i_p| = f_4(i_p)$ are linearized by using the extended describing function method. This is done by approximation of resonant tank and rectifier circuit together. The coefficients are also calculated depending on approximation.

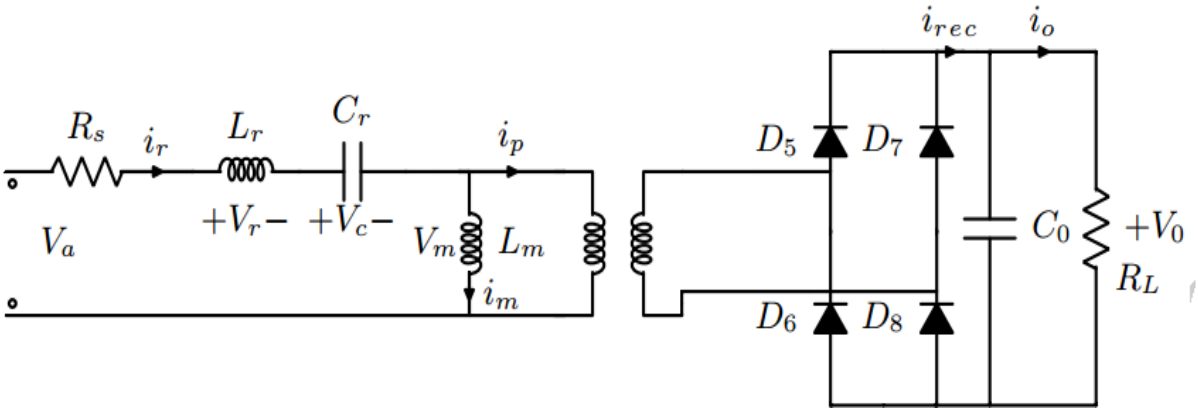

Figure 3.8 Resonant tank and rectifier circuit diagram

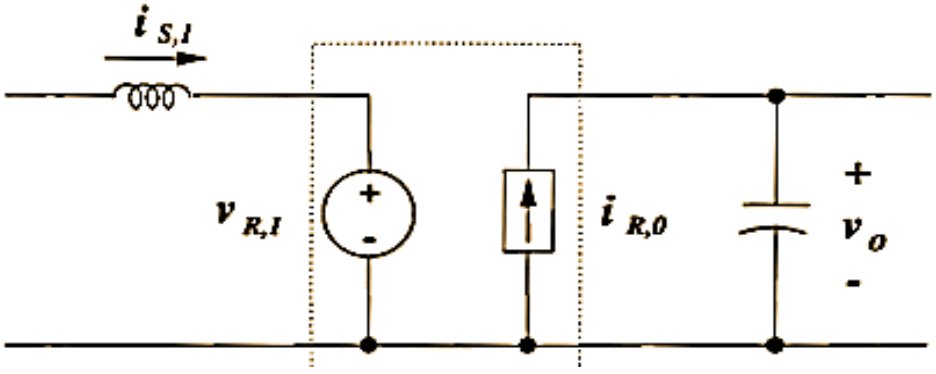

Figure 3.9 Fundamental approximation of resonant tank and rectifier circuit [36]

Since resonant tank is loaded by square wave voltage(V_{RI}) whose amplitude is V_0. This square wave is in phase with resonant current (i_{si}). The fundamental component of V_{RI} is found by applying EDF as:

$$\begin{aligned} V_{abs1} &= \frac{1}{Ts}\int_0^{Ts} V_0 \text{sign}\left(i_r - i_m\right) e^{-j\omega_s t} \\ &= \frac{1}{Ts}\int_0^{Ts} V_0 \frac{\left(i_r - i_m\right)}{|i_r - i_m|} e^{-j\omega_s t} \\ &= 4V_0 \frac{\left(i_{rs} - i_{ms}\right)}{\sqrt{\left(i_{rs} - i_{ms}\right)^2 + \left(i_{rc} - i_{mc}\right)^2}} \sin(\omega_s t) + 4V_0 \frac{\left(i_{rc} - i_{mc}\right)}{\sqrt{\left(i_{rs} - i_{ms}\right)^2 + \left(i_{rc} - i_{mc}\right)^2}} \cos(\omega_s t) \end{aligned} \tag{3.41}$$

Therefore the coefficients are calculated as

$$\begin{aligned} f_2(i_s, i_p) &= \frac{4\left(i_{rs} - i_{ms}\right)}{\sqrt{\left(i_{rs} - i_{ms}\right)^2 + \left(i_{rc} - i_{mc}\right)^2}} \\ f_3(i_c, i_p) &= \frac{4\left(i_{rc} - i_{mc}\right)}{\sqrt{\left(i_{rs} - i_{ms}\right)^2 + \left(i_{rc} - i_{mc}\right)^2}} \end{aligned} \tag{3.42}$$

where $i_s = \left(i_{rs} - i_{ms}\right)$, $i_c = \left(i_{rc} - i_{mc}\right)$ and $i_p = \sqrt{\left(i_{rs} - i_{ms}\right)^2 + \left(i_{rc} - i_{mc}\right)^2}$

The average component of rectified tank current (I_{Ro}) is derived as follows

$$i_{rec} = \frac{1}{\pi}\int_0^{\pi} |i_r - i_m| \sin(\omega t) = \frac{1}{\pi} i_p [-\cos(\omega t)]_0^{\pi} = \frac{2}{\pi} i_p \tag{3.43}$$

where $i_p = \sqrt{(i_{rs} - i_{ms})^2 + (i_{rc} - i_{mc})^2}$

Therefore $f_4(i_p) = \frac{2}{\pi} i_p$

Substituting the coefficients derived using harmonic balance and extended describing function into (3.25-3.28), the overall model of the converter is given as follows.

$$L_r \frac{di_{rs}}{dt} = \frac{4V_{dc}}{\pi} + \omega_s L_r i_{rc} + i_{rs} R_s - V_{Crs} - 4nV_0 \frac{i_{rs} - i_{ms}}{\pi i_p} \tag{3.44}$$

$$L_r \frac{di_{rc}}{dt} = -\omega_s L_r i_{rs} + i_{rc} R_s - V_{crc} - 4nV_0 \frac{i_{rc} - i_{mc}}{\pi i_p} \tag{3.45}$$

$$C_r \frac{dV_{Crs}}{dt} = i_{rs} + \omega_s C_r V_{Crc} \tag{3.46}$$

$$C_r \frac{dV_{Crc}}{dt} = i_{rc} - \omega_s C_r V_{Crs} \tag{3.47}$$

$$L_m \frac{di_{ms}}{dt} = \omega_s L_m i_{mc} + 4nV_0 \frac{i_{rs} - i_{ms}}{\pi i_p} \tag{3.48}$$

$$L_m \frac{di_{mc}}{dt} = -\omega_s L_m i_{ms} + 4nV_0 \frac{i_{rc} - i_{mc}}{\pi i_p} \tag{3.49}$$

$$C_0 \frac{d}{dt} V_0 = \frac{2}{\pi} i_p - \frac{1}{R_L} V_0 \tag{3.50}$$

iv) Equilibrium Point derivation

Consider a nonlinear differential equation

$$\frac{d(x(t))}{dt} = f\left(x(t), u(t)\right) \tag{3.51}$$

where f is a function mapping $R^n x R^m \rightarrow R^n$

A point $\bar{x} \in R^n$ is called an equilibrium state if there is a specific $\bar{u} \in R^m$ (called the equilibrium input) such that

$$f\left(\bar{x}, \bar{u}\right) = 0 \tag{3.52}$$

The steady state operating point of LLC resonant converter is found by equating differential equation in (3.44-3.50) to zero.

$$\frac{4V_{DC}}{\pi} + \omega_s L_r i_{rc} + i_{rs} R_s - V_{Crs} - 4nV_0 \frac{i_{rs} - i_{ms}}{\pi i_p} = 0 \tag{3.53}$$

$$-\omega_s L_m i_{rs} + i_{rc} R_s - V_{Crc} - 4nV_0 \frac{i_{rc} - i_{mc}}{\pi i_p} = 0 \tag{3.54}$$

$$i_{rc} - \omega_s C_r V_{Crs} = 0 \tag{3.55}$$

$$\omega_s L_m i_{mc} + 4nV_0 \frac{i_{rs} - i_{ms}}{\pi i_p} = 0 \tag{3.56}$$

$$-\omega_s L_m i_{ms} + 4nV_0 \frac{i_{rc} - i_{mc}}{\pi i_p} = 0 \tag{3.57}$$

$$\frac{2}{\pi} i_p - \frac{1}{R_L} V_0 = 0 \tag{3.58}$$

Rearranging the above equations in matrix form, equilibrium point states are found as:

$$\bar{x} = (A_0)^{-1} \bar{u} \tag{3.59}$$

where $\bar{x} = \begin{vmatrix} \bar{i}_{rs} \\ \bar{i}_{rc} \\ \bar{V}_{Crs} \\ \bar{V}_{Crc} \\ \bar{i}_{ms} \\ \bar{i}_{mc} \end{vmatrix}$; $A_0 = \begin{vmatrix} R_s + R_{ac} & L_r\omega_s & 1 & 0 & -R_{ac} & 0 \\ -L_r\omega_s & R_s + R_{ac} & 0 & 1 & 0 & -R_{ac} \\ 1 & 0 & 0 & -C_r\omega_s & 0 & 0 \\ 0 & 1 & C_r\omega_s & 0 & 0 & 0 \\ R_{ac} & 0 & 0 & 0 & -R_{ac} & -L_m\omega_s \\ 0 & R_{ac} & 0 & 0 & L_m\omega_s & -R_{ac} \end{vmatrix}$; $\bar{u} = \begin{vmatrix} \frac{4V_{DC}}{\pi} \\ 0 \\ 0 \\ 0 \\ 0 \\ 0 \end{vmatrix}$

v) Jacobean Linearization

Equations (3.44-3.50) have also nonlinear terms in which two states are multiplied together. So, these equations are linearized using Jacobean matrix linearization method at equilibrium point, with disturbance signal applied to the converter. The nonlinear equations (3.44-3.50) can be expressed in general form of state space representation as follows

$$\dot{x} = f\left(x(t), V_{DC}(t), R(t), \omega(t)\right) \tag{3.60}$$

where $x(t) = [i_{rs}, i_{rc}, V_{crs}, V_{crc}, i_{ms}, i_{mc}, V_0]^T$ are state variables, $V_{DC}(t)$ and $R_L(t)$ are time varying input voltage and load resistance respectively, which are considered as disturbances, while $\omega_s(t)$ is control variable and V_0 is controlled variable.

Suppose ($\bar{x}$ $\bar{u}$) is steady state operating state and input. If the system starts at $x(t_0) = \bar{x}$ and apply the constant input $u(t) = \bar{u}$, then the state of the system will remain fixed at $x(t) = \bar{x}$ for all t. Deviation variables are defined to measure the difference between x(t) and $\bar{x}$, if a slightly different input from $\bar{u}$ is applied.

$$\begin{aligned} \delta_{x(t)} &= x(t) - \bar{x} \\ \delta_{u(t)} &= u(t) - \bar{u} \end{aligned} \tag{3.61}$$

The variables x(t) and u(t) are related by the differential equation as

$$\frac{dx(t)}{dt} = f\left(x(t), u(t)\right) \tag{3.62}$$

Substituting (3.61) in (3.62),

$$\frac{d(\delta_{x(t)})}{dt} = f(\bar{x} + \delta_{x(t)}, \bar{u} + \delta_{u(t)}) \tag{3.63}$$

Applying Taylor expansion to the right hand side of (3.63) and neglecting higher order terms

$$\dot{\delta}_{x(t)} = f(\bar{x}, \bar{u}) + \frac{\partial f}{\partial x}|_{(x=\bar{x}, u=\bar{u}}) x(t) + \frac{\partial f}{\partial u}|_{(x=\bar{x}, u=\bar{u}}) \delta_{u(t)} \tag{3.64}$$

At steady state operating point, $f(\bar{x}, \bar{u})=0$; Thus, (3.64) becomes

$$\dot{\delta}_{x(t)} = \frac{\partial f}{\partial x}(|_{x=\bar{x}, u=\bar{u}}) x(t) + \frac{\partial f}{\partial u}|_{(x=\bar{x}, u=\bar{u}}) \delta_{u(t)} \tag{3.65}$$

This differential equation approximately governs the deviation variables $\delta_{x(t)}$ and $\delta_{u(t)}$ as long as they remain small. It is a linear time invariant differential equation, since the derivatives of $\dot{\delta}_x$ are linear combinations of the variable δ_x and the deviation input δ_u.

The linear system

$$\dot{\delta}_{x(t)} = A\delta_{x(t)} + B\delta_{u(t)} \tag{3.66}$$

is called the Jacobian Linearization of the nonlinear system, about the equilibrium point.

where the A and B matrices defined as

$$A = \frac{\partial f}{\partial x}|_{x=\bar{x},u=\bar{u}} \; ; \qquad B = \frac{\partial f}{\partial u}|_{x=\bar{x},u=\bar{u}}$$

The disturbance vector applied to the converter described in the equation (3.60), is given by

$$f(t) = \begin{vmatrix} V_{in} \\ \frac{1}{R_L} \end{vmatrix} = \begin{vmatrix} d_1 \\ d_2 \end{vmatrix} \tag{3.67}$$

where V_{in} and R_L is DC input voltage and load resistance respectively

Then the nonlinear state space representation in equation (3.60) can be rewritten as follows

$$\begin{gathered} \dot{x}(t) = f\left(x(t)\right) + g(x)u(t) + g_1 d_1 + g_2(x)d_2 \\ y(t) = Cx(t) \end{gathered} \tag{3.68}$$

Applying Jacobian linearization method to (3.68)

$$\begin{aligned} &\dot{\delta}_{x(t)} + \dot{\bar{x}} = f\left(\bar{x} + \delta_{x(t)}\right) + g\left(\bar{x} + \delta_{x(t)}\right)u + g_1 d_1 + g_2\left(\bar{x} + \delta_{x(t)}\right)d_2 \\ &\dot{\delta}_{x(t)} + \dot{\bar{x}} = f(\bar{x},\bar{u}) + \left(\frac{\partial f}{\partial x}|_{x=\bar{x}}\,\bar{x} + \frac{\partial g}{\partial x}|_{x=\bar{x}}\,\bar{u} + \frac{\partial g_2}{\partial x}|_{x=\bar{x}}\,\bar{d}_2\right)\delta_{x(t)} + \frac{\partial g}{\partial u}|_{u=\bar{u}}\,\delta_{u(t)} + g_1\delta_{d_1(t)} + g_2(\bar{x})\delta_{d_2(t)} \end{aligned} \tag{3.69}$$

The linear time invariant equation of LLC resonant converter becomes

$$\dot{\delta}_{x(t)} = \left(\frac{\partial f}{\partial x}|_{x=\bar{x}}\,\bar{x} + \frac{\partial g}{\partial x}|_{x=\bar{x}}\,\bar{u} + \frac{\partial g_2}{\partial x}|_{x=\bar{x}}\,\bar{d}_2\right)\delta_{x(t)} + \frac{\partial g}{\partial u}|_{u=\bar{u}}\,\delta_{u(t)} \tag{3.70}$$

where $\dot{\bar{x}} = f\left(\bar{x},\bar{u}\right) = f\left(\bar{x}\right) + g\left(\bar{x}\right)\bar{u} + g_1\bar{d}_1 + g_2\left(\bar{x}\right)\bar{d}_2 = 0$ at steady operating system and $g_1\delta_{d_1(t)} + g_2\left(\bar{x}\right)\delta_{d_2(t)}$ are disturbance variables.

Therefore the transfer function of the converter is derived as

$$G(s) = C(sI - A)^{-1}B + D \tag{3.71}$$

where the matrices A, B, C and D are given as

$$A=\left(\frac{\partial f}{\partial x}|_{x=\bar{x}}\ \bar{x}+\frac{\partial g}{\partial x}|_{x=\bar{x}}\ \bar{u}+\frac{\partial g_2}{\partial x}|_{x=\bar{x}}\ \bar{d}_2\right),\ B=\frac{\partial g}{\partial u}|_{u=\bar{u}},\ C=\begin{vmatrix}0 & 0 & 0 & 0 & 0 & 0 & 1\end{vmatrix}\ \text{and D=0}$$

The state space representation of seven order state converter is given as

$$\begin{vmatrix}\dot{i}_{rs}\\ \dot{i}_{rc}\\ \dot{V}_{crs}\\ \dot{V}_{crc}\\ \dot{i}_{ms}\\ \dot{i}_{mc}\\ \dot{V}_0\end{vmatrix}=\begin{vmatrix}-0.43 & -315736.6 & -22222.2 & 0 & 9626.72 & 1736.6 & -2876.6\\ 312263.41 & -9626.72 & 0 & -22222.2 & 1736.6 & 9626.72 & 518.9\\ 6666666.7 & 0 & 0 & -314000 & 0 & 0 & 0\\ 0 & 6666666.7 & 314000 & 0 & 0 & 0 & 0\\ 7735.8 & 1395.47 & 0 & 0 & -7735.8 & -315395.47 & 2311.56\\ 1395.47 & 7735.8 & 0 & 0 & 312604.5 & -7735.75 & -416.98\\ 64723.78 & -11675.66 & 0 & 0 & 64723.78 & 11675.66 & -1.25E-10\end{vmatrix}\begin{vmatrix}i_{rs}\\ i_{rc}\\ V_{crs}\\ V_{crc}\\ i_{ms}\\ i_{mc}\\ V_0\end{vmatrix}+\begin{vmatrix}-44.7\\ 21.4\\ -454.25\\ -948.25\\ -47\\ 8.65\\ 0\end{vmatrix}(\omega_s) \quad (3.72)$$

Using (3.71) the seven order transfer function is derived as follows

$$G_7(s)=\frac{-6.084e06s^5-3.903e11s^4-3.466e18s^3-1.954e23s^2-1.772e29s+1.222e33}{s^7+2.51e04s^6+5.922e11s^5+1.094e16s^4+5.115e22s^3+2.639e26s^2+2.458e32s-2.672e34} \quad (3.73)$$

3.2.3 Simplified Linearized Model Of The Converter

The linear transfer function derived in equation (3.73) is seventh order which is not suitable for controller design. Moreover, only single state, output voltage, is measurable. The rectifier current should also controlled. But, this needs an observer to design the controller to control the two parameters at the same time. Simple reduction method of seven order to second order system is discussed in [27] and [37]. In equation (3.28) i_p is the current connecting the resonant tank and rectifier circuit which contains all information about resonant variables which was expressed as

$$i_p^{\,2}=i_s^{\,2}+i_c^{\,2}=\left(i_{rs}-i_{ms}\right)^2+\left(i_{rc}-i_{mc}\right)^2 \quad (3.74)$$

Differentiating (3.74)

$$2i_p\frac{d}{dt}i_p=2\left(i_{rs}-i_{ms}\right)\left(\frac{d}{dt}i_{rs}-\frac{d}{dt}i_{ms}\right)+2\left(i_{rc}-i_{mc}\right)\left(\frac{d}{dt}i_{rc}-\frac{d}{dt}i_{mc}\right) \quad (3.75)$$

Subtracting (3.45) from (3.44) and (3.49) from (3.48) gives

$$\frac{d}{dt}i_{rs}-\frac{d}{dt}i_{ms}=\frac{4V_{DC}}{\pi L_r}+\omega_s\left(i_{rc}-i_{mc}\right)+i_{rs}\frac{R_s}{L_r}-\frac{V_{crs}}{L_r}-4nV_0\frac{i_{rs}-i_{ms}}{\pi i_p}\left(\frac{1}{L_r}+\frac{1}{L_m}\right) \quad (3.76)$$

$$\frac{d}{dt}i_{rc} - \frac{d}{dt}i_{mc} = -\omega_s\left(i_{rs} - i_{ms}\right) + i_{rc}\frac{R_s}{L_r} - \frac{V_{crc}}{L_r} - 4nV_0\frac{i_{rc} - i_{mc}}{\pi i_p}\left(\frac{1}{L_r} + \frac{1}{L_m}\right) \tag{3.77}$$

Substituting (3.76) and (3.77) into (3.75) gives

$$\frac{d}{dt}i_p = \left(\frac{(i_{rs} - i_{ms})\left(\frac{4V_{DC}}{\pi} + + i_{rs}R_s - V_{crs}\right) + \left(i_{rc} - i_{mc}\right)\left(i_{rc}R_s - V_{crc}\right)}{L_r i_p}\right) - \frac{4nV_0}{\pi}\left(\frac{1}{L_r} + \frac{1}{L_m}\right) \tag{3.78}$$

Equation (3.78) can be written as follows if the first part is assumed as voltage source (V_n).

$$\frac{d}{dt}i_p = \frac{4n}{\pi}\left(\frac{1}{L_r} + \frac{1}{L_m}\right)\left(V_n - V_0\right) \tag{3.79}$$

where $V_n = \dfrac{(i_{rs} - i_{ms})\left(\frac{4V_{DC}}{\pi} + + i_{rs}R_s - V_{Crs}\right) + \left(i_{rc} - i_{mc}\right)\left(i_{rc}R_s - V_{Crc}\right)}{L_r i_p}$

But, from Figure 2.12 the rectifier current is represented as

$$\begin{aligned} i_{rec} &= 2n\frac{i_p}{\pi} \\ i_p &= \frac{\pi}{2n}i_{rec} \end{aligned} \tag{3.80}$$

Substituting (3.80) into (3.79) and (3.28), the second order differential equation of the LLC resonant converter can be rewritten as follows:

$$\begin{aligned} \frac{d}{dt}i_{rec} &= -L_s V_0 + L_s V_n \\ C_0\frac{d}{dt}V_0 &= -\frac{V_0}{R_L} + i_{rec} \end{aligned} \tag{3.81}$$

where $L_s = 8\left(\frac{n}{\pi}\right)^2\left(\frac{1}{L_r} + \frac{1}{L_m}\right)$, i_{rec} is rectifier current and V_0 is output voltage.

In this simplified model, the full bridge converter, resonant tank and rectifier diodes of the LLC resonant converter are regarded as a switching frequency controlled voltage source connected with a LC filter formed by equivalent inductor (L_s) and output capacitor (C_0) as shown in Figure 3.10.

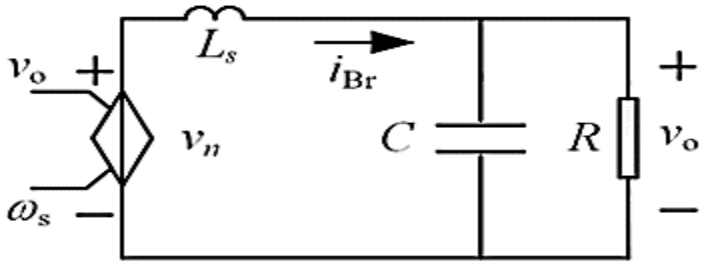

Figure 3.10 Simplified equivalent circuit of LLC converter [27]

Based on this assumption, the resonant variables have reached the steady state during each control period achieving a steady state controlled voltage source which can be written as follows from DC characteristics equation of LLC converter.

$$V_n = \frac{V_{in}}{n\sqrt{\left(1+\frac{1}{k}\left(1-\frac{1}{f_n^{\,2}}\right)\right)^2 + Q^2\left(f_n-\frac{1}{f_n}\right)^2}} \tag{3.82}$$

However, the transfer function between V_n and f_n is still nonlinear. Taylor series is applied to linearize the controlled voltage source which is derived in [37] as follows:

$$V_n = \frac{V_{in}}{n} + \frac{dV_n}{df_n}\Big|_{f_n=1} = \left(1-\frac{2f_n}{k}\right)\frac{V_{in}}{n} \tag{3.83}$$

Then (3.81) becomes

$$\begin{aligned} \frac{d}{dt}i_{rec} &= -L_s V_0 + \left(1-\frac{2f_n}{k}\right)L_s V_{in} \\ C_0\frac{d}{dt}V_0 &= -\frac{V_0}{R_L} + i_{rec} \end{aligned} \tag{3.84}$$

The state space equation of the above linear system is derived as follows

$$\begin{vmatrix} \frac{d}{dt}V_0 \\ \frac{d}{dt}i_{rec} \end{vmatrix} = \begin{vmatrix} -\frac{1}{C_0R_L} & \frac{1}{C_0} \\ -L_s & 0 \end{vmatrix} \begin{vmatrix} V_0 \\ i_{rec} \end{vmatrix} + \begin{vmatrix} 0 \\ -\frac{2L_sV_{in}}{knf_{r1}} \end{vmatrix} f_s + \frac{L_sV_{in}}{n} \tag{3.85}$$

where $\begin{vmatrix} V_0 \\ i_{rec} \end{vmatrix}$, f_s and $\frac{L_sV_{in}}{n}$ are measurable state variables, control signal(u) and disturbance signal respectively.

Substituting the values of the parameters, the state space representation is

$$\begin{vmatrix} \frac{d}{dt}V_0 \\ \frac{d}{dt}i_{rec} \end{vmatrix} = \begin{vmatrix} -125 & 10^6 \\ -324.8 & 0 \end{vmatrix} \begin{vmatrix} V_0 \\ i_{rec} \end{vmatrix} + \begin{vmatrix} 0 \\ -34.21 \end{vmatrix} f_s + f(t); \tag{3.86}$$

$$y = \begin{vmatrix} 1 & 0 \end{vmatrix} \begin{vmatrix} V_0 \\ i_{rec} \end{vmatrix}$$

The second order transfer function is

$$G_2(s)\frac{-3.42x10^7}{s^2+125s+3.248x10^8} \tag{3.87}$$

CHAPTER FOUR

4. CONTROLLER DESIGN

4.1 Super Twisting Second Order Sliding Mode Controller Design

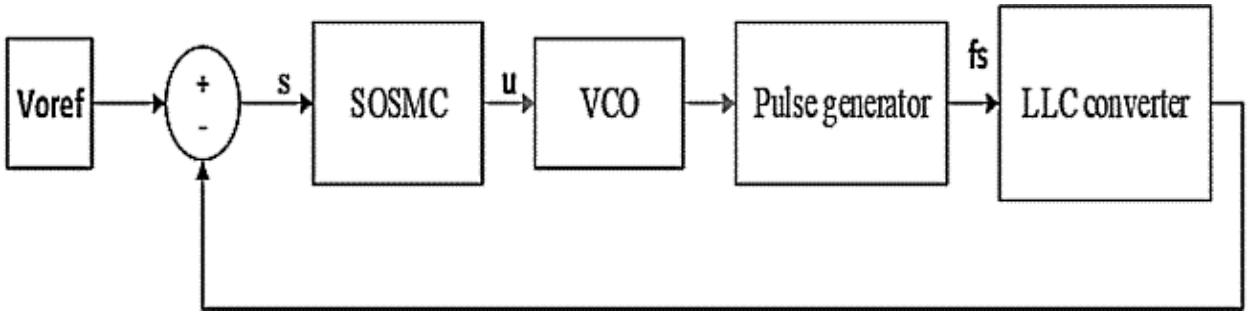

Figure 4.1 Supper twisting controller structure for LLC converter

The block diagram shown in Figure 4.1 describes the second order sliding mode controller used to control output voltage of LLC converter. VCO is used to convert control signal to switching frequency to drive the MOSFET. But, VCO generates triangular wave so that pulse generator is used to convert triangular wave to pulse signal.

The super twisting algorithm (STA) is a continuous sliding mode algorithm among the SOSM algorithms. Therefore, it does not suffer from the chattering problem compared with classical sliding mode method. According to [21] the sliding variable is defined as

$$s(t) = V_0 - V_{ref} \tag{4.1}$$

where V_0 is output voltage and V_{ref} is reference voltage of the converter.

Then the STA is given as follows

$$u(t) = k_\lambda |s|^{\frac{1}{2}} \operatorname{sign}(s) + k_\alpha \int_0^t \operatorname{sign}(s)dt + k_d \frac{ds}{dt} \tag{4.2}$$

where k_λ, k_α and k_d are controller parameters to be designed.

To design the controller parameters, upper bound signal of the controller should be obtained. The upper bound (U) is found by simulation of the converter by increasing the gain of the controller

until the good performance is obtained. The controller parameters are designed using the method discussed in [38]. When the sliding mode control is designed, the stability condition should be considered. In the sliding motion ($s = 0, \dot{s} = 0$), the ideal closed loop dynamics can be expressed as:

$$k_d \frac{\partial^2 e}{\partial t^2} + k_\lambda \frac{\partial e}{\partial t} + k_\alpha e = 0 \tag{4.3}$$

Based on the Routh criterion, the output voltage asymptotically tends toward its reference signal if the following conditions are satisfied.

$$k_d > 0, k_\alpha > 0, k_\lambda > 0 \tag{4.4}$$

Equation (4.3) can be rearranged into the standard second order system form, which relates the sliding coefficients to the dynamic response of the converter during sliding mode operation. The relations can be expressed as functions of the natural frequency and the damping ratio.

$$\begin{aligned} \frac{k_\alpha}{k_d} &= 2\xi\omega_0 \\ \frac{k_\lambda}{k_d} &= {\omega_0}^2 \end{aligned} \tag{4.5}$$

where $\omega_0 = 2\pi f_0$ such that f_0 is one tenth of resonant frequency. k_d Should be selected small.

Selecting $\omega_0 = 34484.5$ and $\xi = 0.707$ the controller parameters are calculated as follows

Table 4.1 control parameters of STA

k_λ	k_α	k_d
$54x10^6$	$1.4x10^{12}$	$1x10^3$

4.2 MRASMC Design

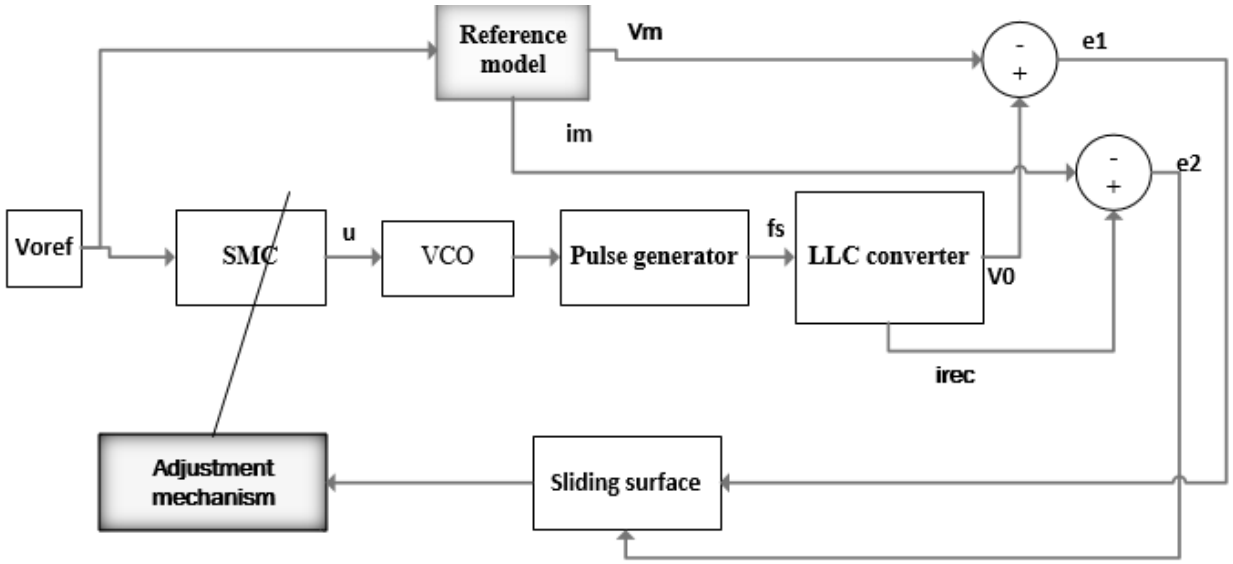

Figure 4.2 Adaptive sliding mode controller structure for LLC converter

Consider the system with parametric uncertainties and disturbance signal defined as

$$\dot{x} = (A + \Delta A)x + Bu + f(t) \tag{4.6}$$

where x(t) the state vector available for measurement, ΔA is the unknown parameter uncertainties of the matrix A and $f(t)$ represents the whole disturbance signal.

The reference model is given by

$$\dot{x}_m = A_m x_m + B_m u_c \tag{4.7}$$

The following assumptions are made to design the controller [19]:

- All eigenvalues of A_m are in the open left half complex plane, and u_c is bounded
- There exists a constant vector $k_1^T \in R^n$ and a non zero constant scalar $k_2 \in R$ such that the following conditions are satisfied $A + Bk_1^T = A_m, Bk_2 = B_m$. These conditions are called the matching conditions.
- ΔA and $f(t)$ have matched and unmatched terms. There exists unknown matrices of appropriate dimension D and G such that $BD(t) + \Delta\tilde{A}(t)$ and $BG(t) + \tilde{f}(t)$. $BD(t)$ and $BG(t)$ are matched uncertainty and disturbance; while $\Delta\tilde{A}(t)$ and $\tilde{f}(t)$ are unmatched

uncertainty and disturbance respectively. From this assumption, equation (4.6) can be rewritten as

$$\begin{aligned}\dot{x} &= A + Bu + \Delta Ax + f(t) \\ &= A + Bu + BD(t) + \Delta\tilde{A}(t) + BG(t) + \tilde{f}(t) \\ &= A + Bu + Bf_m + fu\end{aligned} \tag{4.8}$$

where f_m represents the lumped matched uncertainty and disturbance which is given by

$$f_m = BD(t)x(t) + BG(t) \tag{4.9}$$

The term f_u represents the system lumped unmatched uncertainty and disturbance which is given by

$$f_u = \Delta\tilde{A}(t)x + \tilde{f}(t) \tag{4.10}$$

- The matched and unmatched lumped uncertainty and disturbance f_m and f_u are bounded by known positive parameters α_{m1}, α_{m2} and α_1, α_2 such that

  $f_m \le \alpha_{m_1} + \alpha_{m_2}\|x\|$ and $f_u \le \alpha_{u_1} + \alpha_{u_2}\|x\|$

- The sign of the parameter k_2 is known and the sign of the λB is known, if $\lambda \in R^n$; $|\lambda B| < \beta$, where β is known positive parameter.

The control objective is to determine the plant input u(t) so that the plant state x(t) tracks the reference model state $x_m(t)$ as close as possible for any given reference input u_c. To design the controller, the error between the plant and reference model is defined as

$$e(t) = x(t) - x_m(t) \tag{4.11}$$

The integral sliding surface is defined as

$$s(t) = \lambda e(t) - \lambda\int A_m e(t)dt \tag{4.12}$$

Its derivative is

$$\begin{aligned}\dot{s}(t) &= \lambda\dot{e}(t) - \lambda A_m e(t) \\ &= \lambda A_m e + \lambda(A - A_m)x + \lambda Bu + \lambda Bf_m + \lambda f_u - \lambda B_m u_c - \lambda A_m e(t) \\ &= \lambda(A - A_m)x + \lambda Bu + \lambda Bf_m + \lambda f_u - \lambda B_m u_c\end{aligned} \tag{4.13}$$

Setting $\dot{s}(t) = 0$, the equivalent control (u_{eq}) is given by

$$\begin{aligned}u_{eq} &= -(\lambda B)^{-1}[\lambda((A - A_m)x - B_m u_c)] - f_m - (\lambda B)^{-1}\lambda f_u \\ &= -(\lambda B)^{-1}\lambda(A - A_m)x + (\lambda B)^{-1}\lambda B_m u_c - f_m - (\lambda B)^{-1}\lambda f_u \\ &= \hat{k}_1^{\,T} x + \hat{k}_2 u_c - f_m - (\lambda B)^{-1}\lambda f_u\end{aligned} \tag{4.14}$$

The adaptive sliding mode state tracking controller is designed as

$$u = \hat{k}_1^{\,T} x + \hat{k}_2 u_c - \rho(\lambda B)^{-1}\text{sign}(s) \tag{4.15}$$

where $\hat{k}_1^{T}$ and $\hat{k}_2$ are are the update controller parameter of k_1^{T} and k_2 and ρ is control gain. The design task is to choose adaptive laws to update controller parameters so that the model reference control objective is achievable. The main functions of adaptive update laws for $k_1^{\wedge T}$ and $k_2^{\wedge}$ are to ensure the stability of the closed loop system [19]. The parameter update error is defined as

$$\begin{aligned}\tilde{k}_1 &= \hat{k}_1 - k_1 \\ \tilde{k}_2 &= \hat{k}_2 - k_2\end{aligned} \tag{4.16}$$

Substituting (4.16) into (4.8)

$$\dot{x} = A + B(\hat{k}_1^{\,T} x + \hat{k}_2 u_c - \rho(\lambda B)^{-1}\text{sign}(s) + Bf_m + f_u \tag{4.17}$$

Using the relation $A + Bk_1^{T} = A_m$ and $Bk_2 = B_m$

$$\dot{x} = A_m x + B_m u_c + B_m\left(\frac{1}{k_2}\tilde{k}_1^{\,T} x + \frac{1}{k_2}\tilde{k}_1^{\,T} r(t)\right) - \rho B(\lambda B)^{-1}\text{sign}(s) + Bf_m + f_u \tag{4.18}$$

The tracking error derivative is given as

$$\dot{e}(t) = \dot{x} - \dot{x}_m$$

$$\dot{e}(t) = A_m(x - x_m) + B_m u_c - B_m u_c + B_m\left(\frac{1}{k_2}\tilde{k}_1^T x + \frac{1}{k_2}\tilde{k}_1^T u_c\right) - \rho B(\lambda B)^{-1}\text{sign}(s) + Bf_m + f_u \quad (4.19)$$

$$\dot{e}(t) = A_m(e) + B_m\left(\frac{1}{k_2}\tilde{k}_1^T x + \frac{1}{k_2}\tilde{k}_1^T u_c\right) - \rho B(\lambda B)^{-1}\text{sign}(s) + Bf_m + f_u$$

The integral sliding surface derivative becomes

$$\dot{s}(t) = \lambda\dot{e}(t) - \lambda A_m e(t) \quad (4.20)$$

$$\dot{s}(t) = \lambda A_m e + \lambda B_m\left(\frac{1}{k_2}\tilde{k}_1^T x + \frac{1}{k_2}\tilde{k}_1^T u_c\right) - \lambda\rho B(\lambda B)^{-1}\text{sign}(s) + \lambda Bf_m + \lambda f_u - \lambda A_m e(t)$$

$$\dot{s}(t) = \lambda B_m\left(\frac{1}{k_2}\tilde{k}_1^T x + \frac{1}{k_2}\tilde{k}_1^T u_c\right) - \lambda\rho B(\lambda B)^{-1}\text{sign}(s) + \lambda Bf_m + \lambda f_u \quad (4.21)$$

If the upper bound of the uncertainties and disturbance is not known, adaptive control algorithm can be used to get the upper bound of the uncertainties and disturbance.

Assuming $f_u = 0$,

$$f_m \le \alpha_1 + \alpha_2 \|x\| \quad (4.22)$$

where α_1 and α_2 are unknown positive constants.

The controller estimated gain parameter is given by

$$\rho = \hat{\alpha}_1 + \hat{\alpha}_2 \| x \| \quad (4.23)$$

The controller gain parameter estimation error is defined as

$$\tilde{\alpha}_1 = \hat{\alpha}_1 - \alpha_1$$
$$\tilde{\alpha}_2 = \hat{\alpha}_2 - \alpha_2 \quad (4.24)$$

Define a Lyapunov function as

$$V = \frac{1}{2}s^2 + \frac{1}{2|k_2|}\tilde{k}_1^{T}\tau^{-1}\tilde{k}_1 + \frac{1}{2|k_2|}\tilde{k}_2^{2}\gamma_1^{-1} + \frac{1}{2}\tilde{\alpha}_1^{2}\gamma_2^{-1} + \frac{1}{2}\tilde{\alpha}_2^{2}\gamma_3^{-1} \tag{4.25}$$

The lyapunov function derivative is

$$\begin{aligned}
\dot{V} &= s^{T}\dot{s} + \frac{1}{2|k_2|}\tilde{k}_1^{T}\tau^{-1}\dot{\tilde{k}}_1 + \frac{1}{2|k_2|}\tilde{k}_2\dot{\tilde{k}}_2\gamma^{-1} + \tilde{\alpha}_1\dot{\tilde{\alpha}}_1\gamma_2^{-1} + \tilde{\alpha}2\dot{\tilde{\alpha}}_2\gamma_3^{-1} \\
\dot{V} &= s^{T}[\lambda B_m(\frac{1}{2|k_2|}\tilde{k}_1^{T}x + \frac{1}{2|k_2|}\tilde{k}_2u_c) - \lambda\rho B(\lambda B)^{-1}\mathrm{sign}(s) + \lambda B f_m] + \frac{1}{|k_2|}\tilde{k}_1^{T}\tau^{-1}\dot{\tilde{k}}_1 + \frac{1}{|k_2|}\tilde{k}_2\dot{\tilde{k}}_2\gamma^{-1} \\
&\quad + \tilde{\alpha}_1\dot{\tilde{\alpha}}_1\gamma_2^{-1} + \tilde{\alpha}2\dot{\tilde{\alpha}}_2\gamma_3^{-1} \\
\dot{V} &= s^{T}\lambda B_m\frac{1}{2|k_2|}\tilde{k}_1^{T}x + s^{T}\lambda B_m\frac{1}{2|k_2|}\tilde{k}_2u_c) - s^{T}\lambda\rho B(\lambda B)^{-1}\mathrm{sign}(s) + s^{T}\lambda B f_m] + \frac{1}{|k_2|}\tilde{k}_1^{T}\tau^{-1}\dot{\tilde{k}}_1 \\
&\quad + \frac{1}{|k_2|}\tilde{k}_2\dot{\tilde{k}}_2\gamma^{-1} + \tilde{\alpha}_1\dot{\tilde{\alpha}}_1\gamma_2^{-1} + \tilde{\alpha}2\dot{\tilde{\alpha}}_2\gamma_3^{-1}
\end{aligned} \tag{4.26}$$

Substituting $(\lambda B)^{-1} = \frac{\lambda^{T}B^{T}}{|\lambda^{T}B^{T}|}$, $f_m \le \alpha_1 + \alpha_2\|x\|$ and $\rho = \hat{\alpha}_1 + \hat{\alpha}_2\|x\|$ into (4.26)

$$\begin{aligned}
\dot{V} &= s^{T}\lambda B_m\frac{1}{k_2}\tilde{k}_1^{T}x + s^{T}\lambda B_m\frac{1}{k_2}\tilde{k}_2u_c - s^{T}\lambda B\left(\hat{\alpha}_1 + \hat{\alpha}_2\|x\|\right)\frac{\lambda^{T}B^{T}}{|\lambda^{T}B^{T}|}\mathrm{sign}(s) \\
&\quad + s^{T}\lambda B\left(\alpha_1 + \alpha_2\|x\|\right) + \frac{1}{|k_2|}\tilde{k}_1^{T}\tau^{-1}\dot{\tilde{k}}_1 + \frac{1}{|k_2|}\tilde{k}_2\dot{\tilde{k}}\gamma_1^{-1} + \tilde{\alpha}_1\dot{\tilde{\alpha}}_1\gamma_2^{-1} + \tilde{\alpha}_2\dot{\tilde{\alpha}}_2\gamma_3^{-1} \\
\dot{V} &= |s|\lambda B_m\frac{1}{k_2}\tilde{k}_1^{T}x + |s|\lambda B_m\frac{1}{k_2}\tilde{k}_2u_c - |s|\lambda B\left(\hat{\alpha}_1 + \hat{\alpha}_2\|x\|\right)\frac{\lambda^{T}B^{T}}{|\lambda^{T}B^{T}|}\mathrm{sign}(s) \\
&\quad + |s|\lambda B\left(\alpha_1 + \alpha_2\|x\|\right) + \frac{1}{|k_2|}\tilde{k}_1^{T}\tau^{-1}\dot{\tilde{k}}_1 + \frac{1}{|k_2|}\tilde{k}_2\dot{\tilde{k}}\gamma_1^{-1} + \tilde{\alpha}_1\dot{\tilde{\alpha}}_1\gamma_2^{-1} + \tilde{\alpha}_2\dot{\tilde{\alpha}}_2\gamma_3^{-1}
\end{aligned} \tag{4.27}$$

Substituting $\tilde{\alpha}_1 = \hat{\alpha}_1 - \alpha_1$ and $\tilde{\alpha}_2 = \hat{\alpha}_2 - \alpha_2$ into (4.27)

$$\begin{aligned}
\dot{V} &= |s|\lambda B_m\frac{1}{k_2}\tilde{k}_1^{T}x + \frac{1}{|k_2|}\tilde{k}_1^{T}\tau^{-1}\dot{\tilde{k}}_1 + |s|\lambda B_m\frac{1}{k_2}\tilde{k}_2u_c + \frac{1}{|k_2|}\tilde{k}_2\dot{\tilde{k}}_2\gamma_1^{-1} \\
&\quad - (|s|\lambda B - \dot{\tilde{\alpha}}_1\gamma_2^{-1})(\hat{\alpha}_1 - \alpha_1) - (|s|\lambda B\|x\| - \dot{\tilde{\alpha}}_2\gamma_3^{-1})(\hat{\alpha}_2 - \alpha_2)
\end{aligned} \tag{4.28}$$

For stable control system $\dot{V}$ should be negative semi _definite i.e. $\dot{V} \le 0$ .Therefore

$$
\begin{aligned}
&|s|\lambda B_m \frac{1}{k_2}\tilde{k}_1^{T}x + \frac{1}{|k_2|}\tilde{k}_1^{T}\tau^{-1}\dot{\tilde{k}}_1 = 0\\
&|s|\lambda B_m \tilde{k}_2 u_c + \frac{1}{|k_2|}\tilde{k}_2\dot{\tilde{k}}_2\gamma_1^{-1} = 0\\
&|s|\lambda B_m \frac{1}{k_2}(|s|\lambda B - \dot{\tilde{\alpha}}_1\gamma_2^{-1}) = 0\\
&(|s|\lambda B\|x\| - \dot{\tilde{\alpha}}_2\gamma_3^{-1}) = 0
\end{aligned}
\tag{4.29}
$$

The adaptive parameter update law is

$$
\begin{aligned}
&\dot{k}_1 = -\tau|s|\lambda B_m \frac{|k_2|}{k_2}x = -\tau|s|\lambda B_m \operatorname{sign}(k_2)x\\
&\dot{k}_2 = -\gamma_1|s|\lambda B_m \frac{|k_2|}{k_2}r(t) = -\gamma_1|s|C^{T}B_m \operatorname{sign}(k_2)u_c\\
&\dot{\alpha}_1 = \gamma_2|s|\lambda B\\
&\dot{\alpha}_2 = \gamma_3|s|\lambda B\|x\|
\end{aligned}
\tag{4.30}
$$

The second order equation (3.85) can be rewritten as follows

$$
\begin{aligned}
\dot{x} &= Ax + Bu + f(t)\\
y &= Cx
\end{aligned}
\tag{4.31}
$$

where $A = \begin{vmatrix} \frac{1}{C_0 R_L} & \frac{1}{C_0} \\ -L_s & 0 \end{vmatrix}$, $B = \begin{vmatrix} 0 \\ -\frac{2L_s V_{in}}{knf_{r1}} \end{vmatrix}$, $C = |0 \quad 1|$, $f(t) = \frac{L_s V_{in}}{n}$ (disturbance signal)

However, matrix A can be written as $A + \Delta A$ since there is parameter variation due to L_s and R_L. The second order reference model is chosen depending best dynamic and steady state performance and plant transfer function. The second order system is described as

$$
y_m = \frac{\omega_n^{2}}{s^2 + 2\xi\omega_n s + \omega_n^{2}} \tag{4.32}
$$

Where ω_n is natural frequency and ξ is a damping factor.

The reference model of crically damped second order system is selected as follows with $\omega_n = 10000$ rad/s. The model is selected depending on the plant transfer function derived in (3.87).

$$y_m = \frac{10^8}{s^2 + 20000s + 10^8} \tag{4.33}$$

The nominal controller parameters can be calculated using the following relation

$$\begin{vmatrix} A + Bk^T_1 = A_m \\ \begin{vmatrix} -125 & 10^6 \\ -324.8 & 0 \end{vmatrix} + \begin{vmatrix} 0 \\ -34.21 \end{vmatrix} \begin{vmatrix} k_{11} & k_{12} \end{vmatrix} = \begin{vmatrix} -20000 & 10^8 \\ -1 & 0 \end{vmatrix} \end{vmatrix} \tag{4.34}$$

Substituting the matrices A, B and k

$$\begin{vmatrix} -125 & 10^6 \\ -324.8 + -34.21k_{11} & -34.21k_{12} \end{vmatrix} = \begin{vmatrix} -20000 & 10^8 \\ -1 & 0 \end{vmatrix} \tag{4.35}$$

Solving (4.35)

$$\begin{vmatrix} k_{11} & k_{12} \end{vmatrix} = \begin{vmatrix} 0 & -10 \end{vmatrix} \tag{4.36}$$

From relation, $k_2 B = B_m$

$$\begin{vmatrix} k_2 \begin{vmatrix} 0 \\ -34.21 \end{vmatrix} = \begin{vmatrix} 0 \\ 1 \end{vmatrix} \\ k_2 = -3x10^{-2} \end{vmatrix} \tag{4.37}$$

From the following relation, λ can be calculated.

$$|\lambda B| \geq \beta \tag{4.38}$$

where β is the positive constant

Choosing $\beta = 1$,

$$\begin{vmatrix} \lambda_{11} & \lambda_{12} \end{vmatrix} \begin{vmatrix} 0 \\ -34.21 \end{vmatrix} = 1 \tag{4.39}$$

Solving (4.39)

$$\left|\lambda_{11} \quad \lambda_{12}\right| = \left|\text{-2x10}^{-2} \quad \text{-3x10}^{-2}\right| \tag{4.40}$$

The adaptation gains are selected as follows depending on stability, both steady state and transient response of controller.

$$\tau = \begin{vmatrix} 0.3 \\ 0.3 \end{vmatrix}$$

$$\gamma_1 = 0.009$$

$$\gamma_3 = 80$$

$$\gamma_2 = 100$$

CHAPTER FIVE

5. SIMULATION RESULT and DISCUSSION

5.1 Super Twisting Second Order Sliding Mode Controller Without Disturbance Response

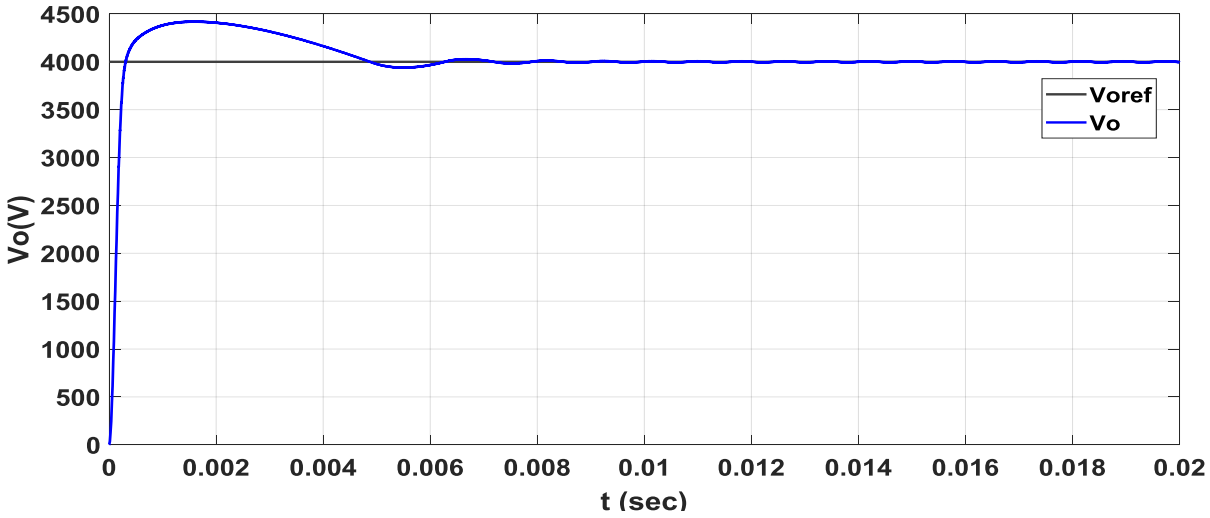

Figure 5.1 Output voltage response without disturbance

The performance of supper twisting controller without any parameter variation is described in table 5.1.

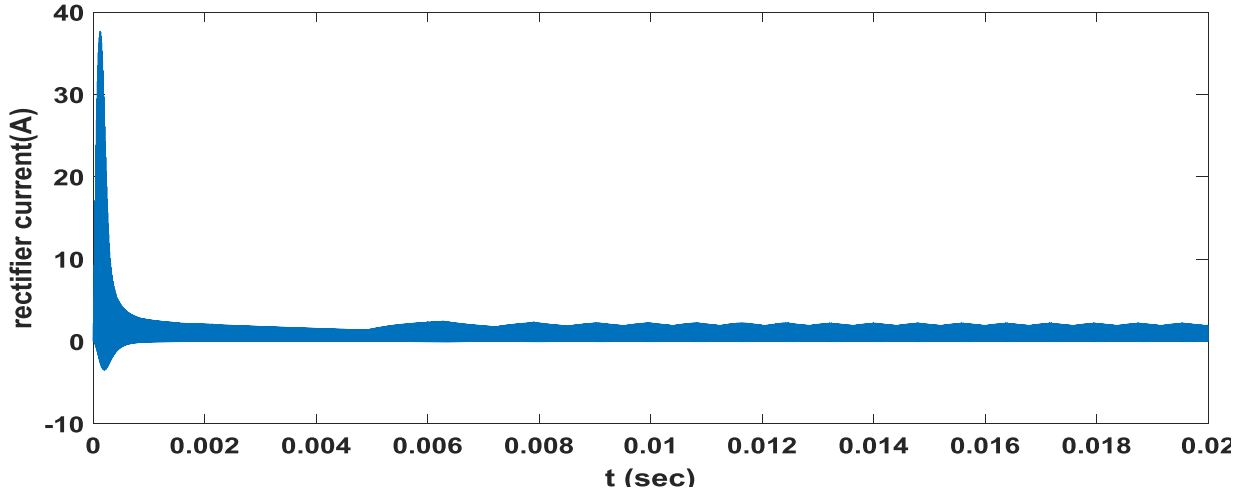

Figure 5.2 Rectifier current without any disturbance

Table 5.1 Performance of STA

Settling time (t_s)	Rise time (t_r)	Maximum overshoot	Steady state error(e_{ss})
4.33msec	182.8μsec	8.784%	0.7%

The error signal between output voltage and reference voltage, shown in Figure 5.3 indicates that there is steady state error of 0.7% due to high switching frequency of STA. The sliding surface is similar with error signal.

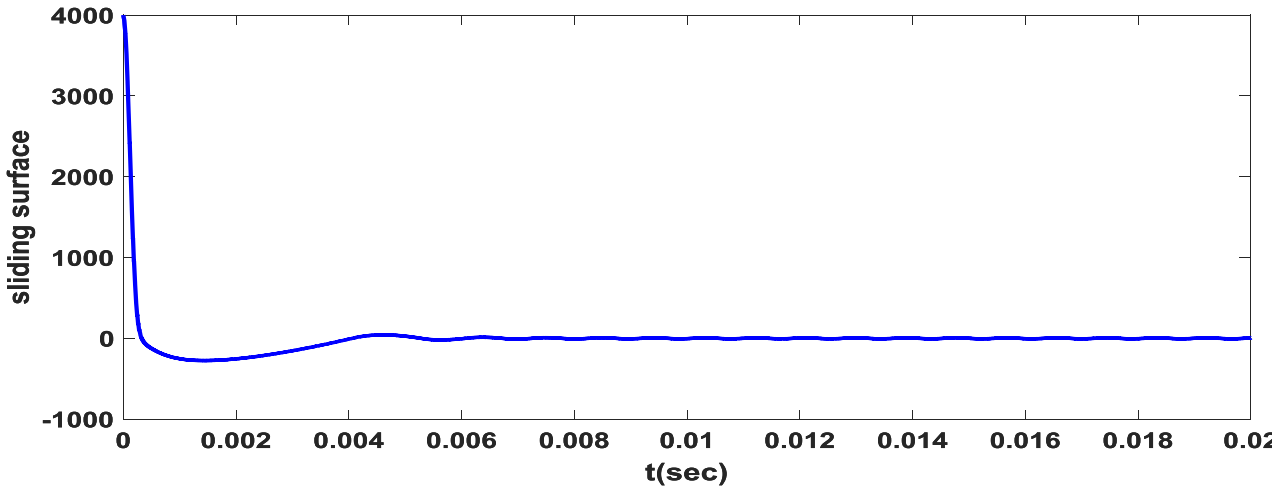

Figure 5.3 Output voltage error without any disturbance signal

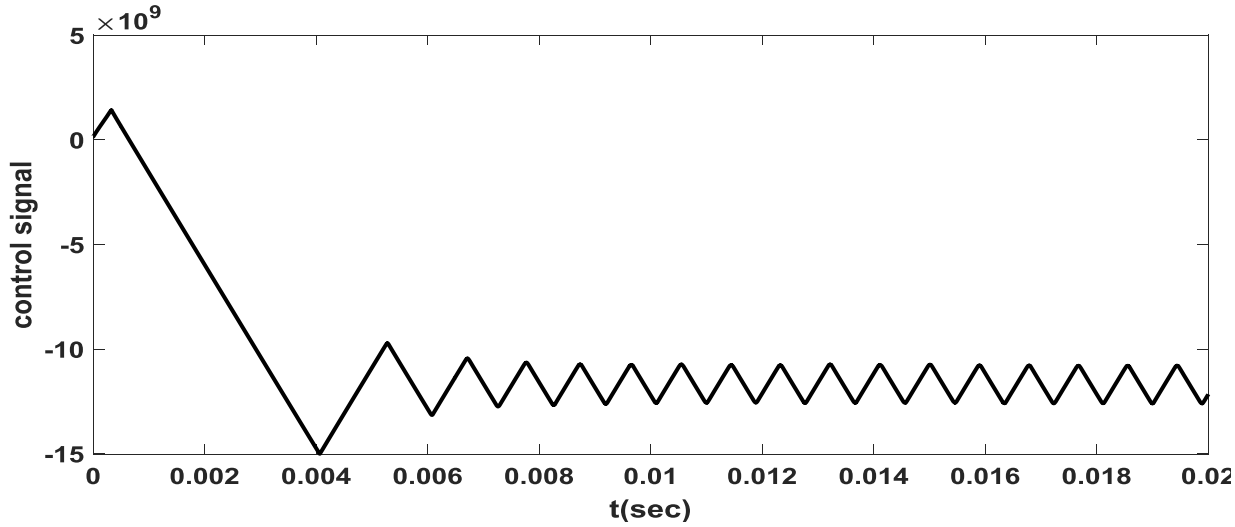

Figure 5.4 Controller output signal

The control signal shown in Figure 5.4 indicates that its value is switching between $-(9-11)\text{x}10^9$ to compensate the nonlinearity in the converter.

5.2 Super Twisting Second Order Sliding Mode Controller With Disturbance Response

5.2.1 Resonant Inductor Variation

The resonant inductor (L_r) variation causes the resonant frequency to be varied. This results in disturbance. It is assumed that about 10% of nominal design value of L_r is increased due to temperature variation or manufacturing error. As shown in Figure 5.5 it is varied from $(45-49.5)\mu H$ within the time $(0.04-0.05)$sec for simulation purpose.

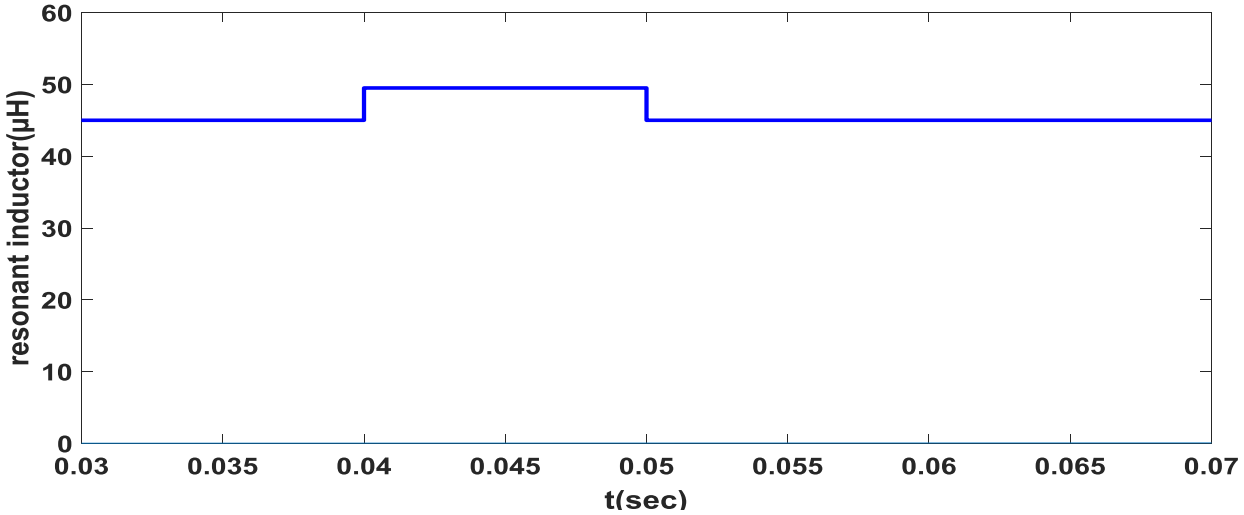

Figure 5.5 Resonant inductor value

The controller performance parameters are the same with STA without disturbance except steady state error.

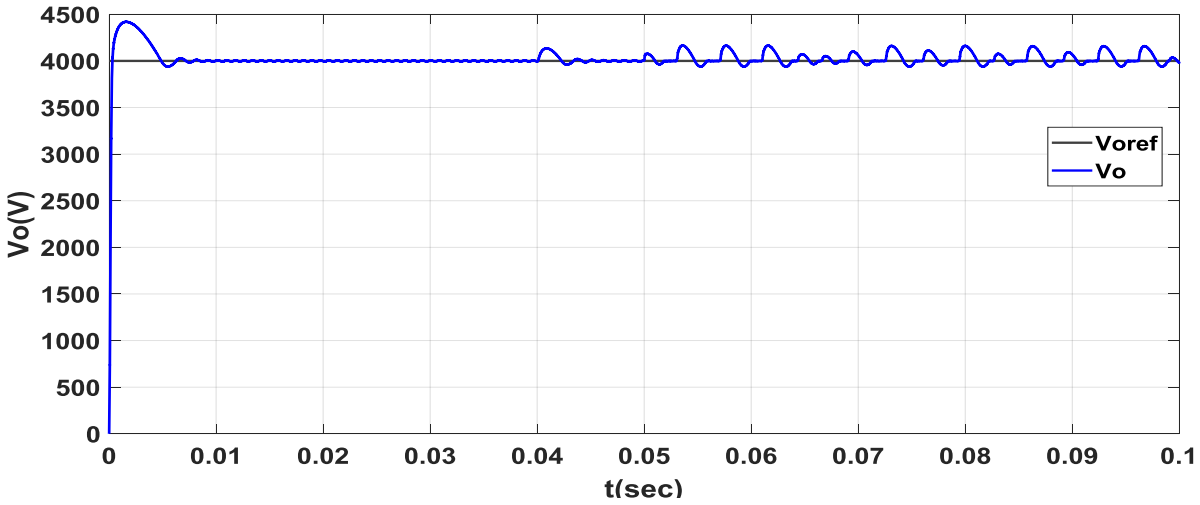

Figure 5.6 Output voltage response to inductor variation

The steady state error increased from 0.7% to 13% as shown in Figure 5.7 when the inductor is varied.

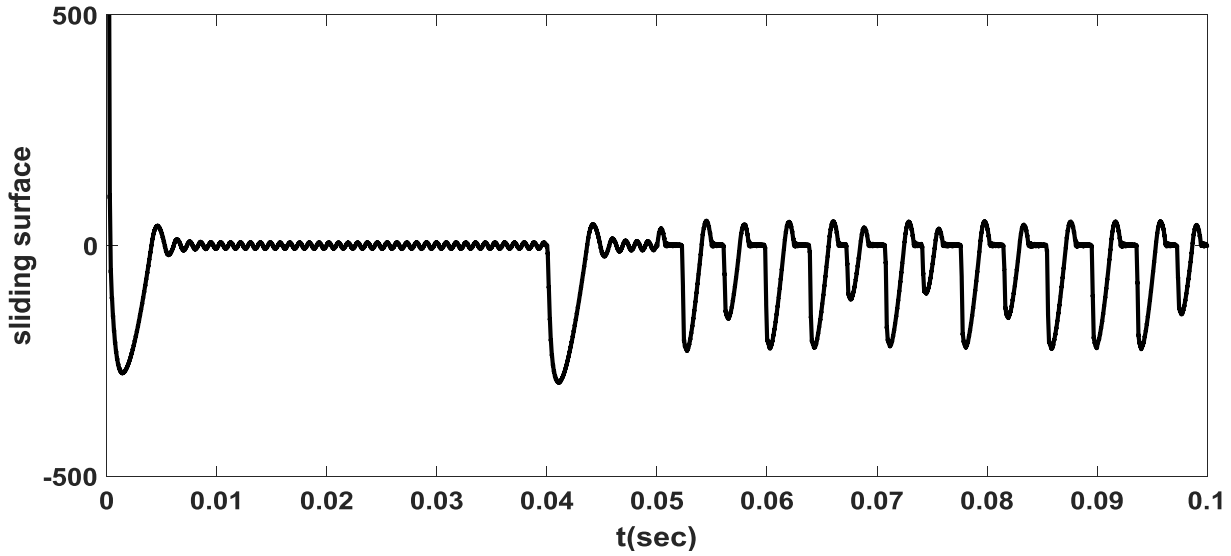

Figure 5.7 Output voltage error after inductor variation

The controller output is changed in order to compensate the variation as follows. But, the controller couldn't reduce the steady state error caused by resonant inductor variation.

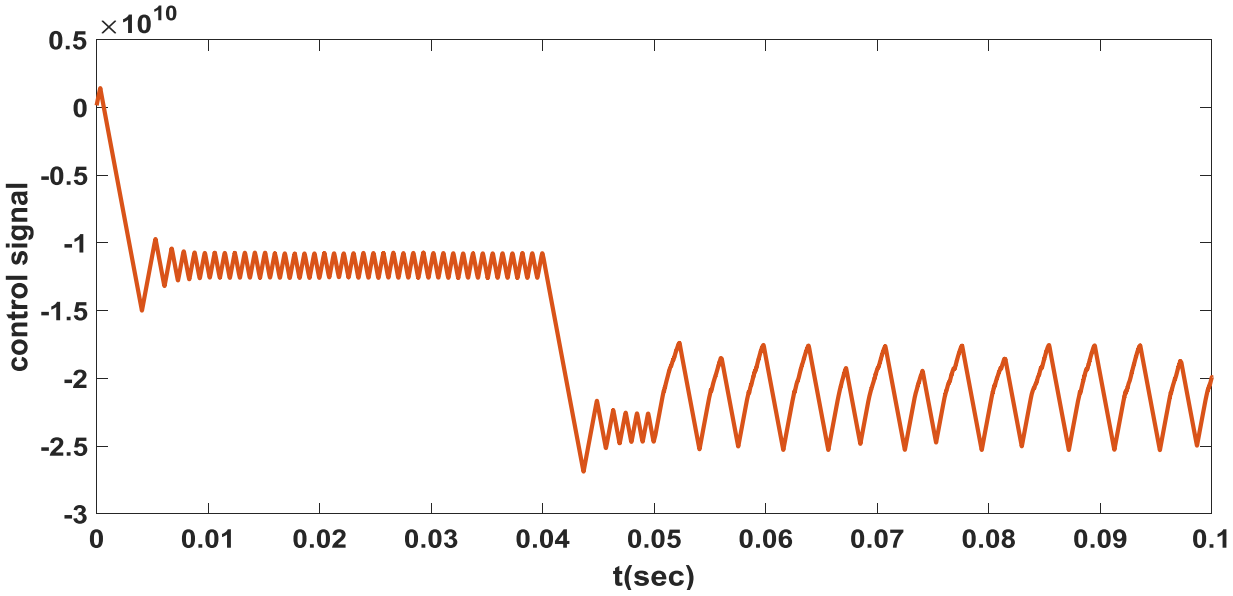

Figure 5.8 Controller signal after inductor variation

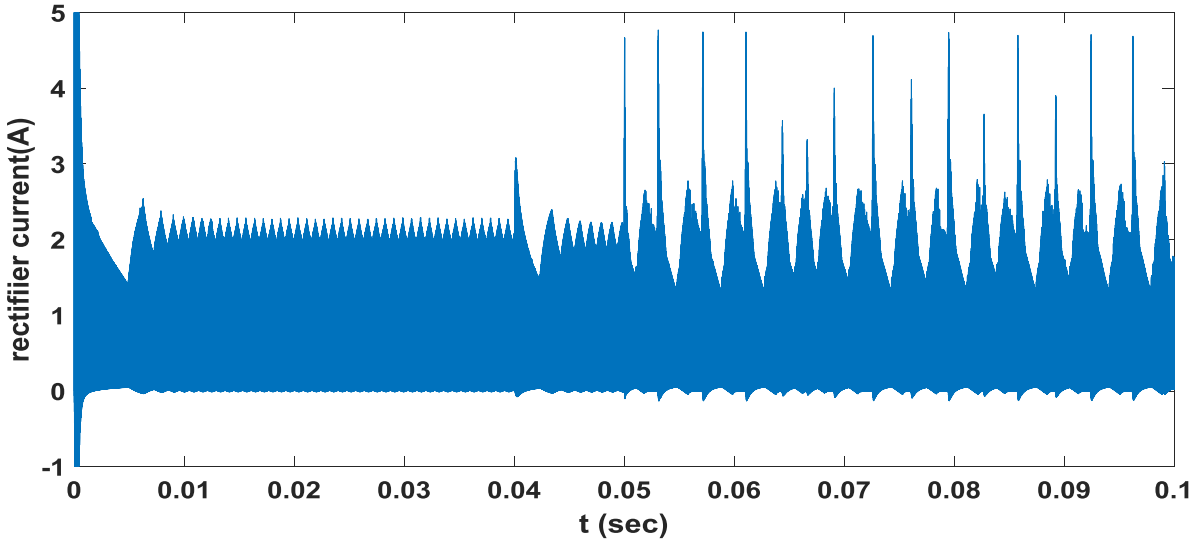

Figure 5.9 Rectifier current after resonant inductor variation

After resonant inductor is changed from nominal value, the rectifier current increased from 2A to 2.5A. The current response shows spike after inductor variation.

5.2.2 Load Resistance Variation

Load resistance can vary due to change in temperature or disturbance in environment. The resistance varied between full load ($R_L = 8000\Omega$) and light load ($R_L = 3000\Omega$).

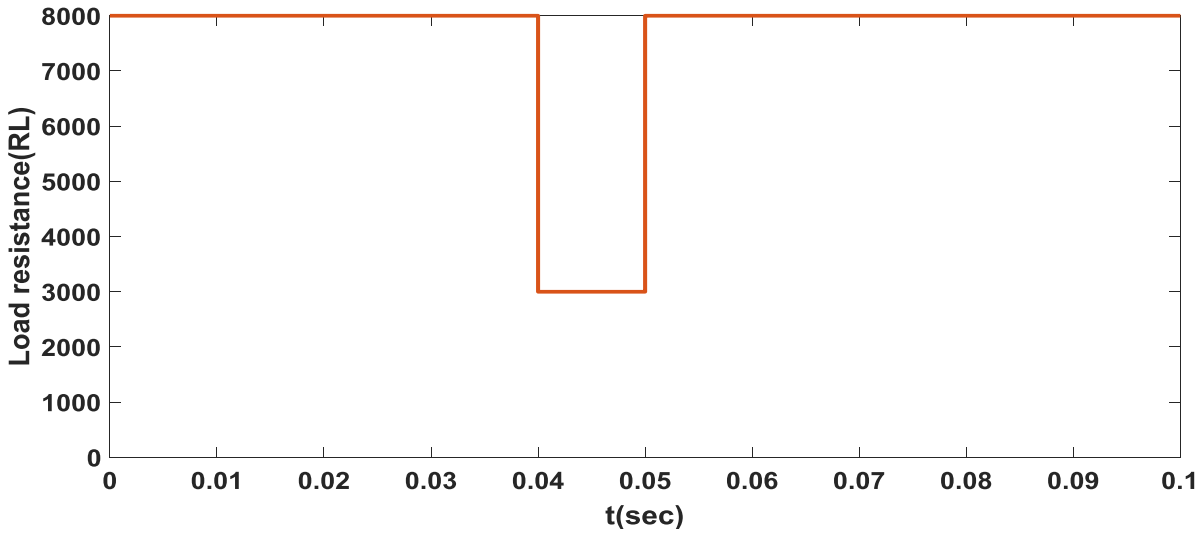

Figure 5.10 Load resistance value

The response of the controller to the load resistance variation is indicated in Figure 5.11 shows that there is output voltage deviation of 397 from reference voltage at a time $(0.04-0.044)$ and $(0.05-0.054)$. All controller performance is similar with the converter without parameter variation.

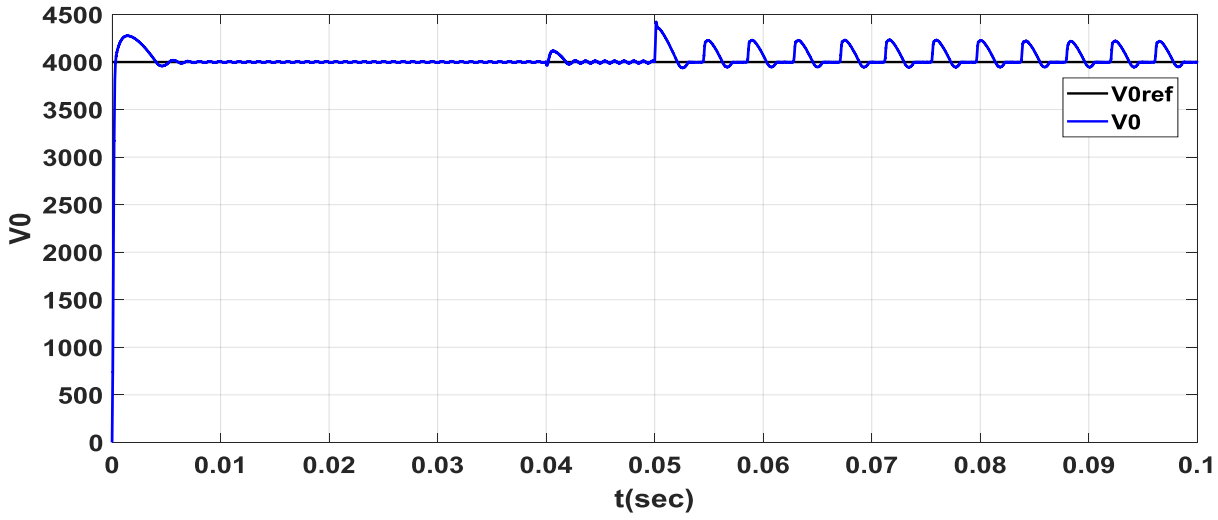

Figure 5.11 Output voltage response to load resistance variation

The error is 397 at a time $(0.04-0.044)$ and $(0.05-0.054)$.

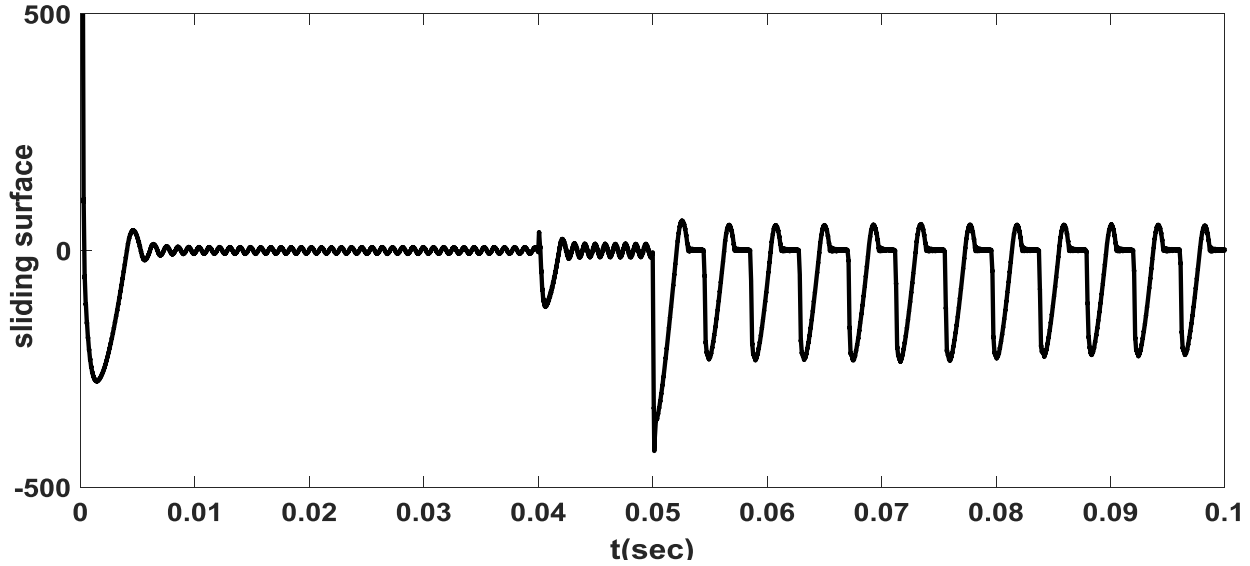

Figure 5.12 Output voltage error after load resistance variation

The control signal switches between $((-1.428)-(-1.245))10^{10}$ for the time $t \le 0.04$ and $t \ge 0.06$, and between $(2.981-1.37)10^{9}$ for the time $0.04 \le t \le 0.06$.

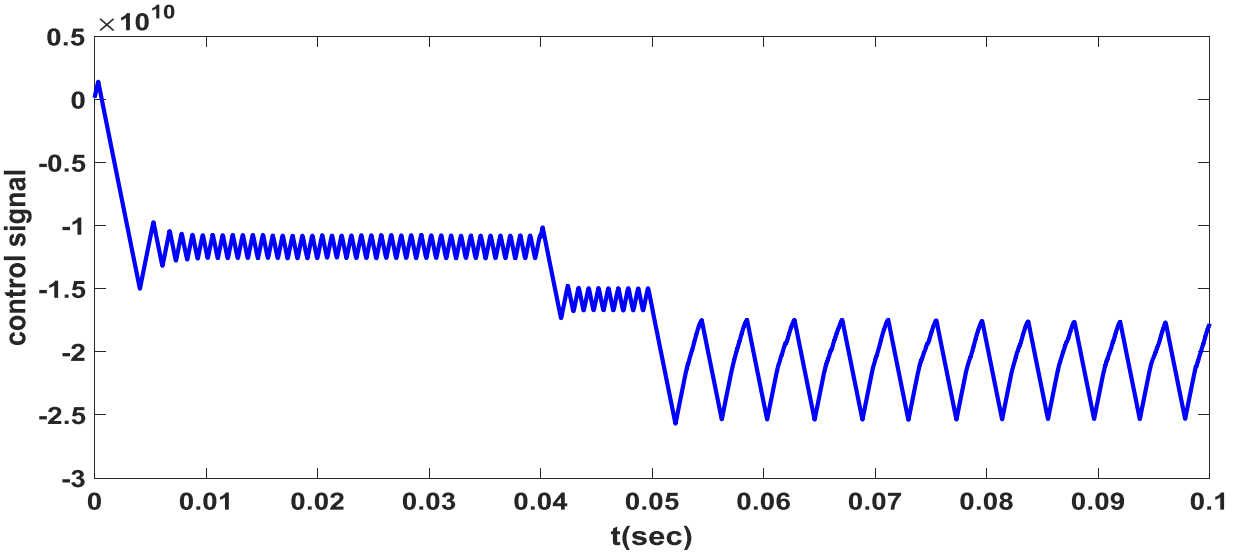

Figure 5.13 Control signal for load resistance variation

5.2.3 DC input voltage source variation

The DC voltage, which can be from PV or rectification of AC source, is not constant i.e. it varies with time due to different conditions. For simulation purpose, it is varied between $(300-400)V$.

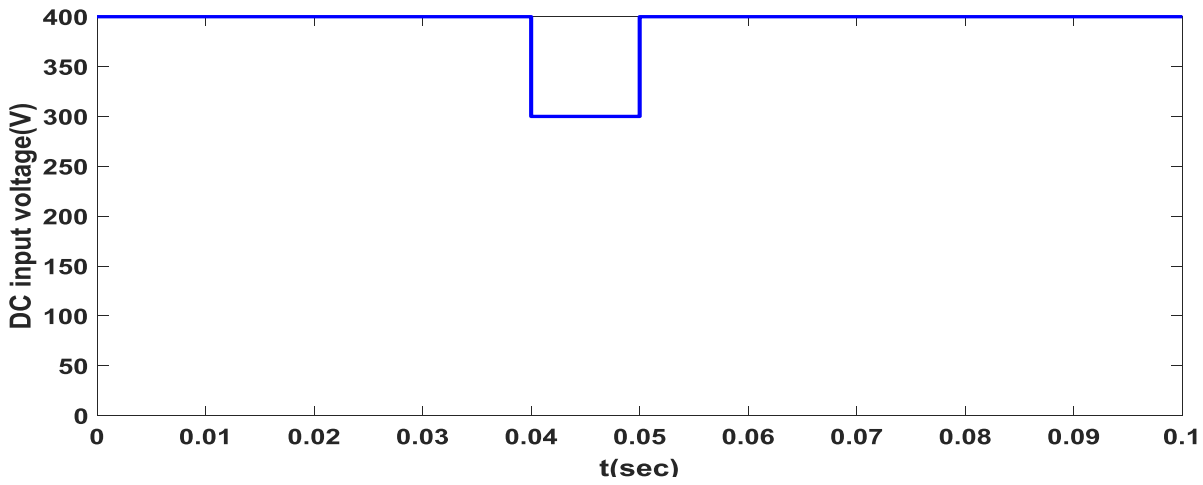

Figure 5.14 DC input voltage value

All controller performance is the same with that of the converter without input voltage variation except error signal. The error is (161) at a time $(0.04-0.044)$ and (-269.9) at $(0.05-0.054)\text{sec}$.

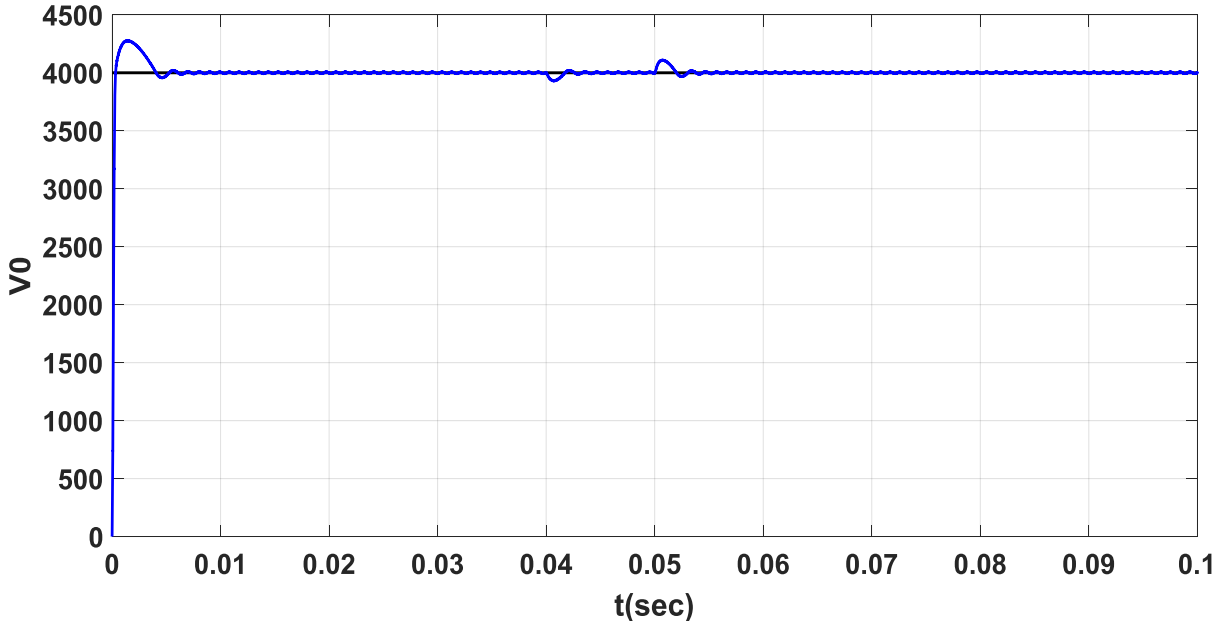

Figure 5.15 Output voltage response for DC input variation

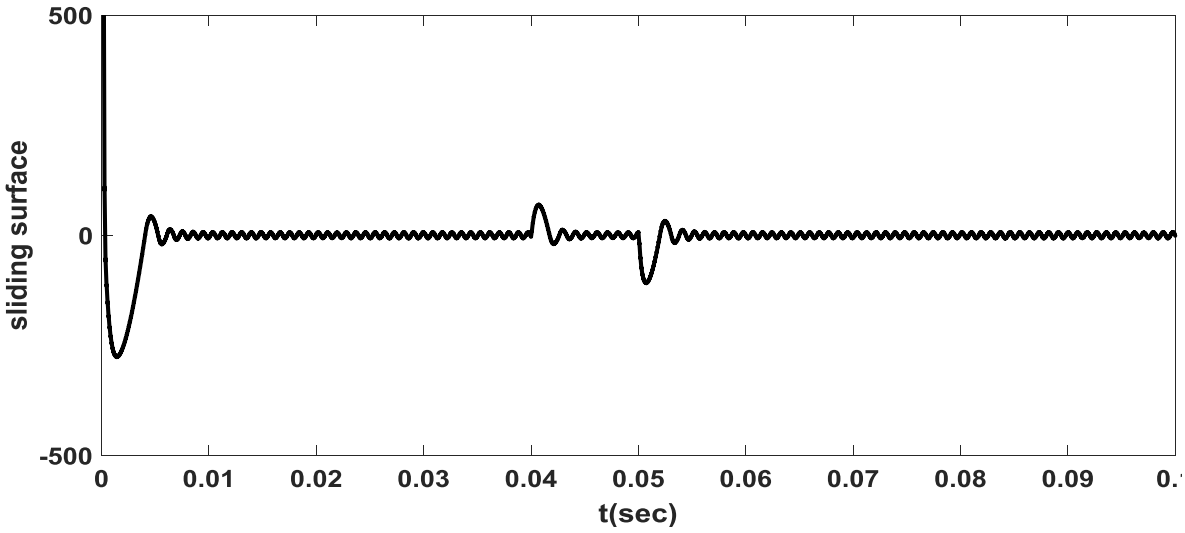

Figure 5.16 Output voltage error for DC input variation

The control signal switches between $((-1.22)-(-1.42))10^{10}$ for the time $t \le 0.04$ and $t \ge 0.06$,and between $((-2.981)10^{9}-(8.45x10^{7}))$ for the time $0.04 \le t \le 0.06$.

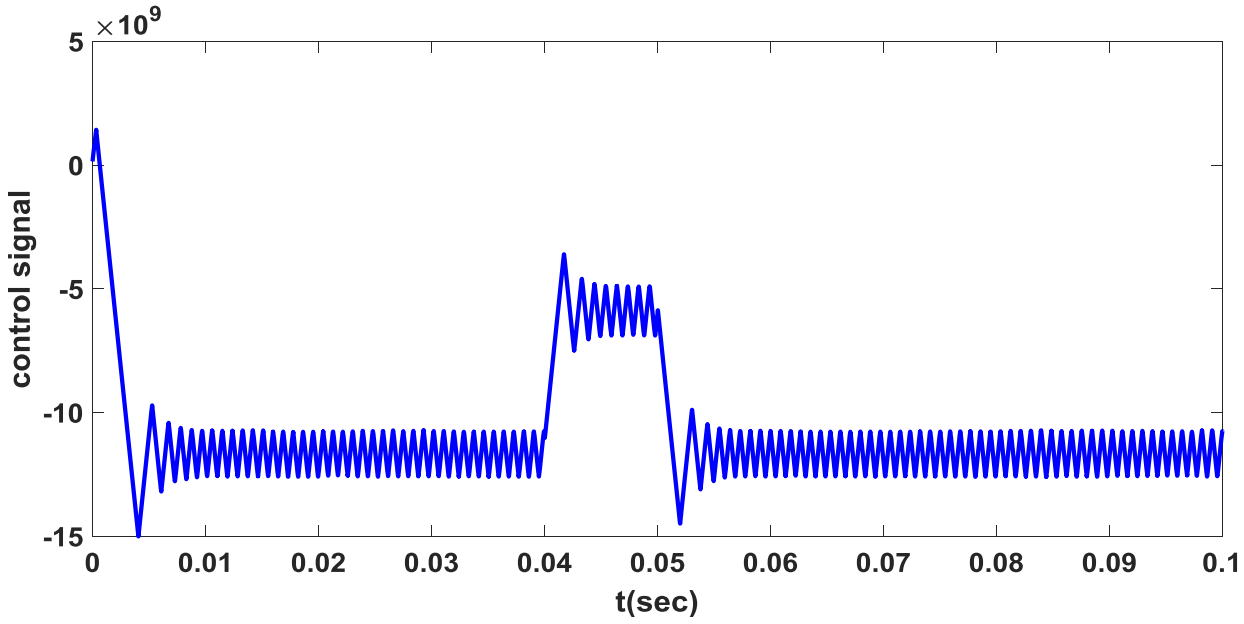

Figure 5.17 control signal for DC input variation

5.2.4 DC Input Voltage, Load Resistance and Resonant Inductor Variation at The Same Time

If DC input voltage, resonant inductor and load resistance is varied at the same time, the response of the output voltage is as follows. The output voltage will not follow the reference voltage after parameter variation at $t = 0.04\text{sec}$.

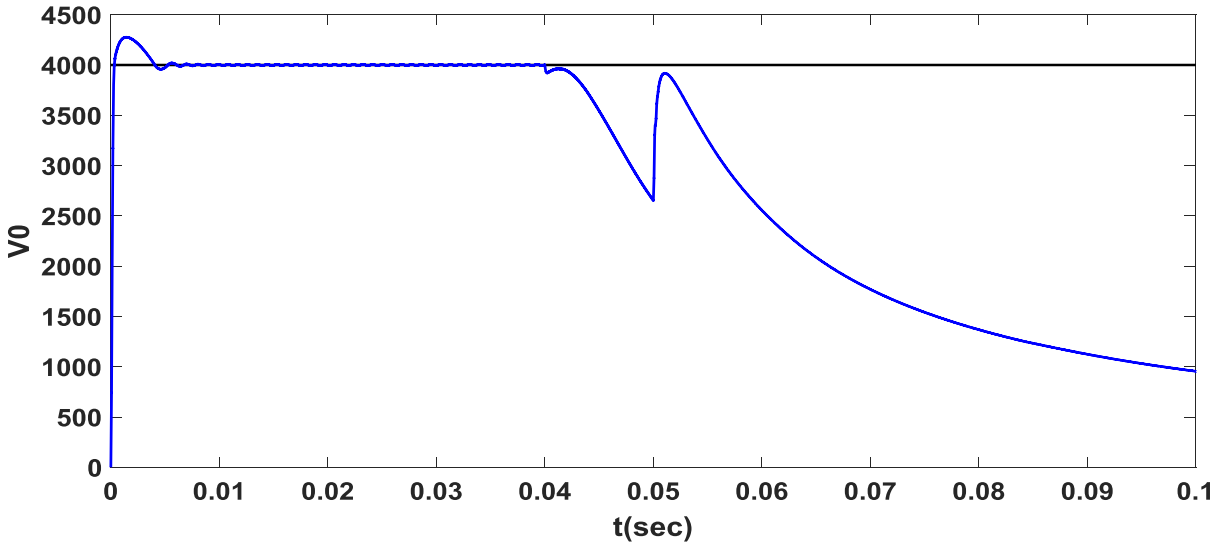

Figure 5.18 Output voltage response after all parameter variation

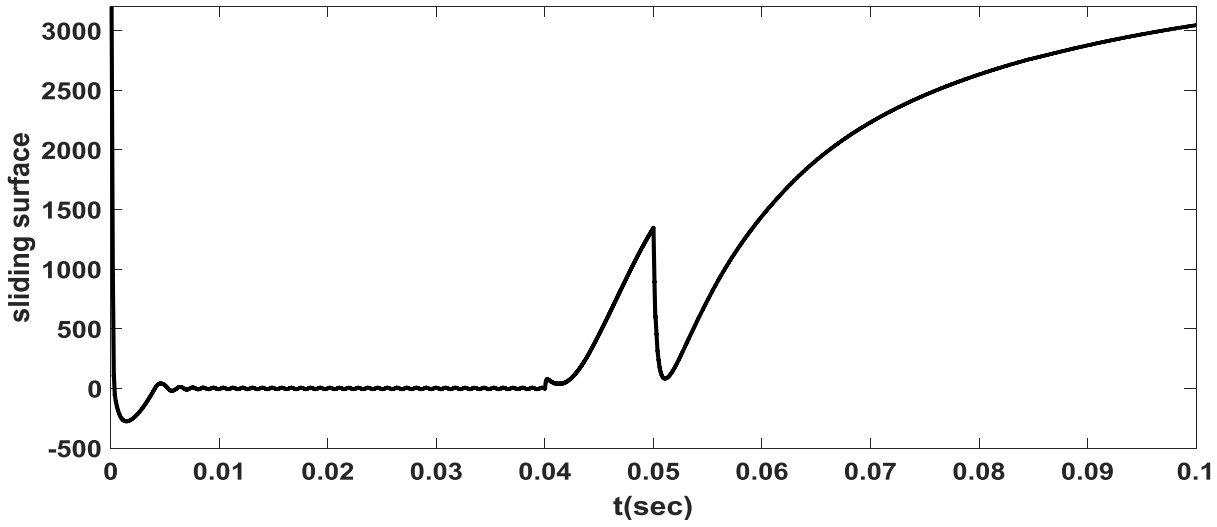

Figure 5.19 Output voltage error after all parameter variation

After three parameters changed from nominal value the voltage error increased from 0 to 3000.

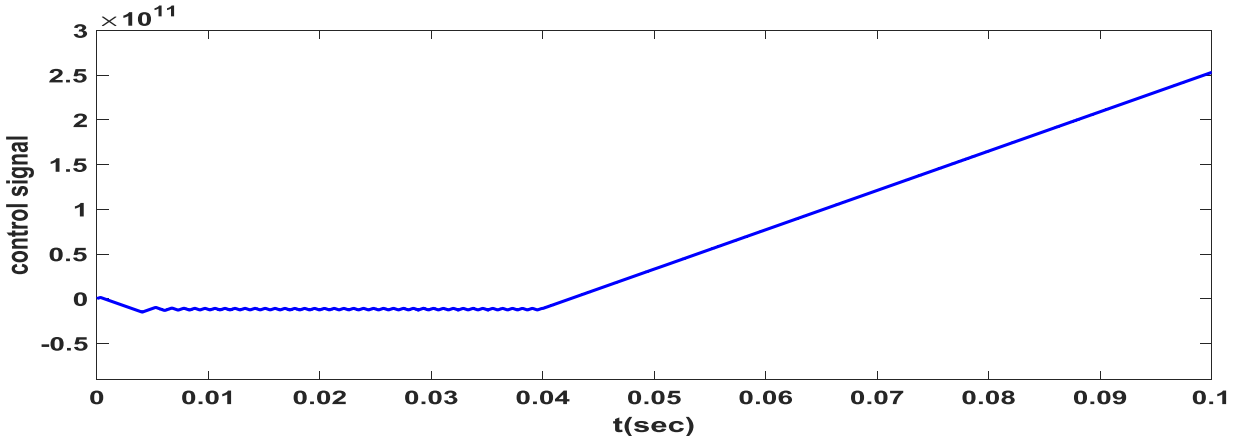

Figure 5.20 Control signal after all parameter variation

5.3 Model Reference Adaptive Sliding Mode Controller Without Disturbance Response

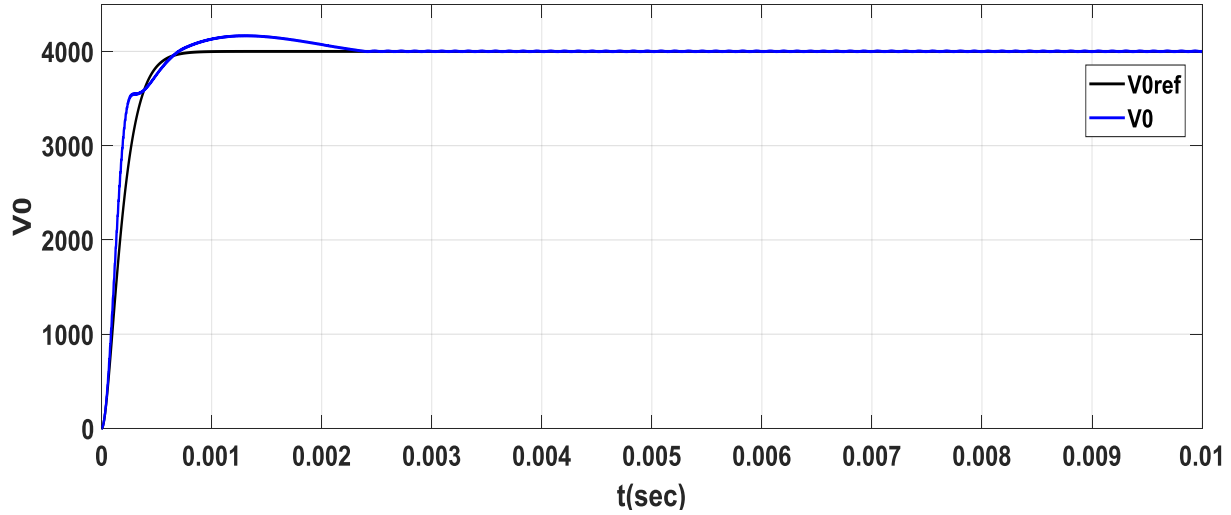

Figure 5.21 Output voltage response without any disturbance

The performance of the ASMC without any disturbance is shown in the following table.

Table 5.2 Performance of ASMC

Settling time (t_s)	Rise time (t_r)	Maximum overshoot	Steady state error(e_{ss})
2.5msec	334μsec	6.37%	0.2%

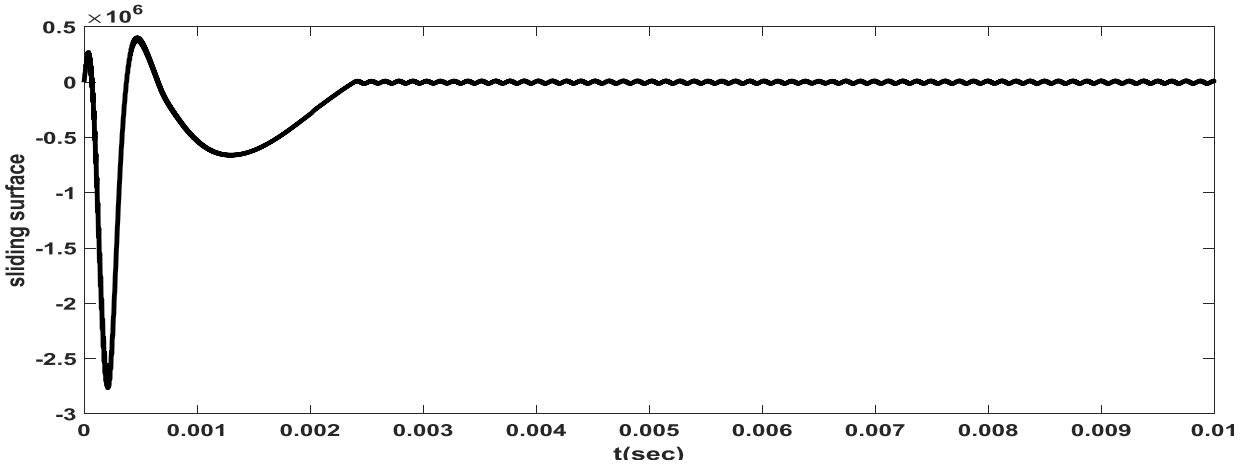

Figure 5.22 Integral sliding surface without any disturbance

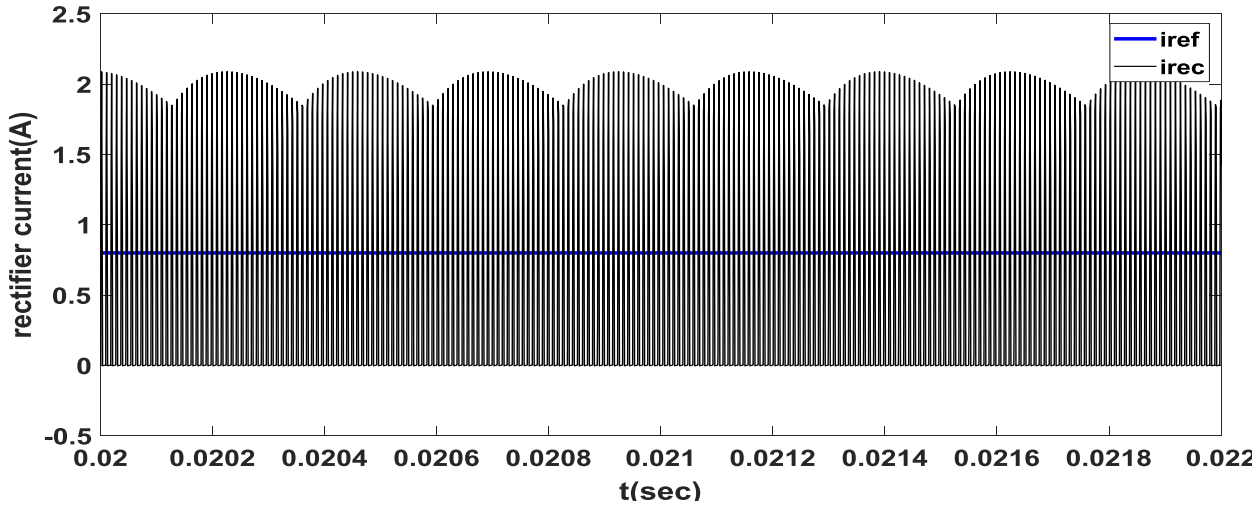

Figure 5.23 Rectifier current for converter without any disturbance

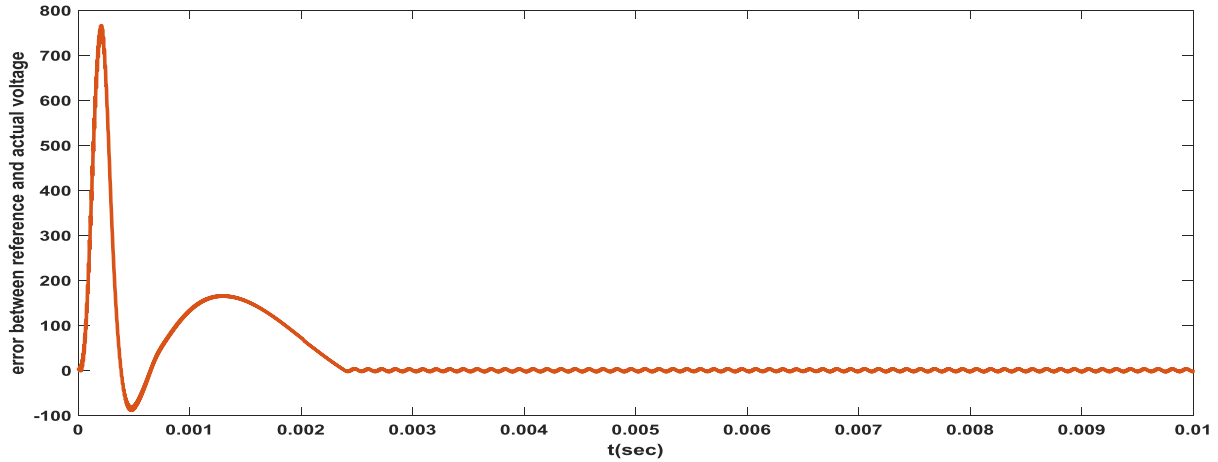

Figure 5.24 Output voltage error without any disturbance

5.4 Model Reference Adaptive Sliding Mode Controller With Disturbance Signal Response

5.4.1 DC Input Voltage Variation

Applying the same signal to ASMC as supper twisting controller, the response to DC input variation indicates that the output voltage follows the reference voltage even though there is DC input voltage variation.

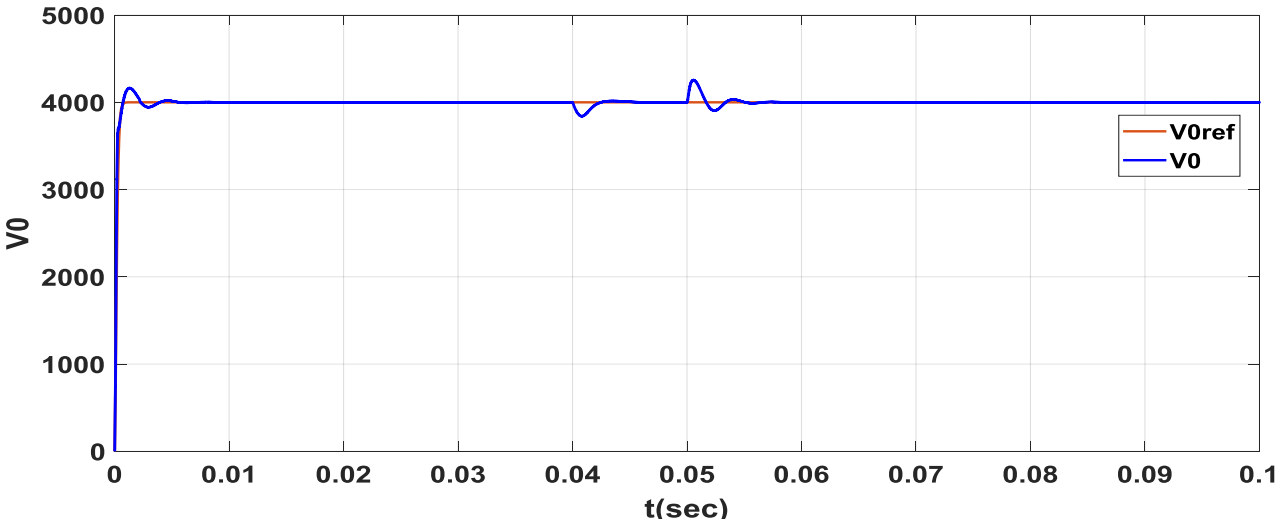

Figure 5.25 Output voltage response with DC input voltage variation

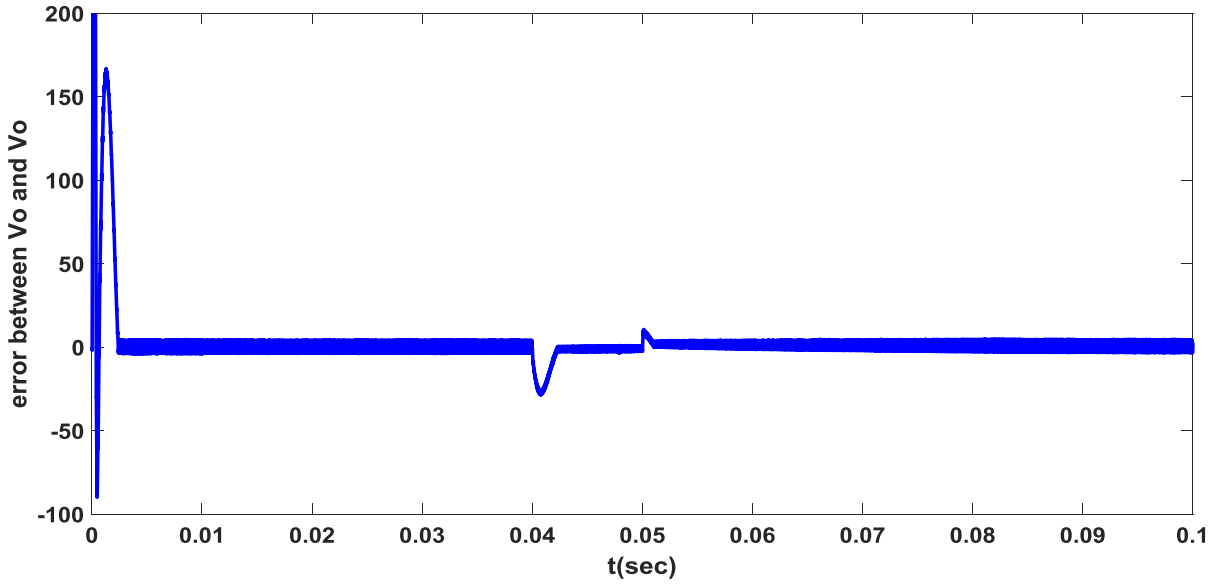

Figure 5.26 Output voltage error signal for DC input variation

The error signal shown in Figure 5.26 is very small (-10) even if there is DC voltage variation.

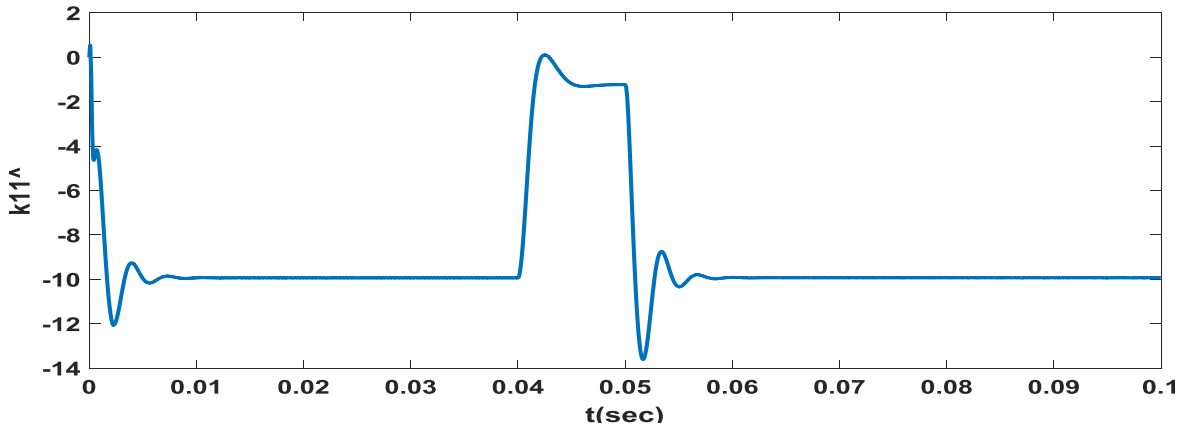

Figure 5.27 Estimated controller parameter of k_{11} for DC input change

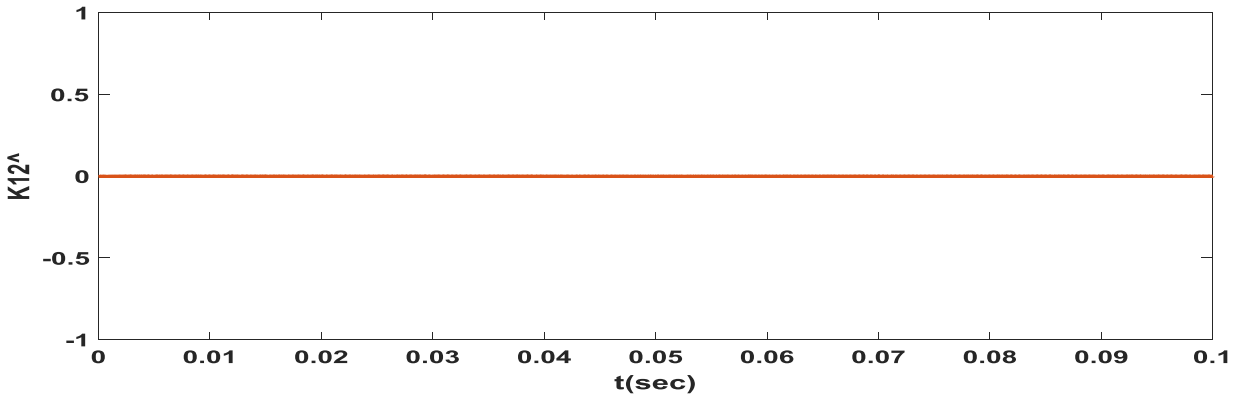

Figure 5.28 Estimated controller parameter of k_{12} after DC input change

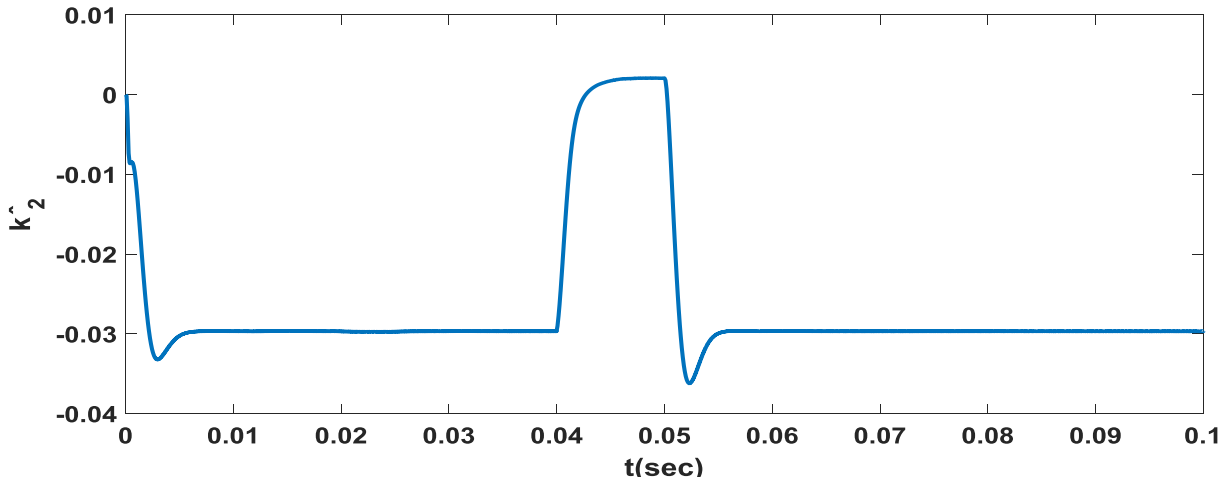

Figure 5.29 Estimated controller parameter of k_2 after DC input change

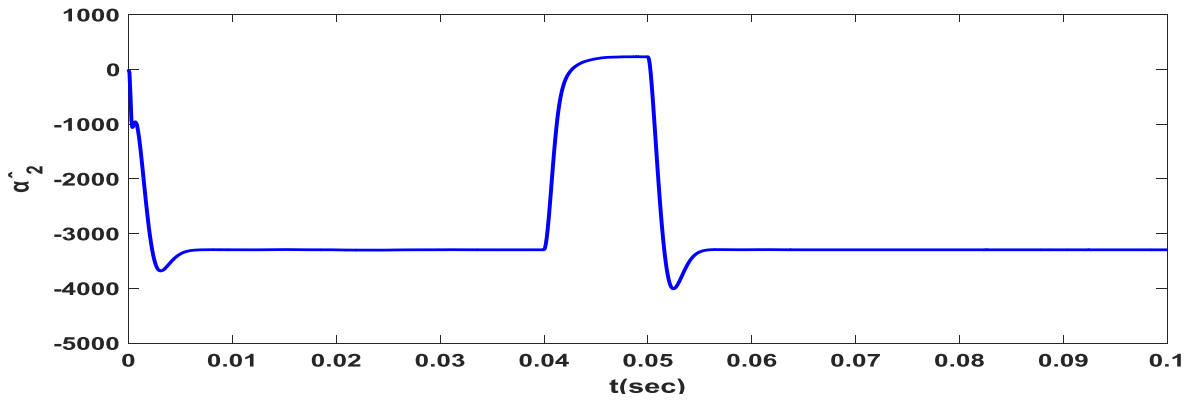

Figure 5.30 Estimated controller parameter of α_2 for DC input change

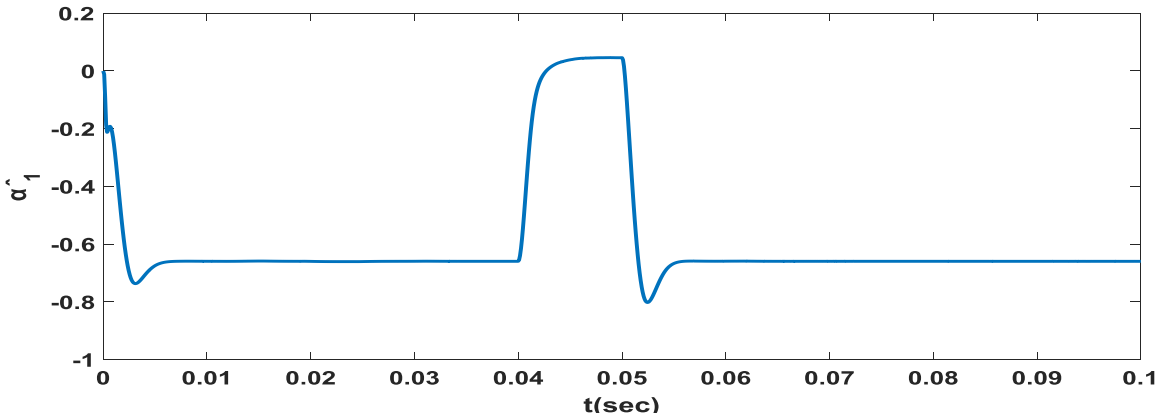

Figure 5.31 Estimated controller parameter of α_1 after DC input change

From figure 5.28-5.31 it is possible to understand that the controller parameter estimated by MRAS update law is the same with original value calculated in controller design part except there is minimum error at the DC input variation point.

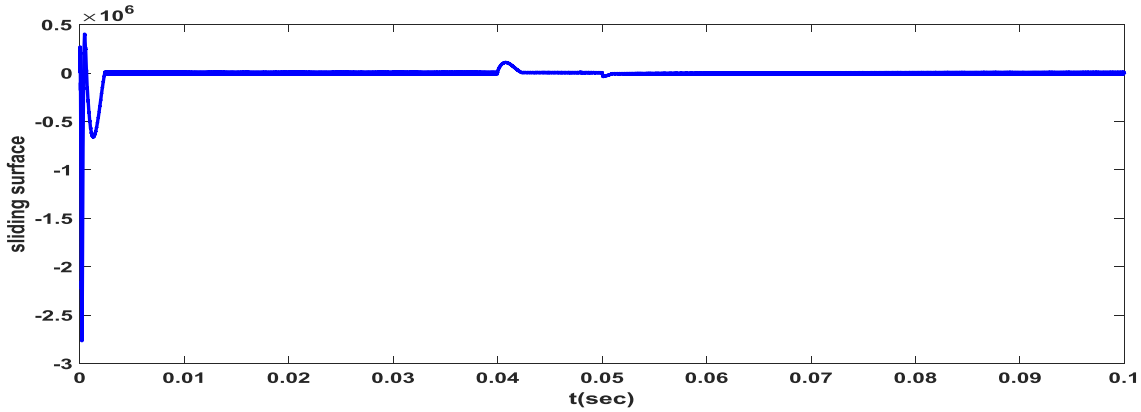

Figure 5.32 Integral sliding surface for DC input Variation

The sliding surface shown in figure 5.32 shows that there is small error occurred due to DC input variation.

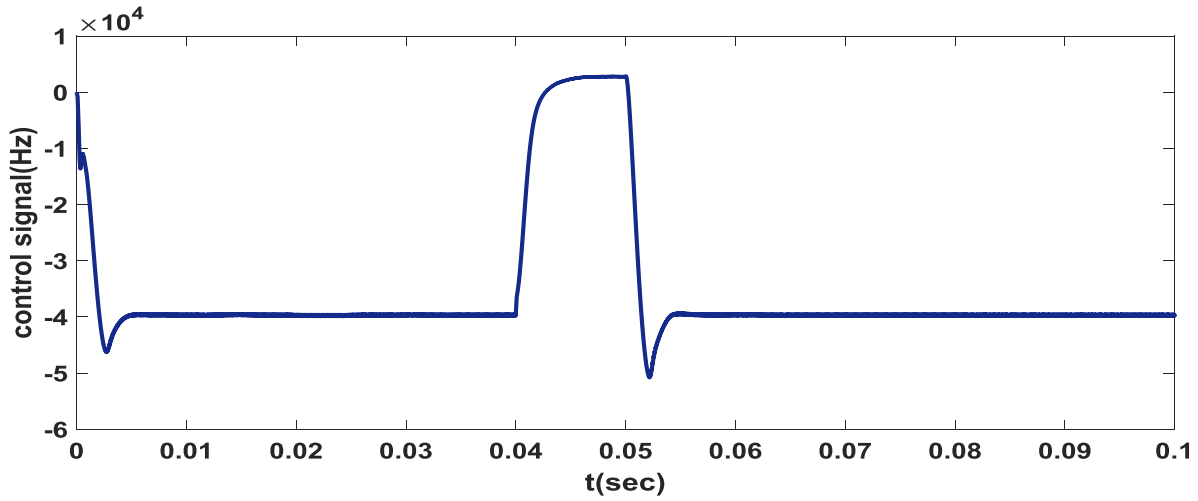

Figure 5.33 Control signal for DC input variation

The control signal value is changed to make the output voltage follow the reference voltage compensating the DC input voltage variation in the converter.

5.4.2 Load Resistance Variation

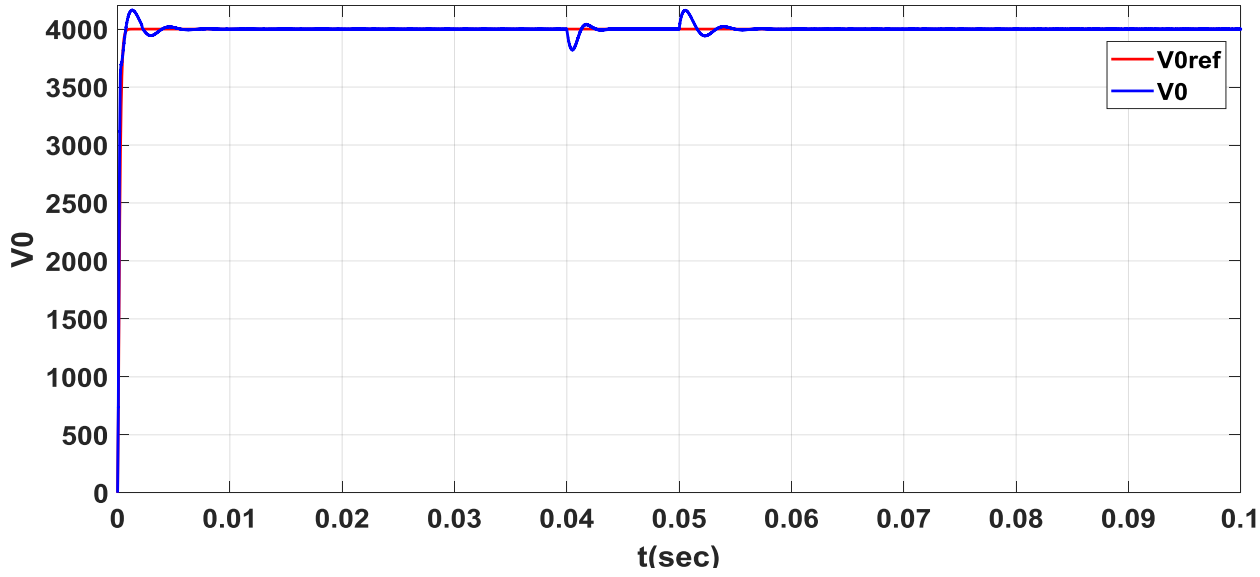

Figure 5.34 Output voltage response after load resistance Variation

The response of output voltage has similar transient response with the response of controller without any disturbance. But, there is about 150 steady state error caused by load resistance variation

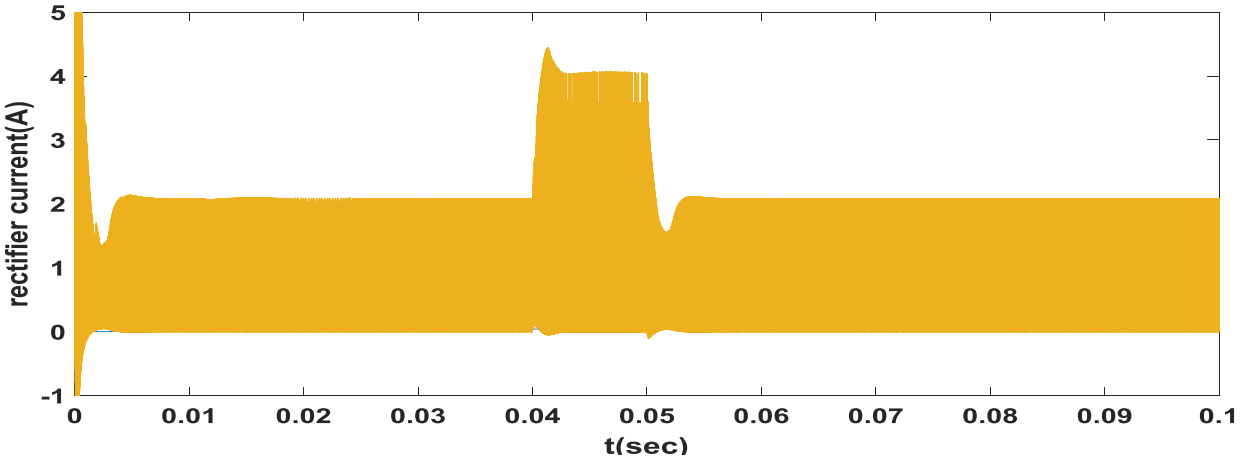

Figure 5.35 Rectifier current after resistance variation

From Figure 5.35 it shown that there is no current spike after load resistance is varied from true value.

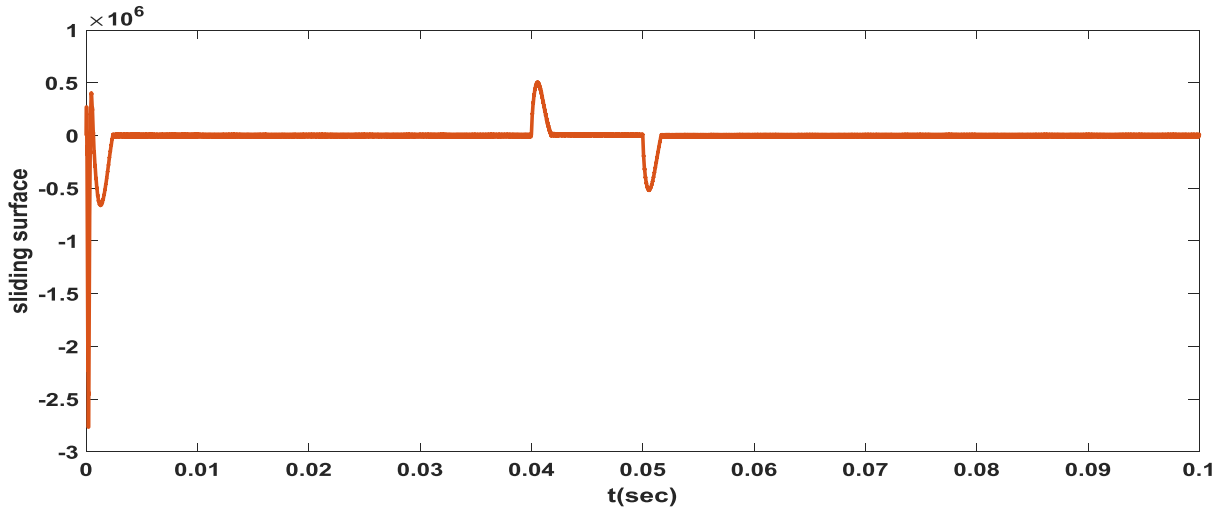

Figure 5.36 Integral sliding surface after resistance variation

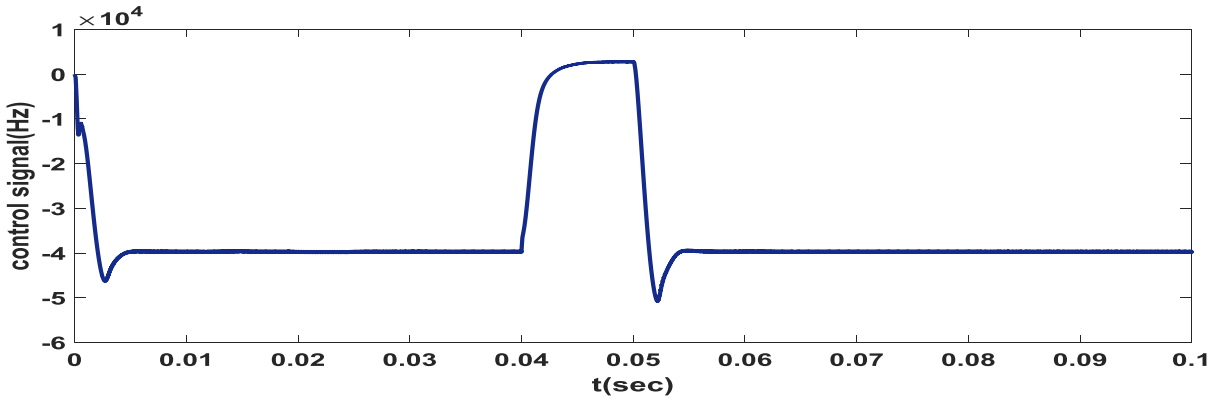

Figure 5.37 Control signal after load resistance change

The control signal value is changed from $-(4)\text{x}10^4$ to $(1)\text{x}10^4$ in order to solve the disturbance caused by load resistance variation.

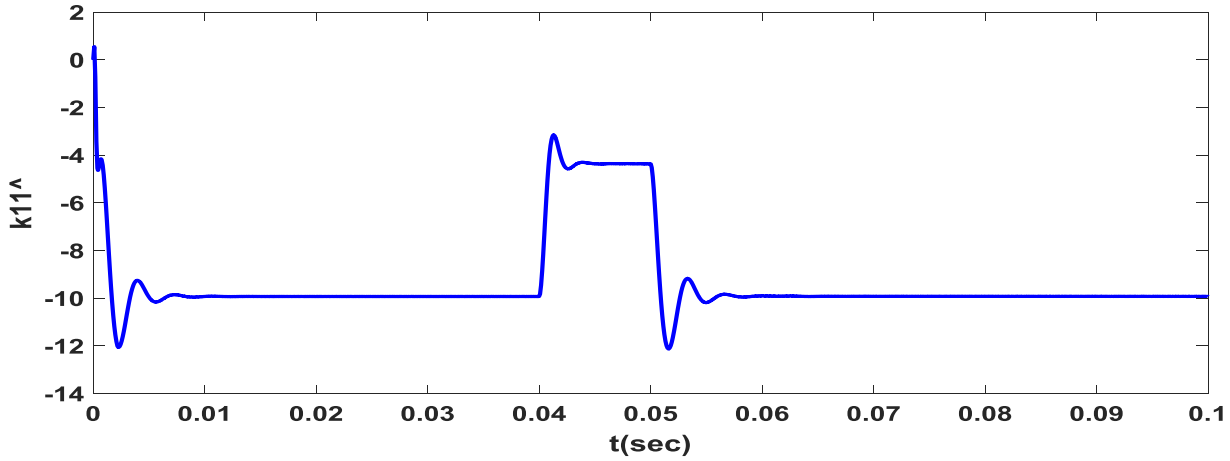

Figure 5.38 Estimated controller parameter of k_{11} after load change

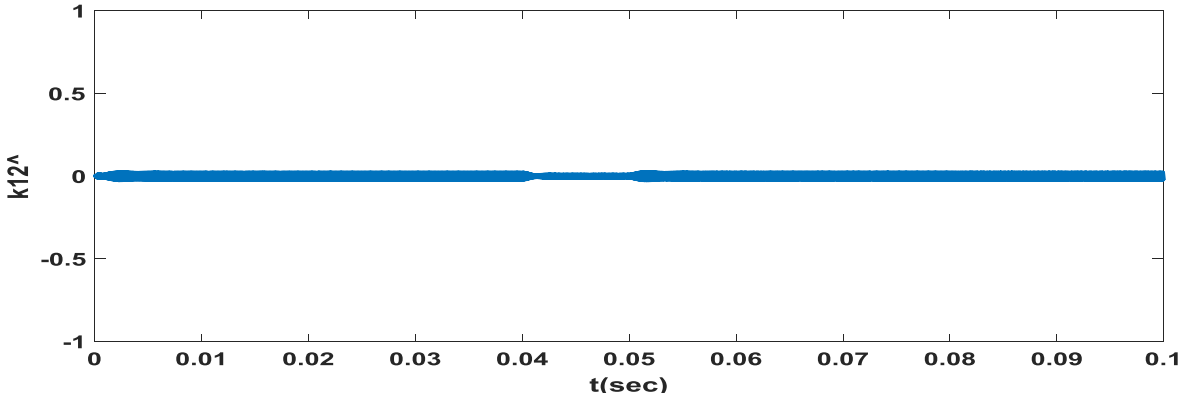

Figure 5.39 Estimated controller parameter of k_{12} after load change

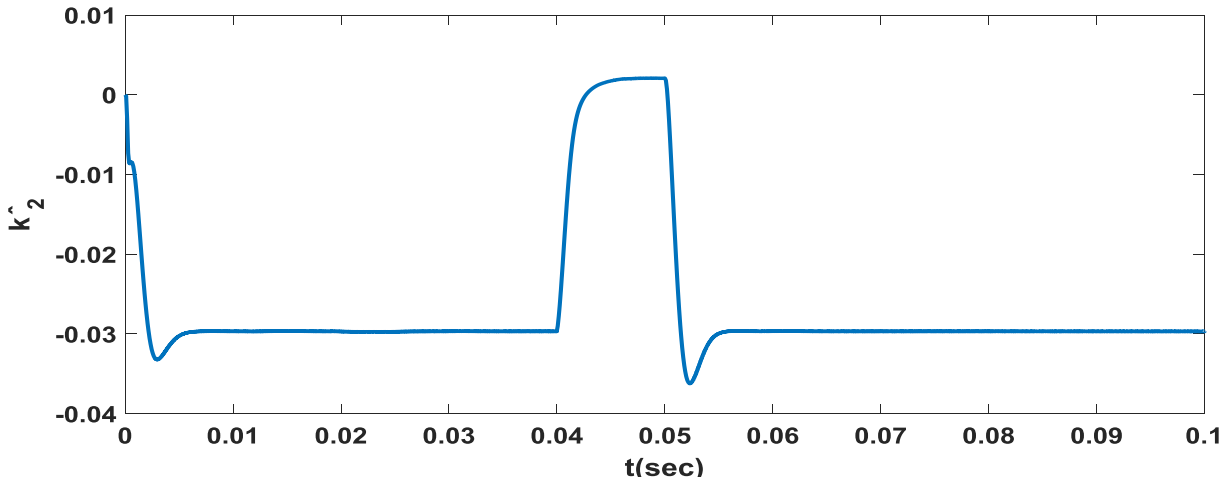

Figure 5.40 Estimated controller Parameter of K_2 after load resistance change

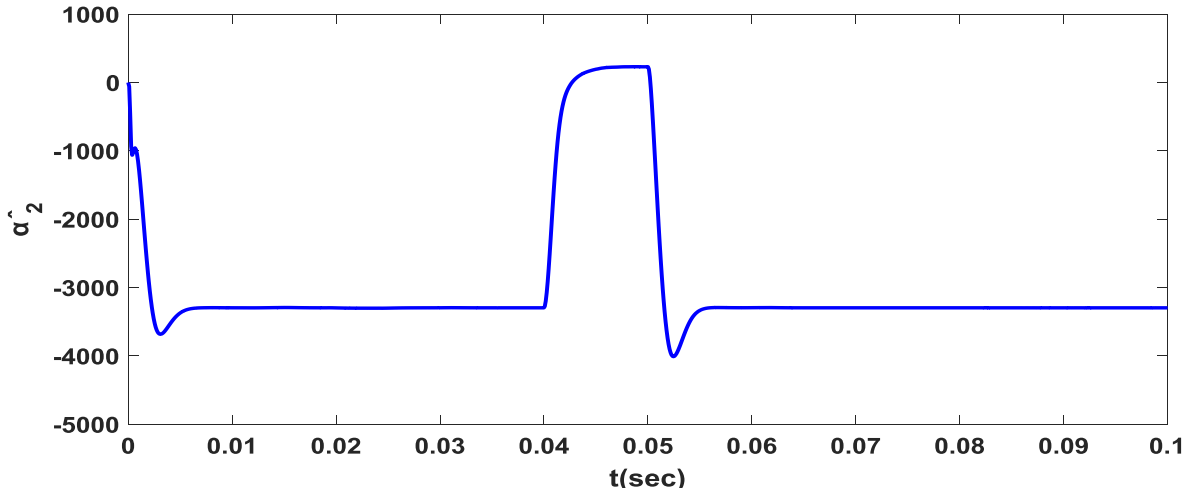

Figure 5.41 Estimated controller parameter of α_2 after load change

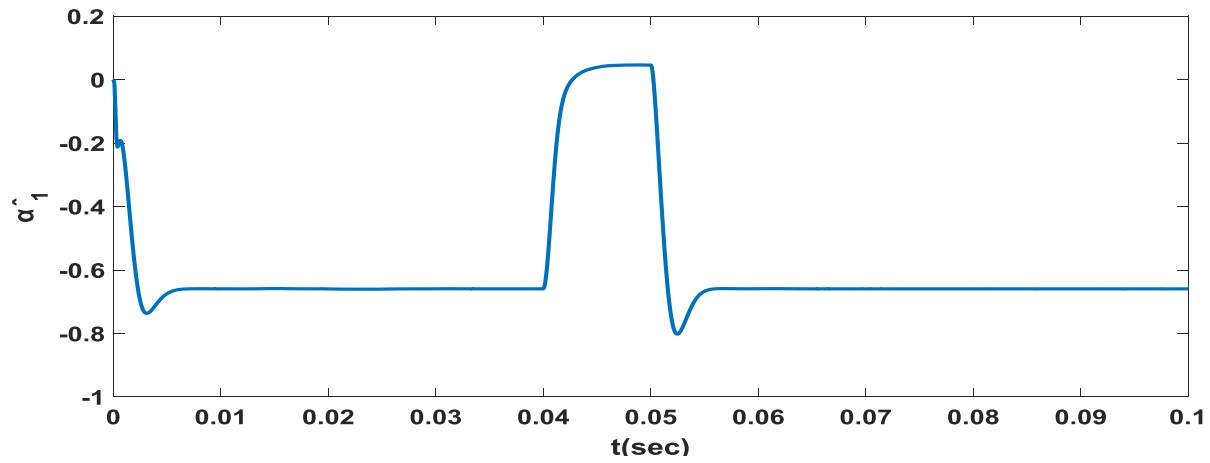

Figure 5.42 Estimated controller parameter α_1 after load resistance change

The output shown in Figure 5.39-5.42 indicates that the estimated controller parameters are the same with the parameter designed in controller design part. This indicates that the estimation error is reduced to zero except at the time (0.04-0.05) sec.

5.4.3 Resonant Inductor Variation

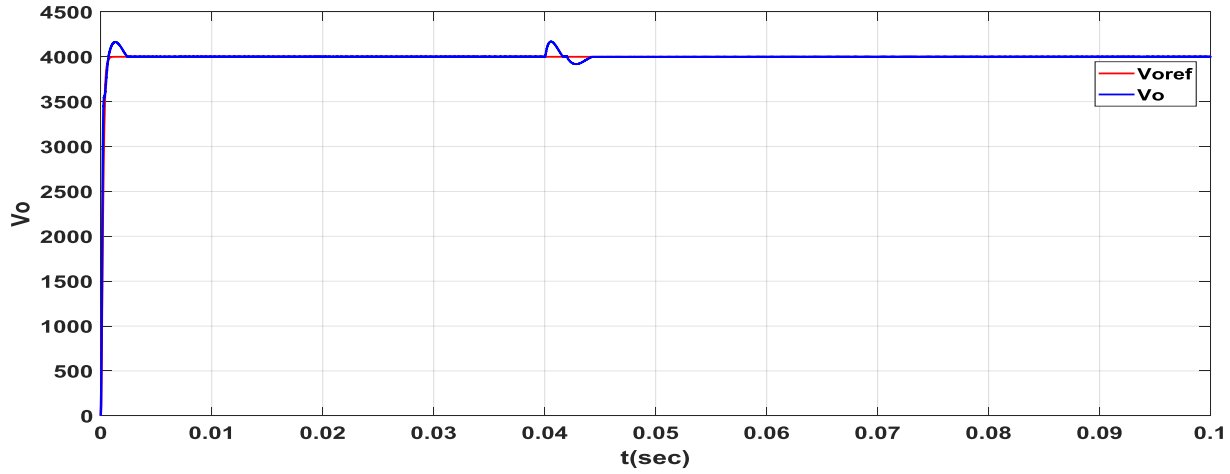

Figure 5.43 Output voltage response after resonant inductor change

The output voltage response has the same transient performance with the controller without any disturbance. But, there is about 200 error caused by resonant inductor variation from nominal value.

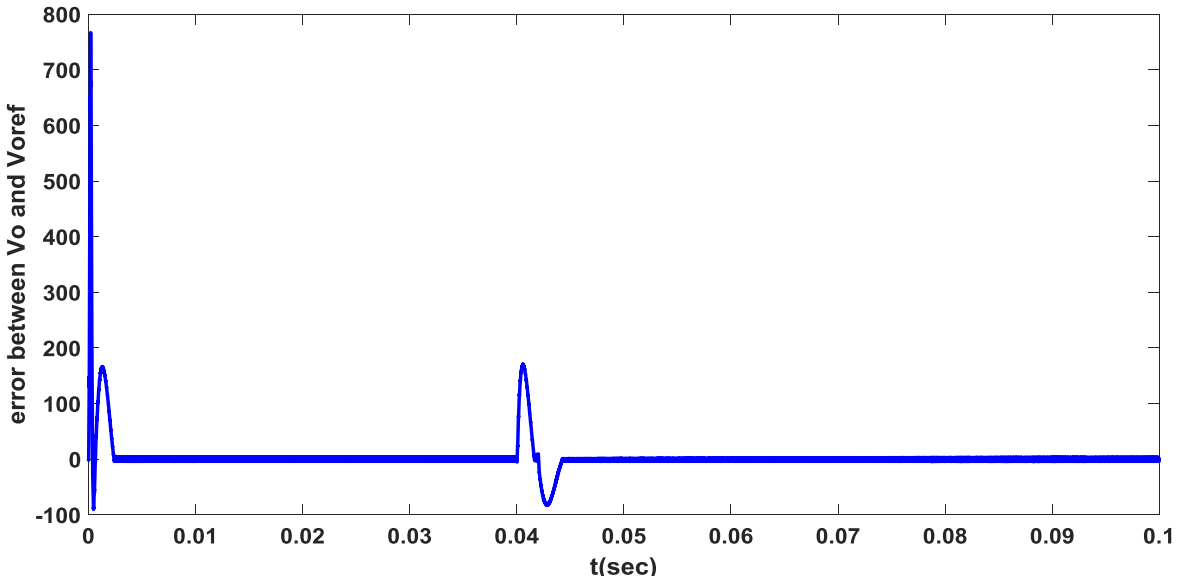

Figure 5.44 Output voltage error after inductor variation

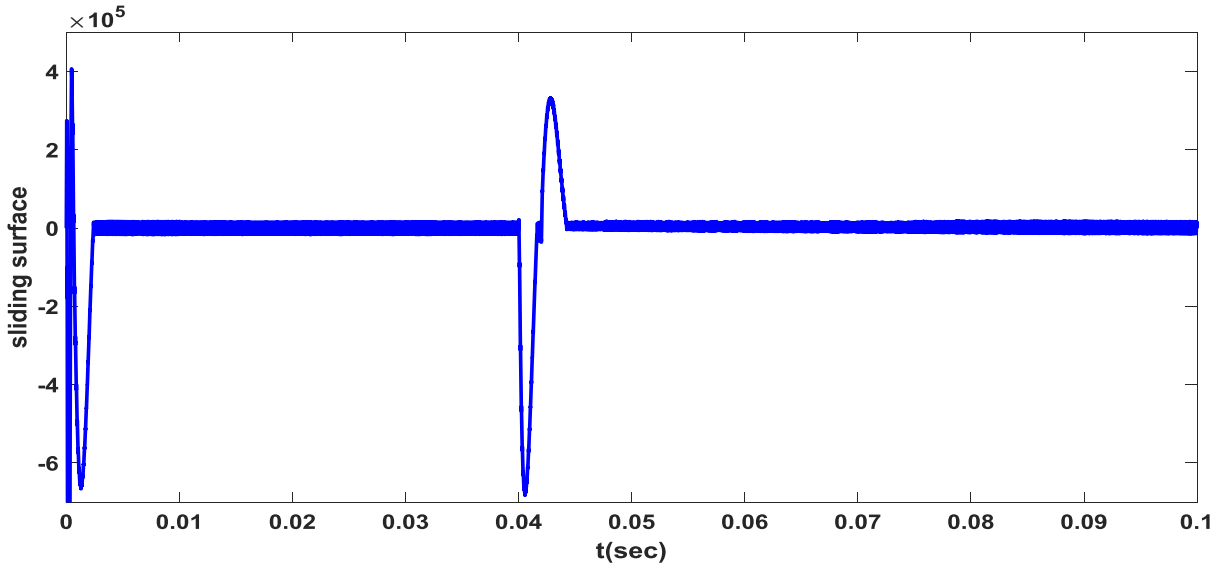

Figure 5.45 Integral sliding surface after inductor variation

5.4.4 DC Input Voltage, Load resistance and Resonant Inductor Variation at the Same Time

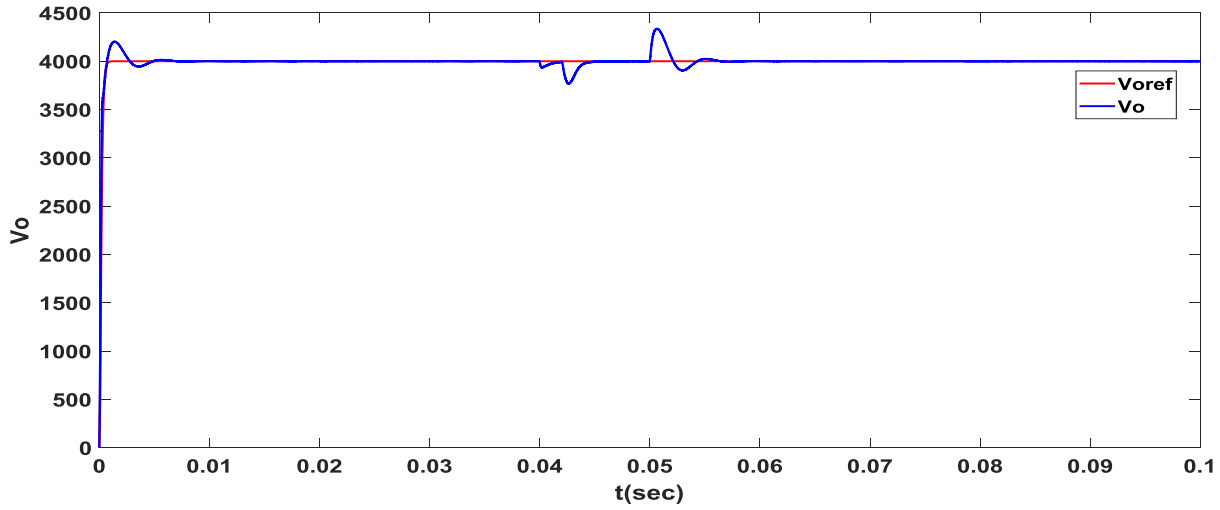

Figure 5.46 Output voltage response after three parameter variation at the same time

The output voltage exactly follows the reference voltage as shown in figure 5.46 even though there is disturbance due to DC input, resonant inductor and load resistance variation at a time between $(0.04-0.05)\,\text{sec}$. The controller has the same transient and steady state response with that of ASMC without any disturbance.

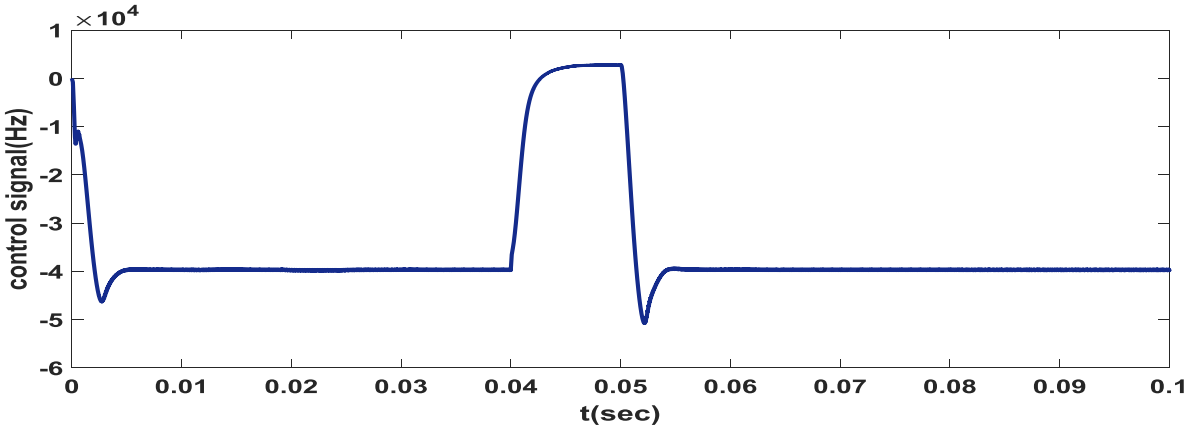

Figure 5.52 Control signal with all parameter variation

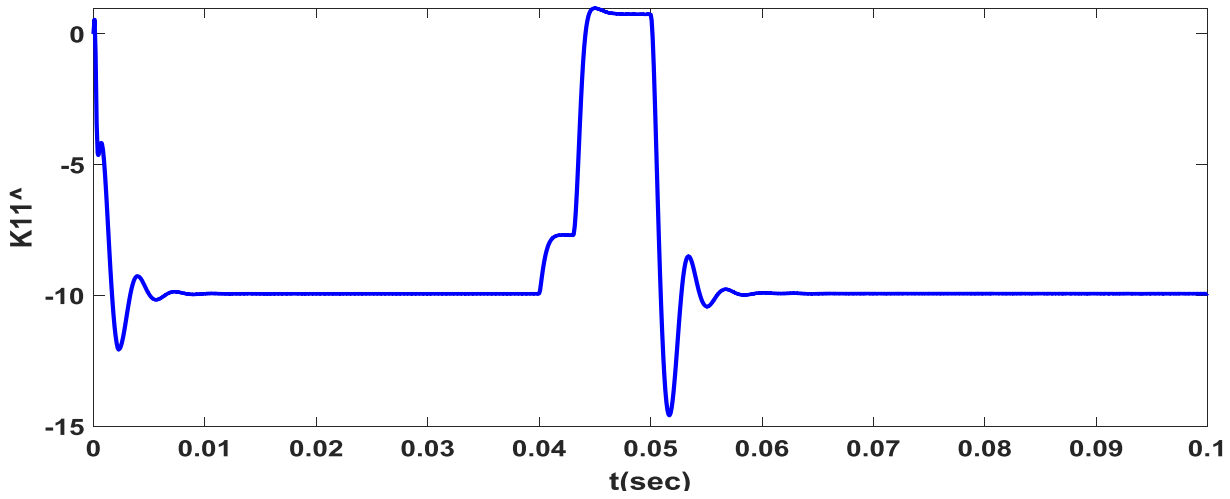

Figure 5.47 The estimated parameter of k_{11} for all parameter change

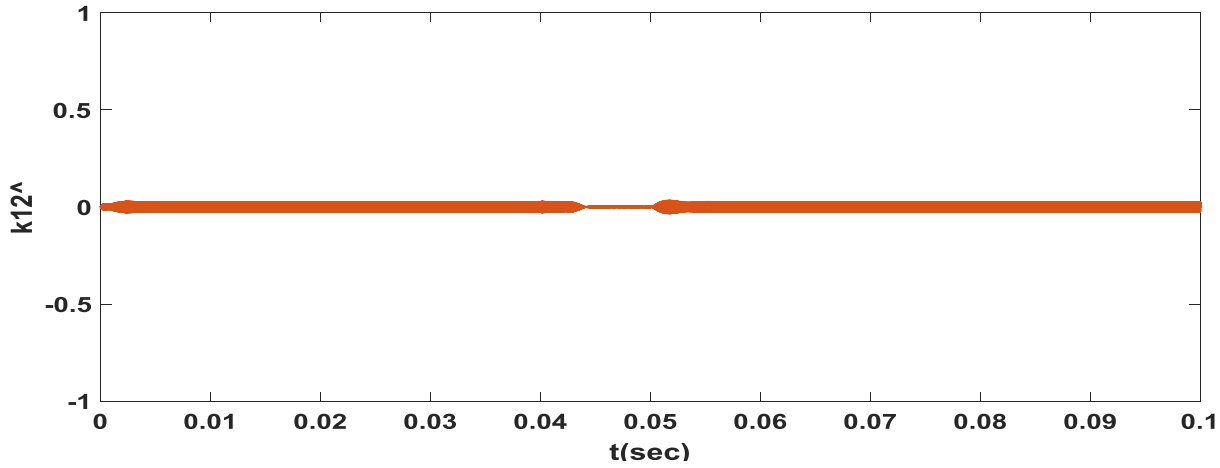

Figure 5.48 The estimated controller parameter of k_{12} for all parameter change

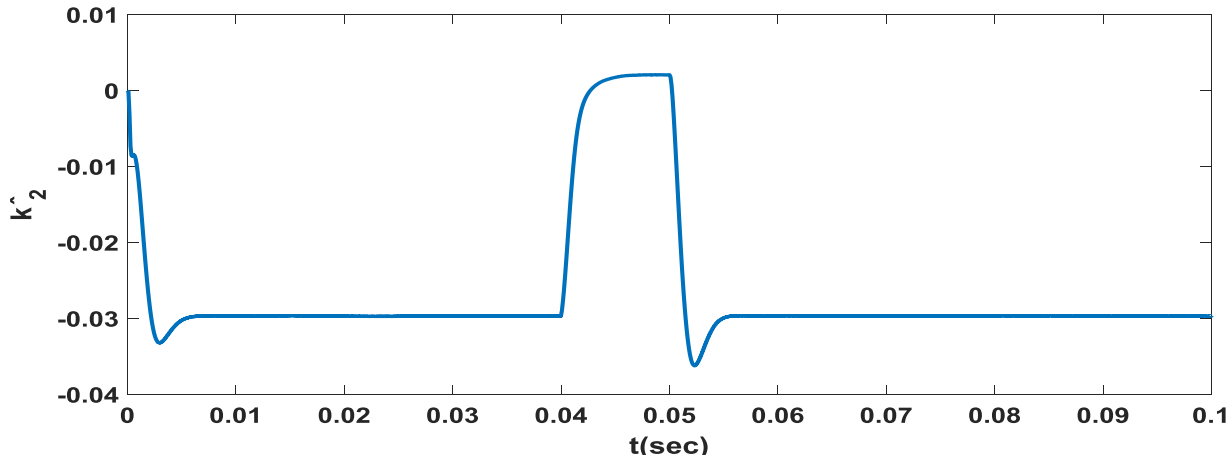

Figure 5.49 Estimated parameter of k_2 for all parameter change

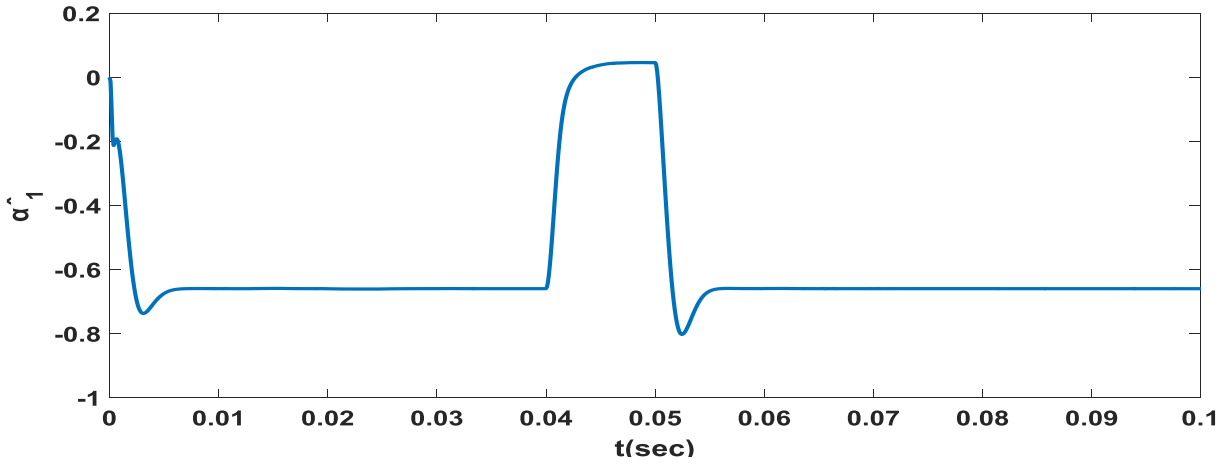

Figure 5.50 Estimated controller parameter of α_1 after all parameter variation

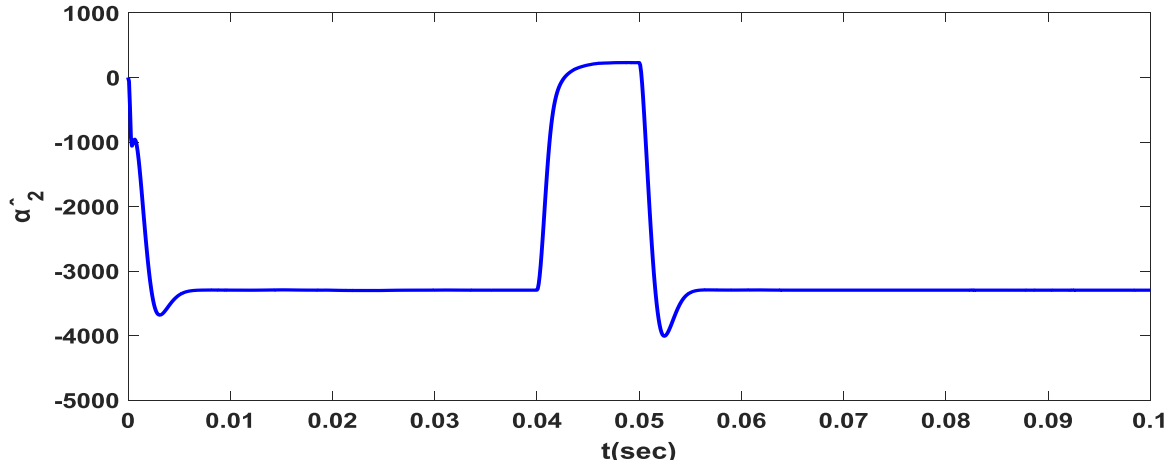

Figure 5.51 Estimated controller parameter of α_2 after all parameter variation

As indicated in figure 5.49, 5.50 and 5.51 the estimated controller parameter is the same with the nominal value calculated in controller design part. The controller parameter error is zero after the disturbance is happened at the time between $(0.04-0.045)\,\text{sec}$.

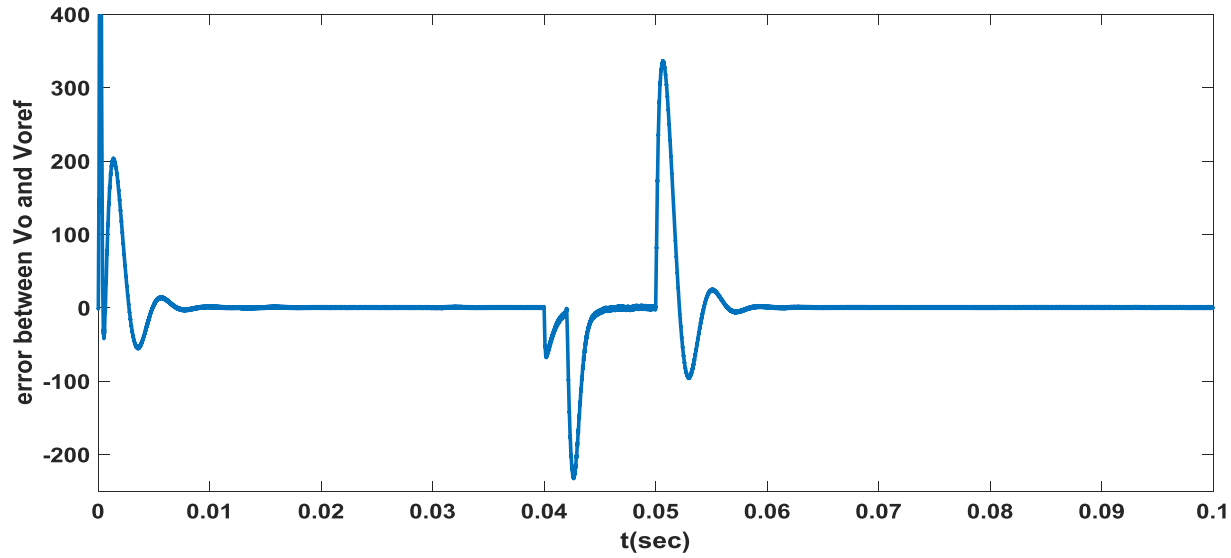

Figure 5.52 Tracking error of ASMC with disturbance

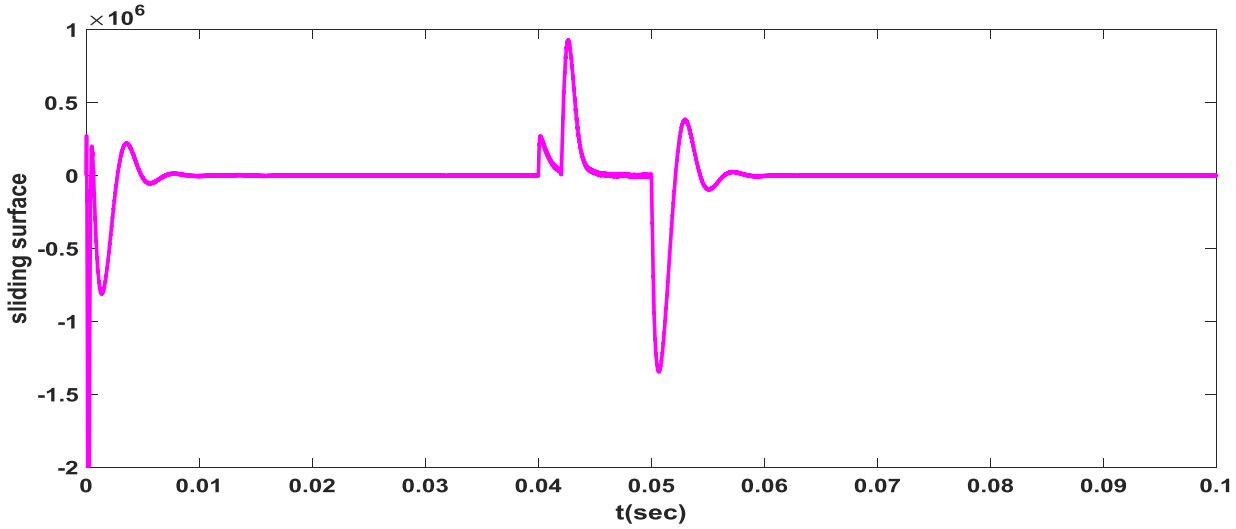

Figure 5.53 Sliding mode surface of ASMC with disturbance

From figure 5.52 and 5.53 it is possible to observe that both tracking error and sliding surface converges to zero, rejecting the disturbance and parameter variation happening between the time $(0.04-0.045)\,\text{sec}$.

5.5 Discussion of the Result

The transient and steady state response of both controllers are compared in the following table.

Table 5.3 Performance of STA and ASMC

Performance parameters	ASMC performance	STA performance
Maximum overshoot (%)	6.37	8.78
Steady state error	0.2%	0.7%
Rise time	334µsec	182.8µsec
Settling time	2.5msec	4.33msec

As indicated in Table 5.3 the ASMC has better transient and steady state response compared to STA.

Both controller can reject the disturbance caused by one parameter deviation individually. During DC input variation the STA controller can perform better than ASMC for large difference of input voltage i.e. (300-400). But, ASMC controller can regulate only (360-400) V range of DC input voltage.

During load resistance adjustment, the ASMC performs better than STA controller. There is 150 error only at a time 0.04 and 0.05 sec. But, there is 397 error value after time 0.05 sec in STA controller. The output voltage follows the reference voltage better in ASMC while it indicates steady state error in STA controller after load resistance alteration.

For resonant inductor change, ASMC has good performance compared to STA. The ASMC shows 200 error at a time 0.04 sec and 0.045 sec. The output voltage exactly follows the reference voltage except at a time 0.04 sec and 0.045 sec. However, in STA controller the error is increased to 397 after a time 0.045.

During load resistance, resonant inductor and DC input voltage variation, the output voltage could not follow the reference signal after time is 0.05 sec in STA controller. But, in ASMC the output voltage follows the reference voltage exactly after 0.05 sec and before 0.04 sec.

CHAPTER SIX

6. CONCLUSION AND RECOMMENDATION

6.1 Conclusion

The LLC resonant converter is preferable for high voltage application since it operates in ZVS region. It reduces switching loss and can be regulated within small frequency range. Large signal modeling of the converter results in nonlinear equations. Small signal modeling of the converter solves the nonlinearity found in large signal modeling equations. The small signal modeling results in linear seven order system. The Taylor series approximation of seven order to second order system makes the controller design easy by reducing the unmeasurable states in small signal modeling. The model reference adaptive sliding mode controller is designed and applied to the converter for different parameter variation. The ASMC performance is improved compared to second order supper twisting sliding mode controller as such the ASMC has settling time 0.0025sec and steady state error 0.2% respectively. Moreover, the tracking error, controller parameter error and sliding surface converges to zero using ASMC. The rectifier current spike shown in STA is removed in case of ASMC. The control effort is also reduced to $4x10^4$ in ASMC while it is switching between $-(9-11)x10^9$ in supper twisting sliding mode controller. The integral sliding surface used in ASMC recovers the steady state error to 0.2% caused by converter parameter and external disturbance. Over estimation of upper bound the disturbance is also reduced by using integral surface in ASMC. Generally, ASMC has better transient and steady state performance than supper twisting controller; even though there is disturbance and uncertainty due to variation in input voltage, resonant inductor and load resistance variation at the same time.

6.2 Recommendation

In this thesis the transformer hysteresis loss and parasitic capacitor is neglected in the design of LLC converter. In addition, only resonant inductor is varied to check the effect of resonant component parameter variation on LLC converter i.e. resonant capacitor change is not considered. Moreover, only 10% of resonant inductor is assumed to vary. The following points are recommended for future work:

- Check the effect of resonant capacitor on LLC converter
- Consider the parasitic capacitor and hysteresis loss in design of LLC converter
- Use optimal sliding surface instead of integral sliding surface during reaching phase
- Use higher order sliding mode controller to avoid chattering problem
- Look forward the best controller which can regulate the output voltage with all these considerations

References

[1] W. Li and H. Xiangning, "Review of nonisolated high-step-up DC/DC converters in photovoltaic grid-connected applications," *IEEE Transactions on Industrial Electronics* , vol. 58.4, pp. 1239-1250, 2011.

[2] Kwasinski, Alexis and N. O. Chimaobi, "Dynamic behavior and stabilization of DC microgrids with instantaneous constant-power loads," *IEEE Transactions on Power Electronics* , vol. 26.3, pp. 822-834, 2011.

[3] Saeedifard, Maryam and I. Reza, "Dynamic performance of a modular multilevel back-to-back HVDC system," *IEEE Transactions on power delivery* , vol. 25.4, pp. 2903-2912, 2010.

[4] Li, Xiaodong and K. B. Ashoka, "Analysis and design of high-frequency isolated dual-bridge series resonant DC/DC converter," *IEEE Transactions on Power Electronics* , vol. 25.4, pp. 850-862, 2010.

[5] B. Yang, "Topology investigation of front end DC/DC converter for distributed power system," Doctorial dissertation,Virginia Tech, 2003.

[6] K. Young, "Asymptotic stability of model reference systems with," *IEEE transaction on Automatic Control,* vol. 22, pp. 2179-281, 1977.

[7] T. Chern and Y. Wu, "Integral variable structure control approach for," *IEE Proc. D. Control theory appl,* vol. 139, pp. 161-166, 1992.

[8] S. Wenlong, L. Yaqiu and S. Liping, "Model Reference Adaptive Integral-type Sliding Mode Control Design for a Class of Uncertain Systems," *IEEE Proceedings of the 6th World Congress on Intelligent Control and Automation,* 2006.

[9] R. W. Erickson and M. Dragan, Fundamentals of power electronics, 2nd ed., Springer Science & Business Media, 2007.

[10] T. Halder, "A comparative study of the hard & soft switching of the flyback converters," *In Power India International Conference (PIICON), IEEE,* vol. 6th, pp. 1-6, 2014.

[11] J. Hung and W. H. J. Gao, "Variable structure control: A survey," *IEEE transactions on industrial electronics,* vol. 40(1), pp. 2-22, 1993.

[12] C. Edwards and S. Sarah, Sliding mode control: theory and applications, 1st ed., London: Crc Press, 1 January 1970.

[13] F. Harashima, H. Hideki and K. Seiji, "MOSFET converter-fed position servo system with sliding mode control," *IEEE Transactions on industrial electronics,* pp. 238-244, 1985.

[14] V. Utkin and S. Jingxin, "Integral sliding mode in systems operating under uncertainty conditions," *Proceedings of the 35th IEEE Conference on Decision and Control,* vol. 4, 1996.

[15] B. Bandyopadhyay, D. Fulwani and S. K. Kyung, Sliding mode control using novel sliding surfaces, vol. 392 lecture Notes in Control and Information Sciences, Springer, 2009.

[16] G. Bartolini and e. et al, Modern sliding mode control theory: New perspectives and applications, vol. 375 of Lecture Notes in Control and Information Sciences, Springer Science & Business Media, 2008.

[17] Z. Ding, Nonlinear and Adaptive Control Systems, 1st ed., London, United Kingdom: The Institution of Engineering and Technology, 2013.

[18] K. J. Åström and W. Björn, Adaptive control, 2nd ed., New York: Dover publications, 2008.

[19] J. Fei, "Adaptive sliding mode control with application to a MEMS vibratory gyroscope," PHD Thesis,University of Akron, 2007.

[20] Lai, S. Yen and H. Y. Min, "On-line auto-tuning technique of switching frequency for resonant converter considering resonant components tolerance and variation," *IEEE Journal of Emerging and Selected Topics in Power Electronics* , 2018.

[21] S. Geng, Y. Zhao, S. Sun, X. Wu, Y. Zheng and J. Liu, "Sliding mode control of LLC resonant DC-DC converters," in *InIndustrial Electronics (ISIE), 2016 IEEE 25th International Symposium on 2016,* 2016.

[22] T. Chen, Q. Chen, L. Lei, L. Zhang and S. Quan, "Research on full bridge LLC resonant converter based on fuzzy self-adaptive PI control," in *In Automation (YAC), 2017 32nd Youth Academic Annual Conference of Chinese Association of,* 2017.

[23] F. Degioanni, G. Z. Ignacio and M. Ordonez, "Dual-Loop Controller for LLC Resonant Converters Using an Average Equivalent Model," *IEEE Transactions on Power Electronics ,* 2017.

[24] B. Amghar, M. Darcherif, J.-P. Barbot and D. Boukhetala, "Modeling and control of series resonant converter for high voltage applications," *Energy Conference (ENERGYCON),IEEE International,* pp. 216-221, 2014.

[25] E. Maguiri, Ouadia and e. al, "Nonlinear adaptive output feedback control of series resonant dc-dc converters," *American Control Conference (ACC),IEEE,* 2010.

[26] Shahzad, I. M, I. Shahid and T. Soib, "LLC series resonant converter with PID controller for battery charging application," *IEEE Conference on Energy Conversion (CENCON),* pp. 84-89, 2014.

[27] F. Zhijian, W. Junhua, D. Shanxu, L. Kaipei and C. Tao, "Control of an LLC Resonant Converter Using Load Feedback Linearization," *IEEE Transactions on Power Electronics,* vol. 33, pp. 887-898, 2017.

[28] Feng, Weiyi, C. L. Fred and M. Paolo, "Simplified Optimal Trajectory Control (SOTC) for LLC Resonant Converters," *IEEE TRANSACTIONS ON POWER ELECTRONICS,* vol. 28, pp. 2415-2426, 2013.

[29] H.-P. Park and J. Jee-Hoon, "Modeling and feedback control of LLC resonant converters at high switching frequency," *Journal of Power Electronics,* pp. 849-860, 2016.

[30] B. Concettina, C. Carlo and L. Hamed, "Observer-based Control of LLC DC/DC Resonant Converter Using Extended Describing Functions," *IEEE TRANSACTIONS ON POWER ELECTRONICS,* pp. 5881-5891, 2015.

[31] N. Azura, S. Iqbal and S. Taib, "LLC resonant DC-DC converter for high voltage applications," *IEEE Conference,* no. Energy Conversion (CENCON), pp. 90-95, 2014.

[32] Rashid and M. H, Power electronics handbook, 2nd ed., Butterworth-Heinemann, 2017.

[33] Person and C. E, "Selection of Primary Side Devices for LLC Resonant Converters ," PHD Thesis,Virginia Tech, 2008.

[34] T. Filchev, D. Cook, P. Wheeler, d. B. A. Van, J. Clare and V. Valchev, "High power, high voltage, high frequency transformer/rectifier for HV industrial applications," *IEEE In Power Electronics and Motion Control Conference,* pp. 1326-1331, 2008.

[35] W. COLONEL and M. T, TRANSFORMER AND INDUCTOR DESIGN HANDBOOK, 3rd ed., California,USA: MarcelDekker, 2004.

[36] E. X.-Q. Yang, "Extended describing function method for small-signal modeling of resonant and multi-resonant converters," PHD Thesis,Virginia Tech, 1994.

[37] Fang, Zhijian, W. Junhua, D. Shanxu, X. Liangle, H. Guozheng and L. Qisheng, "Rectifier Current Control for an LLC Resonant Converter Based on a Simplified Linearized Model," *Energies ,* vol. 3, p. 579, 2018.

[38] Z. Kai, Z. Guodong, Z. Dongfang, L. Jianbing and S. Yin, "Modeling, Dynamic Analysis and Control Design of Full-Bridge LLC Resonant Converters with Sliding-Mode and PI Control Scheme," *Journal of Power Electronics,* vol. 18, pp. 766-777, May, 2018.

Appendix

A. bode plot of second order and seven order transfer function

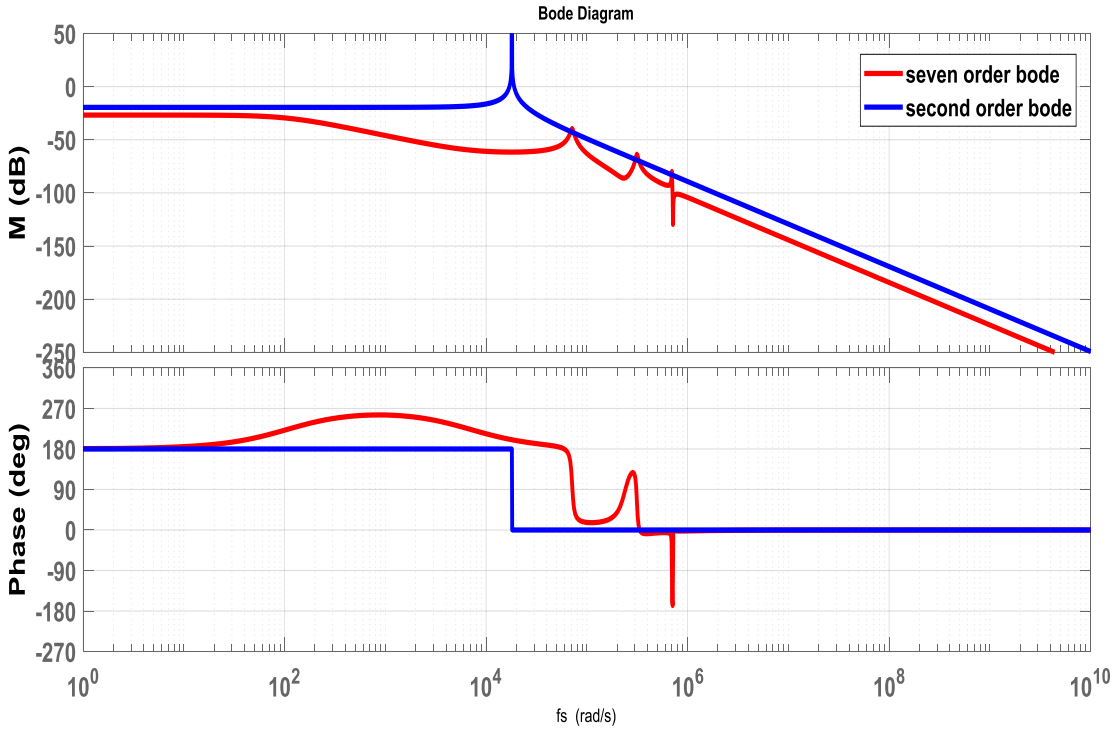

B. LLC resonant converter specification

Table 1 LLC converter specification

Input voltage (V_{DC})	(380-400)V	Switching frequency (f_s)	50kH
Output voltage (V_0)	4000V	Primary resonant frequency (f_{r1})	61.25kH
Output power(P_0)	200W	Secondary resonant frequency	44kH
Output current (I_0)	0.5 A		

C. High voltage, high frequency transformer specification for LLC converter

Table 2 transformer specification for LLC converter

Quantity name	value	Quantity name	Value
V_{rms1}	360V	V_{rms2}	3600
Rms voltage(V_{square})	510 V	Mean length per turn on primary side (Mltp)	19.5 cm
Switching frequency (f_s)	50kH	Resistivity of copper(ρ)	$1.71x10^{-6}$
Efficiency(η)	0.98	Resistance per turn primary(Rs/t)	$418.9x10^{-6}$
Mean length per turn on secondary side (Mlts)	2πx15.5 cm	Cross sectional area of mmg|100|57|44 core transformer(A_c)	24.91 cm^2
Resistance per turn primary(Rp/t)	$8.185x10^{-6}$	Temperature coefficient at 50℃ (ξ)	1.24
Magneticfield density(B_m)	0.5T		